# THE REDOX AND IRON-SULFIDE GEOCHEMISTRY OF SALT POND AND THE THERMODYNAMIC CONSTRAINTS ON NATIVE MAGNETOTACTIC BACTERIA

By

Peter A. Canovas III

B.S., Texas A&M University-Corpus Christi, 2002

Submitted in partial fulfillment of the requirements of the degree of

Master of Science

at the

MASSACHUSETTS INSTITUTE OF TECHNOLOGY

and the

WOODS HOLE OCEANOGRAPHIC INSTITUTION

June 2006



Signature of Author _____

Joint Program in Oceanography/Applied Ocean Science and Engineering
Massachusetts Institute of Technology
and Woods Hole Oceanographic Institution
June 2006

Certified by _____

Katrina J. Edwards
Thesis Supervisor

Accepted by _____

Timothy I. Eglinton
Chair, Joint Committee for Chemical Oceanography
Massachusetts Institute of Technology/
Woods Hole Oceanographic Institution

# THE REDOX AND IRON-SULFIDE GEOCHEMISTRY OF SALT POND AND THE THERMODYNAMIC CONSTRAINTS ON NATIVE MAGNETOTACTIC BACTERIA

Peter A. Canovas III

Massachusetts Institute of Technology / Woods Hole Oceanographic Institution Joint Program in Chemical Oceanography

ABSTRACT

Salt pond is a meromictic system with an outlet to the sea allowing denser seawater to occupy the monimolimnion while the mixolimnion has relatively low salinity and is the site of greater mixing and microbial activity. The density contrast between the two layers allows for a unique geochemical environment characterized by steep redox gradients at the interface. This chemocline is a habitat for magnetotactic bacteria (MB), and the spatial and temporal distribution of MB in the system along with geochemical ($Fe^{2+}$, $H_2S$, pH, $O_2$ (aq), etc.) profiles have been analyzed from 2002 – 2005. It has been previously observed that magnetite-producing cocci occupy the top of the chemocline and greigite-producing MB occur at the base of the chemocline and in the sulfidic hypolimnion. This distribution may be attributed to analyte profiles within the pond; depth profiles show a sudden drop of dissolved oxygen (DO) at the chemocline associated with an increase in dissolved Fe (II) concentrations that peak where both $O_2$ and $H_2S$ are low. In the sulfidic hypolimnion, Fe (II) concentrations decrease, suggesting buffering of Fe(II) by sulfide phases. Maximum concentrations of iron (II) and sulfide are ~31 μM and 3 mM, respectively. Stability diagrams of magnetite and greigite within $E_H$/pH space and measured voltammetric data verify fields of incomplete oxidation resulting in the production of elemental sulfur, thiosulfate and polysulfides. Calculations of the Gibbs free energy in the Salt Pond chemocline for potential microbial redox reaction involving iron and sulfur species indicate abundent potential energy available for metabolic growth. Oxidation of ferrous iron to ferrihydrite in the upper region of the chemocline consistantly has a yeild of over -250 kJ/mol $O_2$ (aq), ~ 12.5 times the proposed 20 kJ/mol minimum proposed by Schink (1997) necessary to sustain metabolic growth. This translates into biomass yeilds of ~ 0.056 mg dry mass per liter of upper chemocline water. If these numbers are applied to the dominant bacteria of the chemocline (MB that are 3% dry weight iron) then there could be up to ~ 1.68 μg of iron per liter of upper chemocline water just in the MB. This iron can be permenantly sequestered by MB into the sediments after death because the organelles containing the iron phases are resistant to degredation. Geochemical and microbial processes relating to the cycling of iron heavily impact this system and perhaps others containing a chemocline that divides the water column into oxic and anoxic zones.

Keywords: salt-stratified pond, magnetotactic bacteria, FeS, magnetite, greigite

# 1. INTRODUCTION

Iron is known to be an essential micronutrient in marine and aquatic systems where it is used in a variety of important metabolic and regulatory processes. Iron serves as a key nutrient in photosynthesis, $N_2$ fixation, methanogenesis, $H_2$ production and consumption, respiration, the TCA cycle, oxygen transport, gene regulation and DNA biosynthesis making it a very influential transition metal in the grand scheme of both the carbon and nitrogen cycles (Andrews, S.C. et al., 2003). In high concentrations this nutrient is considered a toxin, yet it has been found to be a potentially limiting nutrient along with phosphorus, and nitrogen in many systems because of low influx and lowered bioavailability through complexation with numerous organic compounds. Therefore, iron is often considered one of the most reactive elements in aquatic and marine environments, and it is strongly coupled to the cycling of other major biogeochemical elements (e.g. C, O, S, and P) and trace elements (Tessier and Campbell, 1988). Because of this, much attention has been given to the biogeochemical cycling of iron and the roles of microorganisms utilizing this nutrient.

Distribution and speciation of iron in marine systems depends on a host of different processes such as complexation with organic and inorganic ligands, adsorption-desorption, precipitation-dissolution, ion exchange, and redox reactions. Due to the redox nature of iron, some of the most interesting chemistry can be found in basins containing both oxic and anoxic zones in the water column. While the most thermo-dynamically stable oxidation state of iron in the oxic region is Fe(III), which may be mostly in the form of insoluble colloidal iron oxyhydroxides, this changes as it crosses

into the anoxic zone. There it may be made more soluble through reduction to Fe(II), allowing for a much higher dissolved iron concentration (Byrne and Kester, 1976 a,b). Further complications can occur if there is a high sulfide content, as Fe(II) may precipitate as iron sulfide minerals (Emerson et al., 1983). Because of this, reactions occurring across the oxic-anoxic transition zone (OATZ) can have a disproportionate impact on the distribution and speciation of iron. This is very important to microbes residing in or on the boundaries of the OATZ (such as magnetotactic bacteria) because it allows them to exploit the redox disequilibria of the system created from the faster kinetics of the precipitation-dissolution and adsorption-desorption reactions.

Understanding microbial influences on biogeochemical cycling is an integral part of assessing the constraints placed on the biotic and abiotic processes responsible for the cycling of analytes and the potential for microbial growth and their ability to sustain themselves in the system they occupy, and the ones inhabited by magnetotactic bacteria (MB) are no exception. MB biomineralize single-domain, magnetic particles of iron oxides (magnetite) or/and iron sulfides (greigite) into membrane bound organelles called magnetosomes (Bazylinski and Moskowitz, 1997 and Balkwill et al., 1980). This causes the cell to have a permanent magnetic dipole moment and passively align along the Earth's geomagnetic field lines as it swims (Frankel and Blakemore, 1980). In 1970 Blakemore first noticed this behavior and termed it magnetotaxis. Magnetotaxis is believed to aid in maintaining and/or locating the optimal vertical position in a stratified water column with respect to chemical and redox gradients (Frankel et al., 1997).

Iron uptake is accomplished through the utilization of hydroxamate and catechol siderophores, much of whose structure in these organisms is unknown (Calugay, R.J. et al.,2004; Calugay, R.J. et. al., 2003). What is known, is that the action of MB siderophores is strong enough to compete with other well known ligands such as nitrilotriacetic acid (NTA) and may actually strip the iron out of them. *M. magneticum* AMB-1 can incorporate iron so fast in iron replete media that it can deplete the iron in four hours(Calugay, R.J. et al., 2004). The massive uptake of iron by MB is an important factor when considering the availability of iron in a system, especially since the iron sequestered as ferromagnetic inclusions may exceed μM concentrations (Stolz, J.F, 1992). *M. magneticum* has been known to accumulate up to a 10 mM concentration of iron and have a dry weight of ~3% iron (Bazylinski, D and Frankel, R.B, 2004). This is almost 170 times the amount of iron found in *E. coli* (Matsunaga, T. and Okamura, Y., 2003).

Not only are these organisms able to affect the iron cycle by sequestering large amounts of iron while they are alive, but they continue to affect the iron cycle after their cells die and lyse. Biological magnetic particles (BMPs) have a phospholipid bilayer surrounding them and are not degraded quickly or even at all sometimes. These biogenic, single domain, ultra-fine grained magnetic particles have been shown to be a primary remanence carrier in sediments where high numbers of MB have lived, permanently removing iron from bioavailability in the water column. This does come with the added benefit of being able to use older (even fossilized) BMPs as past indicators of environmental conditions (Stolz,J.F, 1992).

This study investigated the geochemistry of the chemocline where the largest populations of MB are located. The major aim was at elucidating the geochemical and thermodynamic constraints imposed on them at these depths concerning the species used for metabolism and BMP formation. Total dissolved iron, iron (II), sulfide, pH, salinity, and dissolved oxygen (DO) were measured at the OATZ and through the anoxic hypolimnion. Data were collected from Salt Pond on Cape Cod Massachusetts between the early summer early fall months of 2003, 2004, and 2005. For this paper, two representative sampling periods (August 11, 2004 and September 22, 2005), comprised of the most consistent and complete data, were chosen for analysis. Speciation and free energy calculations as well as $E_H$ / pH diagrams and species profiles were constructed to assess fluid-mineral equilibria and major complexes of iron sulfide and iron (oxy)hydroxides at the depths relative to the OATZ. This is correlated with data on the spatial and temporal distribution of MB in the pond from these and previous studies in order to investigate the broader relationship between the biogeochemical cycling across the OATZ and the microbiology that may both be contributing to it and be affected by it.

## 2. Methods

### 2.1 Study Site

Figure 1 shows Salt pond, a small (~.29 $km^2$), shallow (4.6-5.8m depth) seasonally stratified, brackish water kettle pond near Falmouth Massachusetts that is surrounded by ~0.02 $km^2$ of salt marsh (Cape Cod Commission, 2001). The pond has salt water inflow from tidal exchange with Vineyard Sound and freshwater inputs from rain, runoff, and groundwater. The daily tidal amplitude for the pond averages ~0.6m

(http://co-ops.nos.noaa.gov/data_res.html). The freshwater input leads to a density stratification that begins in early summer and is accompanied by the generation of sulfidic bottom waters. Later in the year, around mid-October, the thermal stratification of the pond begins to disintegrate. In the epilimnion aerobic process prevail, while the hypolimnion is dominated by hydrogen sulfide from bacterial reduction of sulfate. During the summer the anoxic zone may come within 2-3 m of the surface and the OATZ is characterized by steep gradients (Bazylinski et al., 2000). The epilimnion of this eutrophic pond has been recorded to have chlorophyll concentrations of 70 μg / liter in mid-August (Wakeham et al., 1987).

2.2 Collection of Samples

Samples were collected using an aluminum rowboat at a western, south-central location marked by a buoy in the pond. A YSI 85 profiler (Yellow Springs Inc., Yellow Springs, OH) was used to measure salinity, temperature, and oxygen in order to determine the location of the oxycline. The YSI meter was brought up when sulfide was present so as not to "poison" the electrode. The YSI meter was used in conjunction with a Geotech peristaltic pump (Geotech Environmental Equipment, Inc., Denver, CO) for simultaneous sampling and profiling. The pH was measured at each depth with an Orion 250A field pH meter.

During the 2005 sampling period a YSI 600QS sonde was used because it was capable of retrieving all the data that the YSI 85 was, plus pH, $E_H$ and specific conductivity as well as automatically monitoring depth. Both had a detection limit of ~6 μM for DO. A DLK60 potentiostat was also used during the 2005 sampling period to

measure sulfide, ferrous iron, and thiosulfate as well as test for the presence of elemental sulfur, polysulfides and aqueous iron sulfide. It was used in conjunction with the peristaltic pump and the YSIQS sonde to generate voltammograms across the chemocline. Water Samples were taken every ~0.3 m above and below the oxycline and every ~0.15 m through the oxycline, though in 2005 the advent of a more advanced YSI meter allowed for tighter resolution across the chemocline for all measurements. Samples for iron and sulfide were generally only taken through the oxycline with one sample for iron coming from the surface waters. The samples were withdrawn directly from the pump tubing with a 10-ml syringe and put in the appropriate prepared solutions for analysis at the lab and stored in the dark on ice.

### 2.3 Chemical Analyses

Analyses of Salt Pond were carried out using both laboratory and in situ methods, after which speciation models and $E_H$/pH diagrams were made to analyze the biogeochemical cycling and thermodynamic properties of the system and assess the ramifications to the natural microbial populations. The laboratory analyses consisted of the Cline method (1969) for sulfide determination and the Ferrozine (FZ) method (Stookey, 1970) for the concentrations of total dissolved iron, dissolved iron (II), total iron, and total iron (II). Concentrations for iron (III) were determined by taking the difference between the total iron and iron (II) measurements. Additionally, water samples were collected in 250 ml Nalgene bottles for analysis of magnetotactic bacteria and protists.

#### 2.3.1 Laboratory Analyses

Iron was measured via the Ferrozine method as described in Viollier et al. (2000) and had a minimum detection limit of ~300 nM. Filtered (using 0.4 micron polycarbonate filters) and unfiltered samples were taken for dissolved and total iron, respectively. Before collecting samples, acid washed 15 ml bottles were prepared with 100 µl of 10 mM Ferrozine in 100 mM ammonium acetate and 10 µl of 1 N HCl for Fe(II) while bottles for total Fe only contained 10 µl 1 N HCl. After samples were drawn, a 5 ml aliquot was put into the prepared bottles and then the samples were put back on ice and brought to the lab 1-2 hours later. At the lab, the samples were analyzed using a UV-Vis spectrophotometer. The blank absorbance of the reagents was measured at 562 nm and the spectrophotometer was then set to zero. Iron (II) samples were adjusted to a pH between 5 and 9 using 250 µl (more if necessary) of buffer composed of 10 M ammonium acetate adjusted to a pH of 9.5 with ammonium hydroxide. Total iron samples had 500 µl of the Ferrozine solution and 750 µl of 1.4 M hydroxylamine hydrochloride in analytical grade 2 M HCl. The mixture was then left for 10 minutes at room temperature in the dark for the reduction of Fe(III) to take place. Following reduction, 1.5 ml of buffer (more if necessary) was added to the total iron samples. The blank absorbance for the total iron reagents was then measured at 562 nm for relative absorbance measurements. One ml of each sample was used for spectrophotometric analysis. Standard curves were constructed from a 200 ppm ferrous iron standard in 0.0003 N HCl diluted in 2% NaCl solution. Iron (III) was calculated by taking the difference between total iron and Fe (II). During the summer 2005 sampling session, only total dissolved and particulate iron were obtained using this method.

Sulfide was measured using the Cline method which typically has a minimum detection limit of 1 μM (Cline, 1969). In the field, 500 μl of sample was added to 2 ml tubes that were already prepared with 1 ml of a 2.6% zinc acetate solution. They were then stored in the dark and on ice for 1-2 hours until being returned to the lab for analysis. Once in the lab, 200 μl of a 0.3 % DPDS solution (N,N-dimethyl-p-pheylenediamine in 5.5 N HCl) was added to the samples along with 200 μl of 0.0115 M ferric chloride solution (0.0115 M $FeCl_3$ in 0.6 N HCl). The samples were then incubated for 30 minutes. The absorbance was measured at 665 nm. Standard curves were constructed from 100 mM sodium sulfide solution fixed in 2.6% zinc acetate.

At each sampling depth across the chemocline water samples were collected in 250 ml Nalgene bottles for analysis of bacterial populations. Upon reaching the lab, samples were enriched for north and south seeking magnetotactic bacteria. This is done by placing a magnet next to the bottle to be sampled for one hour. Bacteria were obtained from the water sample using a glass pipette to scrape the side of the Nalgene bottle next to the magnet in order to detach them from the side of the bottle. They were then placed in autoclaved 2 ml microcentrifuge tubes. Samples from the same depth were analyzed at the same time. Examination of the samples was done with differential interference contrast (DIC) microscopy and numerical estimations of MB were done via triplicate dilution counts with deoxygenated artificial seawater (ASW) for both north and south seeking bacteria. The results were recorded and the dominant morphotypes photographed.

2.3.2 In Situ Analyses

Voltammetry was used to investigate the presence and concentration of polysulfide, elemental sulfur, sulfide, iron monosulfide, and ferrous iron across the chemocline and into the anoxic hypolimnion. To do this an Analytical Instrument Systems (AIS) Model DLK-60 voltammetric analyzer was used in conjunction with a solid state three electrode reference system. All the electrodes in the system were prepared using polyethyletherketone (PEEK) tubing. Within the system the working electrode was a 1mm diameter gold-mercury amalgam electrode, the reference electrode was Ag/AgCl and the counter was made of platinum wire. The configuration used for both sampling and calibration can be found in Table 1.

In order to interpret the scans from salt pond standard curves and spiking experiments were done in the lab with purged matrix water filtered through a 0.2 micron filter. This was done by gently heating the matrix water and purging it with $N_2$ for 45 minutes. Standard curves were made for ferrous iron, sulfide, thiosulfate, and oxygen with all prepared solutions being brought to the original pH of the matrix water. The detection limits for ferrous iron, sulfide, and thiosulfate were ~ 1, 0.2, and 2 μM respectively. If the electrodes are conditioned during the scans this method has a precision of ± 1% (Brendel and Luther, 1995).

Ferrous iron standards were made by preparing a 10 mM ferrous chloride stock solution in 10 mM HCl in Milli-Q water. The ferrous chloride crystals were rinsed with purged matrix water prior to weighing to eliminate surface oxidation products. They were then added to the HCl solution which was also purged with nitrogen prior to adding the crystals. After this a 10 mM stock of hydroxylamine HCl in deoxygenated matrix

water was made and buffered back to the original pH of the matrix water with concentrated bicarbonate solution. Sealed Falcon tubes with purged saline solution adjusted to the ionic strength of the matrix water and hydroxylamine added at a 1:4 ratio to that of the ferrous stock were created for concentrations of 1, 5 10 25, 50 and 100 μM. If a ferric iron peak was detected during the scan, the sample was redone with more hydroxylamine HCl added. Scans for all laboratory calibration curves and in situ field measurements were typically performed at a scan range of 1 or 10 μA (though 100 μA was also used for some of the sulfide calibrations or scans in the anoxic hypolimnion) with a two second conditioning step at -0.5 V prior to each scan. The voltage range used was -0.05 to -1.8 V with a scan rate of 1000 mV/s to match the run conditions used in the field where a high scan rate is necessary for peak separation between different sulfide species. Five to ten scans were typically taken for each concentration with the first two scans not being used since they are less accurate due to build up and deposition on the mercury surface between sets of scans. The remaining scans were then averaged to obtain a representative peak height for that concentration.

Thiosulfate standards were made by creating a 10 mM stock solution from sodium thiosulfate in purged matrix water. Dilutions of 1, 5, 10, 25, 50, and 100 μM were made to construct a calibration curve in a manner analogous to that used for the ferrous iron. Sulfide standards of 10 and 10 0mM for calibration curves were made by rinsing sodium sulfide nonhydrate crystals with purged matrix water to remove oxidation products before weighing. Both stock solutions were then buffered back to the pH of the matrix water and concentrations of 1, 10, 100, 250, 500, 1000, 1500 μM were made to construct the

calibrations curves. Standard curves for oxygen were made via two point calibration curve with oxygen saturated matrix water and purged matrix water.

These calibration curves were then used to determine the concentrations of different analytes across the chemocline and into the anoxic hypolimnion. Scans were also analyzed for the presence of polysulfides, elemental sulfur, and aqueous iron sulfides by comparison with scans from that of Rozan et al.(2000). Recognition of different sulfides in the scan is critical for accurate quantitative analysis of analytes present because sulfides will behave differently in the presence of iron. For example polysulfides will give two peaks, each resulting from one part of a two part redox reaction at the electrode surface. One peak is an HS- peak that will exactly over lap that measured by sulfide, adding to the observed sulfide peak height and the other peak is a $S^o$ peak (Fig. 2). The current generated by the HS- peak in polysulfide is 1/3 the current of $S^o$ in polysulfide. This was then subtracted from the total HS- peak signal in the scan in order to obtain the current generated from only sulfide.

2.3.3 Speciation and Solubility Modeling

Speciation and solubility modeling calculations were performed using the Geochemist's Workbench (GWB) suite, specifically the programs REACT and ACT2. REACT uses the basis species in a system to calculate the gas fugacities, saturation states, and speciation of analytes of a system at equilibrium. This is done in a fashion analogous to the Tableux method and incorportates the phase rule to set up a system of equations based on user inputs for activity or concentration and the equilibrium constants associated with reaction occuring in the system. ACT2 works by calculating fields of

stability for analytes based on equalibrium calculations where the boundries for the fields are logrithmic equations of mass balance laws. While ACT2 can perform activity diagrams of almost any two species, the one most relevent for this study is the $E_H$ / pH diagram.

Since a full fluid analysis of the water samples was unable to be obtained for the sampling periods, a two endmember mixing model was created to estimate the concentrations of the major ions. This was done by using data from Berner (1987) and Holland (1978) that was presented by Morel and Herring (1993) depicting average seawater composition. It was assumed that the salinity of the sample would be indicative of the concentration of other analytes based on conservative mixing. In this way all major ions were calculated except chlorinity, which was calculated from the following expression:

$$S(‰) = 1.80655 * Cl(‰) \quad (1)$$

The values obtained from these calculations were used to supplement the measured data entered into the modeling software. When $E_H$ data was available (i.e. the 2005 sampling period) it was also entered into the modeling software with the measured and estimated data. When it was not available (i.e. the 2004 sampling period) $E_H$ data estimated from the $E_H$ values across the chemocline in the 2005 sampling period. In order to estimate the $E_H$, a least squares method was applied to the plot of $E_H$ Vs. depth for only the range across the chemocline. It was assumed that during both sampling periods the top and bottom of the chemocline would have similar $E_H$ values. The equation derived was:

$$E_H = -875.42 * z + 3065.5 \quad (2)$$

Where $E_H$ is the redox potential and z is the depth. $E_H$ values were then calculated using the depth values at which data was obtained during the 2004 sampling period. Tables 2 through 9 indicate data measured and/or entered into REACT. Using the calculated values from REACT, phase diagrams were made using ACT2, another program in the GWB suite, specialized for making stability diagrams. The input files for REACT can be found in Appendices 1 – 6, while the input files for ACT2 can be found in Appendices 7-9.

In order to account for as many species as possible a new database was built by augmenting the standard thermo.dat database with other species from the thermo_wateq4f_gwb4.dat and thermo_minteq _gwb4.dat databases and more accurate thermodynamic data from recent papers for species participating in this system (new database available by request). Species obtained from thermo_wateq4f _gwb4.dat needed the reactions rewritten with $HS^-$ as opposed to $H_2S$ since the latter is not part of the thermo.dat basis (the basis or basis species set is a group of species from which all other analytes in the database are made from in a way that is similar to the Tableaux method). Species from thermo_minteq_ gwb4.dat required no such swapping in the chemical equation, though both data sets needed to have log Ks calculated for STP and also at different predetermined temperatures so GWB could extrapolate to intermediate and elevated values should it be called upon to do so. Calculation of log Ks at elevated temperature to complete the initial parameters for the polynomial used by GWB were accomplished with the following equation (which assumes enthalpy is independent of temperature) when there was enough thermodynamic data:

$$\log \frac{K_{T2}}{K_{T1}} = \frac{\Delta H^o}{2.303R}\left(\frac{1}{T_1} - \frac{1}{T_2}\right) \quad (3)$$

Where $K_{T2}$ and $K_{T1}$ are the equilibrium constants for the reaction at temperatures $T_1$ and $T_2$ (in degrees Kelvin), $\Delta H^o$ is the enthalpy of the reaction (in joules) at standard temperature and pressure (i.e. 25 °C and 1 bar of pressure), and R is the ideal gas constant 8.31451 J $mol^{-1}$ $K^{-1}$. When there were no values for the log K at STP to be used in the preceding formula, one was calculated with the following equations:

$$\Delta G_r^o = \sum v_i \Delta G_f^o x_i \quad (4)$$

$$\Delta G_r^o = 2.303RT \log K \quad (5)$$

Where $\Delta G_r^o$ is the Gibb's free energy of reaction in joules, $v_i$ is the coefficient of the analytes in the mass action equation and is negative for reactants, $\Delta G_f^o$ is the Gibb's free energy of formation of the analyte in question measured in joules, $x_i$ is any analyte in the reaction.

Even if there was not enough data to solve for all the fitting parameters of the thermo.dat database, all species at least had a proper value for log K at STP. Therefore, any absence of thermodynamic data will have no effect on any of the calculations here because this system is so close to STP. Error will occur at elevated temperatures and pressures, i.e. the polynomial will not be able to extrapolate past 100 °C at standard pressure.

All $E_H$/pH phase diagrams were constructed using GWB ACT2 with the augmented database that was also used in REACT. Hematite, goethite, troilite, and pyrite were suppressed during the construction of phase diagrams because they are kinetically

inhibited and would not under ordinary circumstances be able to form in the water column. Also, some phases like troilite never form, while the formation of others such as marcasite, pyrrhotite, or pyrite is delayed. Ostwald's step rule states that the most soluble of phases will be the first to precipitate and that there are intermediary/metastable phases that are precursors to the more thermodynamically stable phases. Some of the suppressed species, such as amorphous iron sulfide would be present simply because of high kinetic favorability, despite the fact that it is not the most thermodynamically stable. Different metastable iron sulfide phases would be present in the water column and have the ability to affect the equilibrium and kinetics of geochemical reactions. It should also be noted that half life of particulate matter in the water column is only a few months; therefore it is not necessarily advantageous to look for the most thermodynamically stable phase in the water column. Many of the metastable phases will have already settled out of the water column before the more thermodynamically favored yet kinetically inhibited phases have a chance to form. One exception to this however, could be the hydrogen sulfide pathway for pyritization which involves the oxidation of iron monosulfide by hydrogen sulfide and has has no intermediaries and is kinetically favorable at STP (Rickard and Luther III, 1997).

## 3. Results

### 3.1 Water column characteristics

Due to freshwater input and solar heating, the pond is highly stratified with this being the most apparent in the temperature, $\sigma_{s,t,p}$ ($\sigma_{s,t,p} = \rho_{s,t,p} - 1000$), and salinity profiles (Figs. 3 and 4). Density calculations for determination of $\sigma_{s,t,p}$ used the international

equation of state for seawater from Unesco (1981). During the August 11, 2004 sampling period the chemocline had a width of approximately 1.1 m and the OATZ occupied the water column between 2.1 to 3.2 m at which point hydrogen sulfide was detectable (Fig. 5). This creates three distinct layers within the water column: an upper oxic layer with lower salinity and warmer temperature (0-2.4 m), the OATZ where there is a drop in oxygen at the top which continues until the concentration is below the detection limit and sulfide is detected (2.1-3.2 m), and a sulfidic hypolimnion where there is no dissolved oxygen (>3.4 m). While the thickness and depth at which each of these zones occurs may change over the season and in each year, they are consistently present and limited to a narrow range within the water column. This is illustrated in the results for the September 22, 2005 sampling period as well as in previous chemical profiles from Bazylinski et al. (2000) and Simmons et al. (2004). The chemocline during the September 22, 2005 period is more compressed, but still showed the same general trends as other dates with the chemocline occurring ~2.76 to 3.65 m where oxygen drops below the detection limit (Fig. 6). In contrast to the DO profile $E_H$ data depicts the chemocline in a different level of the water column i.e. from 3.35 to 3.83 m (Fig. 7). This deeper than the DO and portrays the chemocline to be smaller than in the DO profile, however these may be looked at as placing constraints on the maximum and minimum depth and extent of compaction for the chemocline, which resides between these two measurements. Like the previous sampling period, sulfide is again found to occur at very low concentrations with the DO profile forming a dissolved oxygen and sulfide overlap (DOSO) (Figs. 8 and 9).

3.2 Physical and Chemical profiles

The maximum temperature observed for the 2004 sampling period was 24.8 °C at the surface, while 2.4 m below the surface at the chemocline there was a drop by 1.3 °C which remained constant through the rest of the measurements. The 2005 sampling period had a maximum temperature of 24.07 °C at ~2.77 m and a minimum temperature of 21.09 at 4.154m. The minimum temperature recorded over the two summers was 12.7 °C (May 29, 2003, z = 4.3 m) while the maximum was 27.3 °C (August 15, 2003, z = 1.5 m). Salinity had a minimum of 23.6 ppt at the surface and increased to a maximum of 29.4 ppt by 3.2 m during the 2004 sampling period. During the 2005 sampling period minimum of 24.53 ppt at the surface and increased to a maximum of 29.03 at a depth of 4.121 m (Figs.3 and 4). The salinity extremes over the investigated summers were 30.1 ppt on July 1 2004 at 4.1 m and 7.9 ppt at the surface on June 26 2003. The maximum pH on August 11, 2004 occured at 1.8 m where it measured 8.93 and achieved a minimum of 7.01 at 4.4 m. During the September 22, 2005 sampling period the maximum pH was 7.76 and was found across the depth range of 1.2 to 1.5 m while the minimum pH of 6.71 at depths greater than 4.12 m.

During the 2004 sampling period dissolved oxygen and sulfide actually had a small overlap at 3.2 m where the dissolved oxygen concentration was 2.5 μM and hydrogen sulfide was 193.7 μM. During the 2005 sampling period this overlap was more extensively investigated with the use of voltammetry and a better YSI meter than in previous years and revealed a greater overlap of DO and sulfide. Sulfide first became detectable at 3.15 m with the electrode mounted on the sampler, but oxygen did not drop

below the detection limit of the sonde until 3.5 m. This overlap seemed to be quite normal for this system since only 2 of the 13 sampling periods lacked such a coexistence of the two species. However the readings without the sampler showed less of an overlap and sulfide was not detected until ~3.57 m. This minimizes the overlap of the two species to less than 10 cm. Dissolved oxygen was highest at the surface with a concentration of 240 μM during the 2004 sampling period and 236.88 μM at 1.52 m and dropped below the detection limit at ~3.6 - 3.65 m (Fig 10). During the 2005 sampling period DO started at a concentration of 233.15 μM and began to rapidly decline at 2.76 m where it dropped from ~147 μM to below the detection limit in less than a meter. It should be noted that even though YSI 85 meter used during the 2004 sampling period had a detection limit of ~ 6 μM, this limit was often negated by the presence of sulfide. Sulfide will permanantly bind to the membrane and ruin the meter. Therefore, in the 2004 sampling period "dropped below the detection limit" refers to the depth the electrode was at before sulfide was present. Sulfide was beow the detection limit in the water column down to 3.2 m and reached a maximum of nearly 568 μM at 4.1 m, but went decreased at 4.4 m.

During the 2005 sampling period sulfide first became detectable at 3.12 m with a concentration of 22 μM when the electrodes were mounted on the sampler and at 3.57 m with a concentration of 456 μM when free from the sampler. Sulfide reaches its maximum concentration of 3 mM at 4.15 m without the sampler and 2.8 mM at 3.56 m with the sampler. This concentration is much higher than previous sampling periods and there are two possible causes for its occurrence. The first is that it is later in the season

than when sampling is usually done and a large amount of sulfide could have accumulated below the chemocline prior to overturning. However analysis of data from previous years does not support this since there is no clear trend in readings from month to month. The other possibility is that the sulfide saturation limit of the method used is being approached. Cyclic voltammetry (CV) has a linear response to sulfide until millimolar concentrations are reached (Rozan et. al. 2000). Though previous years have been in the millimolar range, sulfide concentrations this high have never been recorded at Salt Pond. Even though it is entirely possible that the sulfide concentration could be as high as the electrode is asserting, it should be noted that the saturation limit of the method is being approached. Therefore, it can only be said with certainty that the total sulfide measured is over 1 mM, though it may be even be higher than the electrode measured. Figures 10, 11, and 12 show the vertical distribution of measured species relative to each other for the 8-11-2004 and 9-22-2005 sampling periods.

Above the chemocline, concentrations of dissolved iron in both redox states were near zero with particulate iron in the form of iron (oxy)hydroxides. The OATZ had the highest level of total dissolved iron (TDFe) in the water column. For the 2004 sampling period a TDFe maximum of 3.3 μM was achieved 3.4 m below the surface; then it decreased steadily to 1.64 μM at 4.4 m. At the top of the OATZ (~3.2 m) the majority of dissolved iron (2.4 μM ) was iron (III), but as soon as the concentration of oxygen decreased below the detection limit at 3.4 m, the major constituent was dissolved iron (II) which had a concentration of 2.29 μM. Until 4.1 m, DFe(II) was the major form of dissolved Fe and it slowly decreased until 4.1 m where there was a sudden drop to 0.46

μM. Conversely, the opposite trend was observed in DFe(III;, it slowly increased with depth from its minimum value in the OATZ until 4.1 m where it increased suddenly to 1.5 μM (Fig 13).

Iron measurements for the 2005 sampling period were similar to those of the 2004 period after the chemocline with the exception that no observed increase in Fe (III) species was detected. During the 2005 sampling period the Ferrozine method detected a TDFe maximum of 31.11 μM and was achieved a t ~3.22 m, after this the concentration of dissolved iron decreased to a minimum of 5.83 μM at 3.33 m. There was also a corresponding increase in particulate iron as the dissolved iron concentration waned. The electrode data, however were very different from the Ferrozine data and directly contradicted it in some cases (Fig 14). Voltammetric scans across the water column show that between the surface and ~1.5 m there were broad peaks from ~ -200 and -500 mV that are interpreted as Fe(III) complexed with organic material (Fig.15). Below this depth there is no signal from dissolved iron (III). Aqueous iron (II) sulfide complexes were present at various depths from ~ 0.5 m to the bottom of the chemocline as defined by the DO measurements (3.65 m). There are discrepencies in the mganitude of the iron measurements between those done with and without the sampler and also between the electrodes and Ferrozine method. At ~3.5 m the electrodes attached to the sampler read a maximum of 26 μM, while the electrodes alone recorded a maximum concentration of 32 μM. This maximum is where the Ferrozine data measured a minimum. Also, at the point where the Ferrozine method measured a maximum (3.22 m), there is only a concentration

of ~5 μM recorded by the electrode measurements without the sampler and Fe (II) is below the detection limit for the electrodes when they are on the sampler at that depth.

The profiles with the sampler are much more compact and may be attributed to the advective flow created by the pumping of the sampler and the disruption of the chemocline. It appears that this has the affect of sampling the average concentration of the water above and below the opening of the sampler in the range of ten, or maybe even twenty centimeters. This does not just extend to the analyses done with the electrodes but also to those done using the Ferrozine method where the water from different depths is being unevenly drawn up through the tubing due to the rocking and drifting of the boat. This would explain why the samplings done with this method are sometimes erratic. As for the voltammetric analysis, it appears to have the consequence of truncating or shrinking the profiles. Because of this it appears that Fe (II) is only present across a very small range of the chemocline, 3.249 to 3.56 m. Iron measured without the sampler was first detected at 3.06 m and did not drop below the detection limit until a depth of 3.645 m. Sulfide and thiosulfate profiles are altered as well. Sulfide, when measured without the sampler, is first detected at 3.57 m, while with the sampler is first detected at 3.12 m. The profiles with the sampler appear similar to those obtained without the sampler when viewed seperately, except the analyte concentrations are shifted. Figure 16 depicts the differences between the two measurements – with and without the sampler.

Cyclic voltammetry was also used for to detect elemental sulfur, iron sulfide, and polysulfides. Elemental and aqueoud iron monosulfide are found above the chemocline with detection of elemental sulfur occuring at depths as shallow as ~2.44 m and detection

of iron monosulfide occuring throughout the upper water column. While elemental sulfur and polysulfide are found throught the anoxic hypolimnion, ironmonosulfide is only detected once in that region. Thiosulfate on the other hand is only in a few scans, mainly between ~3.32 and 3.65 m (Fig.17). The $E_H$ as measured by the YSI displays the chemocline to be between the depths of 3.52 and 3.83 m, where it drops from ~107 mV to -319 mV. This differs from that of the DO readings which place it to be 2.76 to 3.65. Interestingly enough it is across the overlap between 3.52 and 3.65 m that the presence of thiosulfate, polysulfide, sulfide, elemental sulfur, and aqueous iron sulfide are first realized across the same interval in the water column (Tables 5 and 9 and Figs. 18 and 19).

**4. Discussion**

From the voltammetric data it is seen that thiosulfate, polysulfide, sulfide, elemental sulfur, and aqueous iron sulfide are present across the chemocline at different depths relative to each other. The placement occurs because of differences in the reactivity of each one with DO, which is declining across the chemocline. Oxidation occurs in the order of sulfite, thiosulfate and sulfide, elemental sulfur, and finally aqueous iron sulfides and polysulfides. This is evident in the log K values for the redox reactions listed below as well as depth profiles as sulfide drops below the detection limit before thiosulfate, which drops below the detection limit before ferrous iron. Using the following basic redox reactions a simple representation of what is happening abiotically within the water column can be displayed, though it should be noted that complete oxidation may not be achieved in the natural environment:

$$2SO_3^{2-} + O_2(aq) = 2SO_4^{2-} \qquad \log K = 92.5 \qquad (6)$$

$$\frac{1}{2}S_2O_3^{2-} + O_2(aq) + \frac{1}{2}H_2O = SO_4^{2-} + H^+ \qquad \log K = 73.45 \qquad (7)$$

$$\frac{1}{2}HS^- + O_2(aq) = \frac{1}{2}SO_4^{2-} + \frac{1}{2}H + \qquad \log K = 69.17 \qquad (8)$$

$$\frac{1}{2}H_2S(aq) + O_2(aq) = \frac{1}{2}SO_4^{2-} + H^+ \qquad \log K = 65.70 \qquad (9)$$

$$\frac{1}{8}S_5^{2-} + \frac{1}{2}H_2O + O_2(aq) = \frac{5}{8}SO_4^{2-} + H^+ \qquad \log K = 65.09 \qquad (10)$$

$$HS^- + O_2(aq) = \frac{1}{2}S_2O_3^{2-} + \frac{1}{2}H_2O \qquad \log K = 64.9 \qquad (11)$$

$$\frac{2}{3}S^o + \frac{2}{3}H_2O + O_2(aq) = \frac{2}{3}SO_4^{2-} + \frac{4}{3}H^+ \qquad \log K = 62.15 \qquad (12)$$

$$S_2O_3^{2-} + H_2O = SO_4^{2-} + HS^- + H^+ \qquad \log K = 8.56 \qquad (13)$$

$$S_2O_3^{2-} + H_2O = SO_4^{2-} + H_2S(aq) \qquad \log K = 1.94 \qquad (14)$$

Partial oxidation of sulfides in environments where DO is at a concentration of a few micromolar can provide a variety of different paths for reactions to follow with standard free energies ranging between -800 and -200 kJ/mol. Additivity model calculations from Williamson and Rimstidt (1992) predict the order by which this happens is $HS^- > S_2O_3^{2-} > S_3O_6^{2-} > SO_3^{2-}$, yet it should be noted that the reaction between $S_2O_3^{2-}$ and $O_2$ will not proceed in the absence of a catalyst such as pyrite (Xu and Schoonen, 1995) and that the production of thiosulfate itself may be from the oxidation of pyrite, typically by Fe(III) hexahydrate (Luther 1987, 1990; Moses et al. 1987, and Moses and Herman 1991).

.4.1 Vetical distribution of analytes across the OATZ

The distribution of analytes across the OATZ is characterized by the most oxidized species occurring at the top of the chemocline with reductive processes dominating the lower portion of the chemocline and probably extending into the anoxic hypolimnion. Iron in the ferric form as particulate iron (oxy)hydroxides is present at the top of the chemocline before suboxic conditions are realized with a transition to the ferrous form taking place via reductive dissolution throughout the rest of the chemocline. As dissolved ferrous iron is released it diffuses through the chemocline forming ferrous oxides and hydroxides at the top of the chemocline and iron sulfides deeper in the chemocline where sulfide is present. Inevitably solid iron sulfides such as amorphous iron sulfide or mackinawite form and precipitate out of the water column. By this way iron is quantitatively removed from the water column and settles on the bottom of the pond where it will steadily go through aging processes ultimately leading to pyrite. While this is happening through the chemocline, DO is being depleted through the oxidation of sulfide. Both sulfide and DO are being replenished to the top of the chemocline at a rate greater than the oxidation of sulfide leading to a dynamic overlap of both DO and sulfide causing a region of incomplete oxidation. In this region numerous alternate pathways for sulfide oxidation occur and lead to the production of elemental sulfur, polysulfides, and thiosulfate among other species which are stable at different positions in the water column. These analytes take part in a complex cycling of sulfur and iron across the chemocline that is influenced by many different factors including biotic and abiotic processes (Fig.20).

Aside from redox and kinetic factors affecting the vertical distribution of analytes, the measuring process itself had a large impact. The sampler affected the chemocline by causing eddy diffusion and entraining water from above and below the sampling port through addvecitve flow. Because of this species had different distribution patterns when measured with the sampler. Fortunately the electrodes mounted to the sampler play little or not part in the disruption of the sampling process, allowing them to provide a direct measurement of the disruption to the system from using a sampler to draw water. As seen in Figure 16 there is no numeric operation that can be performed to accurately relate the shift of analytes between the two measurements, only a qualitative relationship between the two can be acheived. The reason why the profiles mimic each other is because of the nature of the analytes being measured. Sulfide measured while the sampler is engaged is detected much earlier and increases to a maximum much quicker because the sampler is disrupting the stratification of the water column across the chemocline. When this happens, species that are diffusing from a high production source like sulfide have the physical barrier of the stratification taken away. The same would be true for DO reading taken with the sampler i.e. DO would be present at a greater depth. For analytes like ferrous iron, sulfite, thiosulfate, etc. the complete opposite occurs. These analytes are produced within a particular stable part of the water column across the chemocline. In their case the stratification actually helps protect them. Therefore when the chemocline is distrurbed by the sampler, more DO is allowed to mix with analytes that are already at realatively low concentratonis compared to sulfide. This is what causes the profiles with the sampler for ferrous iron and thiosulfate to have lower

maximum concentrations at the same points as the measurement without the sampler. Disruption of the water column causes detection of these analytes to occur at greater depth and drop below the detection limit at a shallower depth. Knowing the basic relationship between the two will allow for better constraints to be put on measurements with the sampler. Unfortunately, the actual mechanics of advective flow caused by the sampler in conjunction with its shape and how much disruption in the water column occurs from it are far to complex to be completely elucidated. The extent of disruption to the water column will rely not only on the properties of the sampler and pump rate but also on the tides, water temperature, currents, winds and many other factors at the time of sampling.

4.1.1 Vertical distribution of iron across the OATZ

Chemical speciation and distribution of iron is governed by the redox transitions within the OATZ. The dominant trend observed is a maximum of iron at the redox boundary before the system starts to become sulfidic, followed by a decline in the amount of dissolved as well as particulate iron in the system (O'Sullivan, 1997; Simmons 2004). However, in the upper layer of the water column where there is still oxygen, a majority of the iron should be in the (+3) valence state as particulate iron in the form of iron oxyhydroxides and colloids, dissolved iron would be complexed as iron hydroxides such as $Fe(OH)_4^-$ or $Fe(OH)_2^+$ as well as a number of Fe(III)-organic complexes. Smaller concentrations of Fe (II) are found in oxygenated parts of the water column above the OATZ and could have originated from a number of sources. Major sources could be from the turbulent diffusion of Fe (II) from the maximum, microbial reduction of Fe(III),

or photochemical reduction of Fe(III) (O'Sullivan et al., 1997). Because of the high levels of organic matter found in systems like this, it is quite possible that one of the sources of Fe(II) in oxygenated parts of the water column is from photochemical reduction (Cunningham et al.,1985; Sulzberger et al. 1989; Barbeau et al. 2001). Since microbial reduction of iron in oxygenated surface seawaters has not yet been recorded, and oxidation generally dominates over diffusion, Fe(II) in surface waters is most probably from photochemical reduction.

At the onset of the OATZ iron concentrations start to increase with a maximum located at the bottom of the OATZ where there are low concentrations of dissolved oxygen and sulfide. Though particulate iron was not determined in this study, it is known from previous studies in this system and elsewhere that a large portion of particulate iron (III) will also be present (Bazylinski et al., 2000; Simmons et al., 2004; O'Sullivan et al., 1997). Since iron oxidation will still be happening at low DO concentrations from interactions with organic matter (Liang et al., 1993), Fe (III) minerals (Kostka and Luther, 1994; Luther et al. 1992; Sulzberger et al., 1989), and dissolved iron(III) complexes (Luther et al. 1996), some of the Fe(III) may be ascribed to abiotic oxidation. However, this is a region where there is typically a large microbial population, and there will be a contribution from microbial oxidation of Fe (II) (Oguz et al. 2001; Emerson and Moyer 1997). It is important to note that where there is an appreciable level of Fe (III) there will not be large levels of hydrogen sulfide because Fe(III) is a strong oxidant for reduced sulfide species (Luther et al. 1996).

After crossing into the anoxic zone where DO levels are below the detection limit and sulfide starts to become a major constituent in the water column, ferrous iron is completely removed and the most probable form of iron is as iron sulfide phases (Figs. 18 and 19). Higher concentrations of iron (II) where DO and sulfide overlap (DOSO) are attributed to reductive dissolution of iron (III) oxyhydroxides and results in increased free $Fe^{2+}$, iron sulfide complexes, and a minor amount of precipitation of insoluble iron sulfide minerals due to consumption of sulfide from the DO still present. As the sulfide concentration increases, total iron (composed mainly of Fe (II)) starts to decline, which is most likely due to the precipitation of iron sulfides until there is very little iron left (Figs. 11, 12, 16, 18, 19). While the process of pyritization is probably occurring to some extent as long as sulfide is present, the dramatic drop in iron when dissolvec oxygen drops below the detection limit is most probably from the onset of pyritization through the hydrogen sulfide pathway. One unusual characteristic of this is the apparent increase of DFe (III) in the 2004 data, which has another high in the anoxic region that is far beyond its solubility. The most likely reason for this is that there exists an iron sulfide phase inaccessible to Ferrozine, thereby making the DFe(III) seem higher than it really is, though it should be noted that some Fe(III) may exist due to incomplete reductive dissolution of iron oxyhydroxides and hydroxyl complexes.

4.1.2 Vertical distribution of sulfide, sulfate, and DO

At the top of the chemocline the large drop in DO is mainly the result of consumption from the oxidation of sulfide and to a minor extent that of ferrous iron and iron sulfides. As can be seen from Figure 18, there is a large overlap of both DO and

sulfide, the top of which corresponds to a point in the chemocline where there is a maximum of ferrous iron. The DOSO is unique because it represents one of the few natural regions in a water column where diffusive transport is acting on a timescale shorter than that of the relatively fast reactions of sulfide oxidation and redox reactions involving $Fe^{2+}$ and $Fe^{3+}$.

As the chemocline is further traversed to the midpoint DO, drops below the detection limit and sulfide starts to increase exponentially. This transition marks a region where the diffusive transport of sulfide is high enough to overwhelm that of DO allowing for the complete consumption of DO through the oxidation of sulfide. It is also at this depth that there is most likely a large contribution to sulfide production through microbially mediated reduction of sulfate, though it should be noted that sulfate reduction is happening throughout the anoxic region of the water column:

$$2H^+ + SO_4^{2-} + 2(CH_2O) = 2CO_2 + H_2S + 2H_2O \qquad (15)$$

As a result of this process there may not be a completely linear mixing curve to describe the total sulfate in the system. However, even if all the hydrogen sulfide in the system were a result of the reduction of sulfate present from the seawater contribution to the system via conservative mixing, it would not change the calculated sulfate contribution by more than 10 %, based on the measured sulfide concentrations.

As a result of the depletion of DO through the oxidation of sulfide, the sulfide is left free to interact with ferrous iron to form different iron sulfide phases. One such iron sulfide is:

$$Fe^{2+} + HS^- = FeS + H^+ \qquad (16)$$

The creation of this particular specie (either as a precipitate or an aqueous complex) might be able to lower the pH of the system. Therefore it could be the cause of the pH drop that occured as DO and $Fe^{2+}$ decreased and explain the 0.5 drop in pH that occurred when DO was ccompletely depleted.

4.1.3 Vertical distribution of incompletely oxidized species

Across the DOSO the incomplete oxidation of sulfide is responsible for the creation of species such as elemental sulfur, polythionates, thiosulfate, sulfite, and polysulfides. There are many different mechanisms explaining the production and cycling of sulfides across the chemocline and it is often difficult to ascertain the extent to which microorganisms are participating in the cycling. Thiosulfate has one of the more complex cycles since it has the ability to act as an intermediate between both reduction and oxidation reactions involving different sulfur species. It is also a known product of pyrite oxidation and polysulfide decomposition. Thiosulfate is readily produced from the incomplete oxidation of sulfide:

$$2HS^- + 2O_2 = S_2O_3^{2-} + H_2O \qquad (17)$$

The creation of thiosulfate in this manner takes place across the DOSO from 3.22 to 3.69 m, but there are many other reactions involving thiosulfate across this region of the chemocline. It will also be undergoing disproportionation reactions such as:

$$H^+ + S_2O_3^{2-} = HSO_3^- + S^o \qquad (18)$$

The above reaction favors thiosulfate under alkaline conditions such as those found in marine sediments (Chen and Morris, 1972), but at the circumneutral and slightly acidic pH of this system. it may be another pathway for the removal of thiosulfate and the

production of sulfite. The most important mechanism for production of sulfite across the chemocline will be:

$$HS^- + 1.5\ O_2 = SO_3^{2-} + H^+ \quad (19)$$

These reactions will be occurring throughout the DOSO, but at the bottom where DO drops below the detection limit, sulfite and thiosulfate can be reduced to sulfide by any reductant that would normally be reducing sulfate. In Salt Pond one way this may be happening is through the formation of iron monosulfide from ferrous iron and sulfide. This is subsequently transformed to pyrite through the hydrogen sulfide pathway producing hydrogen gas that can then reduce either sulfite or thiosulfate to sulfide:

$$8\ FeS + 8\ H_2S = 8\ FeS_2 + 8\ H_2 \quad (20)$$

$$8\ H_2 + 2\ S_2O_3^{2-} = 4\ HS^- + 6\ H_2O \quad (21)$$

At the top of the chemocline these species are oxidized to sulfate, though thiosulfate needs catalyst such as pyrite before $O_2$ (aq) can oxidize it. With this in mind the oxidation of thiosulfate is probably happening through two different reactions – one involving particulate pyrite that has been transported to the upper part of the chemocline and acts as a catalyst for oxidation and the other involving oxidation by ferric iron which will be in abundance toward the top of the chemocline as iron oxyhydroxides undergo reductive dissolution and ferric iron is able to diffuse across the top of the chemocline.

Across the DOSO elemental sulfur is produced either as $S_8$ rings or simply as an aggregate of elemental sulfur ($S^o$).

$$2\ HS^- + O_2 = 0.25\ S_8 + 2OH^- \quad (22)$$

The production of elemental sulfur has many consequences including facilitating polysulfide production:

$$HS^- + 0.5\ O_2 = S^o + OH^- \quad (23)$$

$$HS^- + (n\text{-}1)\ S^o = S_n^{2-} + H^+ \quad (24)$$

One of the more complex mechanisms for polysulfide production is:

$$H_2S + Fe^{3+} = H_2S^{\bullet +} + Fe^{2+} \quad (25)$$

$$FeS + Fe^{3+} + 2\ H^+ = 2Fe^{2+} + H_2S \quad (26)$$

$$H_2S^{\bullet +} + H_2O = H_3O^+ + HS^{\bullet} \quad (27)$$

$$2\ HS^{\bullet} = 2\ H_2S_2 \quad (28)$$

This reaction may continue cycling as:

$$H_2S_2 + Fe^{3+} = H_2S_2^{\bullet +} + Fe^{2+} \quad (29)$$

or

$$H_2S_2 + HS^{\bullet} = H_2S + HS_2^{\bullet} \quad (30)$$

(Schippers and Sand 1998)

Polysulfides and elemental sulfur are able to react with each other, sulfide, sulfite, thiosulfate, iron monosulfide, pyrite, and other iron species through different pyrite pathways as well as a multitude of redox cycles across different parts of the chemocline. These incompletely oxidized species form complex cycles where products and reactants are constantly replenished through the disequilibrium associated with the chemocline and often times there are large microbial communities associated with them.

4.2 Speciation and calculations from GWB REACT

Speciation of iron across the chemocline is governed by many factors including $E_H$ and the presence or absence of sulfide. Toward the top to the chemocline where sulfide is absent, iron is mainly in the form of ferrous iron, comprising over 70% of the available iron in the system at these depths. Sulfate is the major form of sulfur, with only a very small amount predicted to be in the form of ferrous sulfate. Through the DOSO however there is a drastic change in the speciation of iron and sulfur. As sulfide becomes a major component of the system iron is mainly in the form of different iron sulfides, many of which are precursor to pyrite in some way depending on the pathway examined. Sulfate is still the major constituent of sulfur in the system, but the high concentration of sulfide, the majority of which is not complexed, provides a very important redox endmember for sulfur at this point in the chemocline where many of the fore mentioned reactions are occurring. Toward the bottom of the chemocline $Fe_2HS^{3+}$ shifts from being predicted as the dominant species to being one of the more minor ones with $FeHS^+$ and $Fe(HS)_2$ being the two most dominant complexes while there is still iron present in the water column. Past this point though, in the anoxic hypolimnion there is no detection of soluble iron.

Despite the lack of data for dissolved organic carbon (DOC) at these depths, some basic assumptions can still be made concerning its contribution to complexation. O'Sullivan (1997) was able to propose constraints on the importance of organic Fe (II) complexes in the anoxic waters of Pettaquamscutt Estuary (Pettaquamscutt, RI), a system very similar to Salt Pond. It was seen that with a DOC content of 3.9 mg $l^{-1}$ and assuming the carboxylic acid groups are responsible for the complexation of Fe (II) and

similar to that of glutamate (log K = 4.6), less than 0.01% of the Fe(II) would be complexed by DOC (Liang et al. 1993).Landing and Lewis (1991) noted that it is possible that Fe(II) can be complexed by thiol containing compounds present in anoxic waters. Thiol containing compounds have been measured in anoxic waters with concentrations up to several hundred nanomolar (Luther, et al. 1991). Calculations from O'Sullivan in Pettaquamscutt using cysteine as a model ligand for complexation and a log K=12.2 found that less than 0.001% of the dissolved Fe(II) would be complexed by thiols.

4.2.1 Chemical speciation of iron

Metal sulfides play a key role in biogeochemical cycling in marine systems because of their control on complexation, solubility and bioavailability of nutrients. It has even been noticed that trace levels of hydrogen sulfide can be transported to oxygenated surface waters due to enhanced stabilization by trace metal complexes (Cuttter and Krahforst, 1988; Luther and Tsamakis, 1989). There also exists considerable evidence that iron sulfide complexes are important precursors in iron sulfide precipitation (Rickard, 1989; Rickard and Luther III, 1997). Due to the presence of high iron and sulfide concentrations within the chemocline and below it, complexation calculations were performed to analyze the speciation and precipitation of iron sulfides. In the upper region of the chemocline, where sulfide is absent the majority of the iron was in the free ion state with no accompanying complexes to bind to it. This would mean there is a large reserve of free iron (II) with nothing sequestering it from use, however it has been shown that typically more than 99% of iron in seawater is complexed to numerous,

unhcaracterized organic ligands (Witter et. al., 2000, Rue and Bruland, 1995) whose influences on iron speciation can not be determined through modeling at this time.

As can be seen from Figures 21 through 26, as soon as there are appreciable levels of sulfide in the water column, the dominant iron species are $Fe_2HS^{3+}$, $Fe(HS)_2$ , and $FeHS^+$. This is important since $FeHS^+$ has been suggested as a precursor to pyrite formation and $Fe(HS)_2$ has been suggested as a precursor to the formation of amorphous FeS (Luther and Ferdelman, 1993; Rickard and Luther, 1997). Other sulfide and iron sulfide complexes such as polysulfides ($S_8$ and $S_x^{2-}$) and neutral polynuclear $Fe_2(HS)_4$ have also been identified as potential agents in pyritization (Rickard and Luther, 1997; Davison et al. 1998). It should be noted that there are other possible complexes involving thiosulfate and polysulfides that GWB was not able to account for because the thermodynamic data were not included in the database. One such complex would be that of iron pentasulfide. Iron pentasulfide is of interest because it would easily decompose to iron sulfide and sulfur, both of which are important components in pyritization. The complexation of iron with pentasulfide itself could be a possible mechanism for pyritization as well (Luther, 1991).

During the 2005 sampling period use of a YSI 600 QS and a new database for GWB provided more accurate speciation models. Input files for GWB REACT for 8-11-2004, 9-22-2005 with the sampler, and 9-22-2005 without the sampler can be found in Appendices 1,2, and 3 respectively. Input files for GWB ACT2 for 8-11-2004, 9-22-2005 with the sampler, and 9-22-2005 without the sampler can be found in Appendices 4, 5, and 6 respectively. Only contributing species with molalities greater than 1 nM are

reported on and discussed. Iron (III) complexation below 4.1 m was also excluded from the analysis since the anomalously high readings after the OATZ in the 2004 data are most certainly from the artifact in the FZ method previously mentioned.

One of the original problems with the 2004 sampling period arose in the model when trying to calculate the $E_H$ of the system. The calculation from the iron data did not support the given assumption that total dissolved iron was equal to the sum of the dissolved iron (II) and (III). Conversely, the $E_H$ data from the 2005 sampling period does not support the high concentrations of ferric iron observed in the chemocline and especially not in the sulfidic hypolimnion as seen in the 2004 data. The reason for this artifact of the Ferrozine method is most likely due to the presence of colloidal or aqueous ferrous iron sulfides and/or complexes that the Ferrozine method could not account for in the first step of the method, i.e. the part that calculates the concentration of ferrous iron. On top of this there is bound to be some amount of oxidation happening to the sample no matter how well it is handled. In order to overcome this, a linear approximation representing the change in $E_H$ across the chemocline was created from the 2005 data and applied to the 2004 sampling period data. Calculations using the theoretical $E_H$ of the system at locations where iron was present indicated that an insignificant portion of iron would be in the ferric form. This allowed REACT to perform speciation and complexation calculations assuming that ferrous iron was equivalent to total iron. From there the $E_H$ was used in REACT to calculate the activity of ferric iron from the newly calculated ferrous iron activity.

The 2004 sampling period data used by REACT for model calculations utilized the calculated $E_H$ data in order to obtain reasonable ferric iron speciation and solubility from abiotic processes. Without the $E_H$ data there would be no approximation availible for ferric iron in the system despite the fact that it is known that this particular system has ferric iron present in it, though in very low concentrations when sulfide becomes present. One of the most prominent differences between the 2004 data and the 2005 data are the speciation of iron and sulfide across the middle and bottom of the chemocline. Not only is the concentration of iron in the 2004 sampling period much lower than in the 2005 sampling period, but there was also a greater region of sulfide coexisting with ferrous iron. The fact that this sampling time was earlier in the season than the 2005 sampling period and that there is a large overlap of sulfide and ferrous iron are both indications that this chemocline is not as stratified as the one in 2005 and will have more diffusion and mixing throughout its depth. This would mean the region of disequilibrium is much larger than in the 2005 sampling period. Unfortunately, the equipment being used during the 2004 sampling period was not designed to examine such a system and the measured data does not depict the changes across the chemocline as accurately as in the 2005 data without the sampler. It is important to acknowledge what measurements are missing because the effects to the system and the microorganisms there are quite significant. For instance, the larger the disequilibrium, the more favorable it will be for microorganisms to exploit the redox pathways available to them in the system. The larger overlap also means greater concentrations of partially oxidized sulfides and iron sulfides for

metabolism (such as thiosulfate) and fewer constraints on the type and number of different pyritization processes occurring.

4.2.2 Chemical speciation of sulfur

The speciation of sulfur throughout the system is dominated by sulfate complexes. This is only natural since the system has a direct outlet to the sea and derives the majority of its properties from the water circulated through the pond from the winds and tides that affect it. The sulfate ion is the most prominent of all sulfur species with several related major complexes being formed from the presence of the three cations with the highest concentration in seawater – sodium, magnesium, and calcium respectively. These four analytes collectively represent ~98.8% of all sulfur species in the system. Despite their great abundance, they are of relatively little importance across the chemocline with the exception that many microorganisms use sulfate reduction as a major source of energy.

Sulfides are the second most abundant sulfur species in the system even though they are but a fraction of the total sulfur budget. Ferrous iron and the incomplete oxidation of sulfide from ferric iron and oxygen are the most important species and processes when considering the sulfide/sulfur speciation in this system. The most abundant sulfur species, other than sulfate, are hydrogen sulfide and bisulfide. These two species represent ~94.9% of all sulfide species across the chemocline and even more in the sulfidic hypolimnion. Though the remaining sulfides are a small part of the sulfur budget they have the greatest consequences both biotically and abiotically for the system. As discussed earlier, different incompletely oxidized sulfide species will be present at different regions of the chemocline and will interact with different iron sulfide species. It

should be pointed out that toward the top of the chemocline where DO is present, thiosulfate is one of the major species, but it was unable to be added to the database for calculations by GWB (Figs. 11, 12, 16, 18, 19). Runs using the thermo_minteq _gwb.dat data base to incorporate thiosulfate speciation into the overall results for the system showed that thiosulfate, when present, was primarily in the (-II) form and only formed notable complexes with several of the major cations – sodium, magnesium, and potassium. Typically the fore mentioned comprised ~ 8, 2, and 0.5 % of the thiosulfate budget. Other complexes had concentrations in the nanomolar range or less.

As for the sulfide complexes that were taken into account for the initial runs of GWB, $FeHS^+$ had the highest concentration excluding hydrogen sulfide and bisulfide. All the major complexes and forms of sulfide aside from hydrogen sulfide and bisulfide were different forms of iron sulfide complexes. The extent of polysulfide complexation and the concentration of elemental sulfur were not able to be determined from the voltammetry, so their contribution to the sulfur budget is not accurately known. It is known though that they are quite abundant and that some of the ferrous iron could actually be complexed with polysulfides, mainly in the form of iron pentasulfide. Soluble elemental sulfur will be in the form of $S_8$ rings when present.

4.3 Solubility and predictions from GWB REACT

GWB REACT and ACT2 were used together to depict the solubility and phase transitions occurring through the chemocline. REACT calculations were performed with and without the precipitation of minerals. The trend as the chemocline is traversed is for the most oversaturated mineral phase to switch from hematite to pyrite. This occurs

through other phases as DO decreases and sulfide increases with hematite generally being the most oversaturated phase until sulfide is present, at which time there is a shift to greigite being the most oversaturated phase. As sulfide increases pyrite ultimately becomes the most oversaturated mineral phase in the water column.

Analyzing the 3.58 m data without the sampler from the 2005 sampling period provides a snapshot of some of the processes occurring in the water column at a point where greigite is actually the most oversaturated mineral phase. Calculations from REACT when minerals were allowed to precipitate predicted three minerals to be in equilibrium with the fluid: dolomite, pyrite, and greigite. The original calculations that do not account for mineral precipitation have 8 natural phases oversaturated with respect to the fluid. Even though greigite is the most oversaturated mineral in the water column it is not as thermodynamically stable as pyrite, meaning that even as this phase precipitates out it will be undergoing a continuous process of reduction to the point of pyrrhotite, marcasite, or probably pyrite, which is why the model predicts both phases to be in equilibrium with the fluid after allowing precipitation.

While the predictions from the 2004 sampling period are similar to the 2005 predictions, the transitions are more abrupt (Figs. 27, 28, 29). Concerning the predictions without the precipitation of minerals, the top of the chemocline characterized by hematite being present as the most oversaturated phase with magnetite and goethite being oversaturated as well. However as soon as sulfide is present, pyrite is immediately the most oversaturated phase and it is also the only iron sulfide that is predicted to be oversaturated. This is very different from the 2005 predictions where several iron

sulfides were predicted to be oversaturated. Predictions from REACT that assume mineral precipitation, lack anything but the most thermodynamically stable phase being in equilibrium with the fluid leaving everything else undersaturated. This is also different than the 2005 predictions which, at depth 3.85 m, allowed both greigite and pyrite to be in equilibrium with the fluid after mineral precipitation. Furthermore the 2004 sampling calculations predict hematite to be the only iron oxide to come to equilibrium with the fluid at the top of the chemocline. At every depth where DO was below the detection limit, pyrite is the only phase predicted to be in equilibrium with the fluid. Part of the reason why there is such a discrepancy between the two sampling periods is the low concentration of iron detected across the chemocline. The effect of this is to lower the ion activity product and therefore lower the saturation index of iron sulfides and oxides present in the water column. This in turn forces the most thermodynamically stable and kinetically favorable phase to be predicted as the most oversaturated phase and it also occludes intermediate or metastable phases that may be partially oxidized.

One problem concerning these predictions is the resolution of the data and the manner in which it was collected. The resolution for 2005 is nearly twice that of 2004 (~10 cm per reading versus ~20 cm) and the 2005 sampling period did not use the sampler to obtain ferrous iron measurements. This means the iron measurements for the 2005 period are literally from discreet depths in the water column, while data obtained with the sampler (like that in the 2004 sampling period) has already been shown to have a considerable amount of error due to advective flow and disruption of the chemocline. If the same techniques and with the same resolution were applied to the 2004 sampling

period it is quite probable that a more gradual transition from the most oxidized and thermodynamically stable mineral phase to the most reduced and thermodynamically stable mineral phase will occur across the chemocline from top to bottom. Furthermore, if the resolution were even higher for the 2005 period, phases such as goethite, magnetite, and mackinawite may also have been predicted as being the most oversaturated phases at depths corresponding to their oxidation state in the water column. It may be summed up that whenever there are very low concentrations of DO with a significant concentration of both dissolved ferrous iron and sulfide at low $E_H$ values and circumneutral pH, pyrite will be the most thermodynamically stable mineral phase with greigite, mackinawite, and other iron sulfides having the potential to serve as metastable transition phases.

4.3.1 Controls on the solubility of iron and sulfide

In systems where there are high concentrations of iron and sulfide, it is quite common for the solubility of different iron sulfides to be exceeded. Due to the low level of kinetic inhibition, amorphous FeS should be one of the first precipitates to form despite having a $pK_{sp}$ close to 3.0 (Emerson et al. 1983). Ferrous iron and sulfide should remain in the water column even if large quantities of amorphous FeS are precipitating because of its relative solubility. However there is a large possibility this is not the only phase precipitating out. Other phases may include, but are not limited to, mackinawite, marcasite, greigite, pyrrhotite, and pyrite.

Analysis of the data dictate that the concentration of DFe (II) in the water column under conditions of high sulfide is a function of the precipitation of different iron(II) sulfide phases. From Figure 30, which shows the thermodynamically stable field for the

depth of 3.05 m in the water column during the 2004 sampling period, it can be seen that before there is any sulfide present magnetite is the most oversaturated mineral in the water column. The converse is also true concerning greigite in Figure 31. It should be noted that goethite, hematite and pyrite are suppressed in the diagram so the meta-stable mixed valence phase magnetite is not occluded. Although these minerals are not necesarrily kinetically inhibited and are no doubt also present with the partially oxidized intermediates, the purpose of the diagrams was to show the stability field boundaries and limitations of the intermediary iron and sulfide phases that will be present as iron sulfides are oxidized to goethite or hematite or vice versa. This is better seen in the 2005 phase diagrams which have tighter depth resolution. While magnetite should be stable through the upper part of the chemocline, greigite should be stable under reducing conditions where there is sufficient $S^{2-}$ (Demitrack, 1985). Also, under small partial pressures of oxygen in solutions saturated with hydrogen sulfide greigite was found to precipitate (Berner, 1964). This area can be found from ~3.05 -3.4 m for 2004 sampling period and is marked by the oversaturation in Figure 27 and the large stability field for greigite in Figure 31. The mixed valence iron oxide, magnetite, should be forming around ~2.9-3.2 m in the water column whereby it will precipitate out of the water column falling through the anoxic zone. Upon entering this zone it will be reduced and possibly dissolved before reprecipitating as an iron sulfide. In this zone of iron sulfide precipitation, the precipitation of amorphous iron sulfide typically occurs first followed by an aging process leading to mackinawite (Rickard, 1989). In water columns without oxidizing

agents, mackinawite has been suggested as the first crystalline product (Rickard, 1969; Morse et al, 1987; Wang and Morse, 1996).

This is important because mackinawite can be a precursor to pyrite formation via a greigite intermediary. Because this reducing system is not devoid of any other reactant than hydrogen sulfide it means mackinawite is not a stable form of iron sulfide and that formation of pyrite is favored (Benning et al., 2000). Examination of the phase diagrams and saturation indices of the 2005 sampling period (Figs. 27 - 39) clearly show that not only is mackinawite not a stable phase, but neither is amorphous iron sulfide. This means any mackinawite present in the system will be converted to pyrite, which will likely happen via the mixed valence phase greigite. Mackinawite is most likely going to be undersaturated because it is continually being redissolved or changed into a more stable phase such as pyrrhotite or greigite. Conversions of this nature indicate that there are multiple mechanisms at work to suppress mackinawite through the pyritization process in the water column. Despite such a low saturation state of the most kinetically favored precipitates, they are continually produced from fresh supplies of reductively remobilized Fe (II) and S (-II) in the anoxic part of the water column. Voltammetric scans across the chemocline indicate that aqueous iron sulfide phases, i.e. the precursors to amorphous iron sulfide and mackinawite, are in great abundance throughout the upper water column as well as the top layer of the chemocline. Since there are removal processes working simultaneously with production, it is as if a pseudo-steady state is maintained (Davison et al., 1998). Therefore the profiles in the saturation states of different minerals should be constant throughout the summer.

4.4 Pyritization and formation of metastable iron sulfide phases

Pyritization is one of the most important processes occurring in the water column because it controls the biogeochemical cycling of iron and sulfide by sequestering the elements in a stable phase to undergo burial. In part, pyritization played a role in keeping the oxygen content of the atmosphere at a relatively constant level during the Phanerozoic by changes in the reduced carbon and sulfur reservoirs such as organic carbon and pyrite and oxidized reservoirs of carbon and sulfur in the form of carbonate and sulfate (Berner and Raiswel, 1983 and Holland, 1984). The effects of pyrite and its contribution to the biogeochemical cycling of carbon, iron and sulfur can be seen in the geologic record through the actions of sulfate reducing bacteria. These bacteria had a large impact on the global sulfur and oxygen cycles, which have been recorded in the isotopic data of pyrite in the Archean and Proterozoic sedimentary rocks. Along with this Keller et. al. (1994) have suggested that it is also possible that the redox energy associated with pyrite formation aided in the formation of amide bonds which was a vital step in initiating the origin of life.

Despite the importance of redox reactions involving pyrite in biogeochemial cycling, there are still many questions as to which mechanisms are the most viable for the formation of pyrite in different systems and to what extent different intermediates contribute. The most abundant type of pyrite in natural systems is that of framboidal pyrite, but there is more than one way to create this end product, though usually only one pyritization pathway in any one body of water is the major contributor. Also the greigite intermediate that may form through some pathways is only created under a very

particular set of conditions, specifically those where there is ferrous iron, sulfide, and an oxidant at a relatively low concentration. Under the right circumstances greigite may be stable for an indefinite period of time, however it will always be metastable with respect to pyrite, marcasite, or pyrrhotite (Berner, 1967, Wada, 1977, Dekkers and Schoonen, 1994). Some of the known mechanisms for pyritization include FeS oxidation by:

The polysulfide pathway (Luther, 1991; Rickard, 1975)

$$FeS(s) + S^0(s) = FeS_2(s) \quad (31)$$

$$FeS(s) + S_n^{2-} = FeS_2(s) + S_{n-1}^{2-} \quad (32)$$

The Ferrous iron loss pathway (Wilkin and Barnes, 1996)

$$2FeS(s) + 0.5H_2O + 0.75O_2 = FeS_2(s) + FeOOH(s) \quad (33)$$

The hydrogen sulfide pathway (Drobner et al., 1990; Rickard, 1997; Rickard and Luther, 1997)

$$FeS(aq) + H_2S(aq) = FeS_2(s) + H_2 \quad (34)$$

It is through intermediaries from incomplete oxidation of FeS to pyrite in these reactions that greigite may be formed. Note that for pyritization, bisulfide cannot be an electron acceptor in a reaction with FeS because its lowest unoccupied molecular orbital (LUMO) has a high positive value. However, it may react with $FeSH^+$ to form pyrite, which is a probable pathway to be occurring in Salt Pond considering $FeSH^+$ is one of the major aqueous complexes of iron (Rickard and Luther III, 1997).

Pyritization should be occurring throughout the chemocline in Salt Pond which would make it one of the few well studied water bodies where pyritization is occurring in the water column itself as opposed to the sediments. Other well studied systems where framboidal pyrite formation has been observed within the water column at the OATZ

include the Black Sea, Framvaren Fjord, and Pettaquamscutt estuary (Murramoto et al., 1991, Skei, 1988, and Wilkin, 1995). Salt Pond mirrors the conditions present at these larger water bodies except on a smaller scale. Considering the proximity of Salt Pond to scientific laboratories and its relatively small surface area and shallow depth, it would be the smallest water system where pyritization is occurring within the water column and also one of the easiest to study.

4.4.1 Pyritization through the suboxic region of the chemocline

The upper and middle region of the chemocline, i.e. the DOSO from ~3.5 – 3.7 m is a candidate for pyritization to be occurring through all three of the pathways previously mentioned. In the DOSO iron monosulfide, elemental sulfur, and polysulfide are all present in relatively large quantities along with DO. Also the pH is between ~6.7 and 7.3, indicating that the concentrations of bisulfide and hydrogen sulfide are nearly equivalent. This means every component for each pathway is present here and none of them necessarily preclude the occurrence of any of the others. Based on kinetic experiments by Rickard and Luther (1996), it would seem that the hydrogen sulfide pathway would be responsible for the majority of the pyrite formed. The rapidity of pyritization via this process may be responsible for the quantitative consumption of ferrous iron at the bottom of the DOSO and why iron monosulfide is basically absent after this point as well. The polysulfide pathway is the other mechanism competing with the hydrogen sulfide pathway and is of great importance through the DOSO because it will be the one responsible for the production of other iron sulfide species such as mackinawite and greigite.

will be the one responsible for the production of other iron sulfide species such as mackinawite and greigite.

Greigite is a possible intermediary in the pyritization process and is promoted by weakly reducing conditions where there are weak oxidants present to react with mackinawite and form greigite (Wilken and Barnes, 1997). For this reason it seems to be promoted at low oxygen levels and where there is zero valence sulfur present. Some of the more familiar equations displaying this are:

Addition of elemental sulfur (Berner, 1967)

$$3FeS\ (s) + S^0 = Fe_3S_4 \qquad (35)$$

This reaction does not require the iron monosulfide specie to reside in a highly reducing zone where it would immediately precipitate out as pyrite as in the previous reactions. The above reaction is potentially occurring at the chemocline where the iron maximum is located. As in the ferrous loss pathway, it is quite possible to form stable iron sulfide phases other than pyrite in the presence of oxygen. The sulfur addition pathway is an example of such a pathway (Berner, 1970; Sweeney and Kaplan, 1973).

$$3\ FeS\ (s) + HS^- + 0.5\ O_2 + H^+ = Fe_3S_4 + H_2O \qquad (36)$$

The above reaction is one that has the potential to dominate other reactions in the DOSO. Due to the nature of the equations governing greigite formation, it is easy to see that all the required elements for this process are available across the OATZ. After the formation of greigite, it should be metastable under the conditions of the water column as it rains down to the underlying sediments. There, conditions will be more favorable to expedite the process of pyritization, leading to removal of greigite from the system. This is in

good accordance with the voltammetry scans which show higher concentrations of FeS in the DOSO region of the chemocline. At the bottom of the chemocline and into the hypolimnion FeS is quantitatively removed along with ferrous iron.

4.5 Consequences for microbial populations across the OATZ

A stable OATZ in a water column characterized by a narrow zone where sulfide and DO coexist leading to diverse environmental gradients that various microbes can exploit. The chemocline is generally characterized by a large population of microbes, including MB, that seem to have two major regions of inhabitance, one at the top of the OATZ and one toward the bottom of the OATZ near the annoxic hypolimnion where sulfide starts to become detectable (Bazylinski, et al. 2000; Simmons et al. 2004). This is displayed quite well in Figure 40 from Simmons et al. (2004) and can be realized in Figures 41 and 42 showing data on magnetotactic protists and magnetotactic bacteria where the maximum population is at the same depth where the voltammetric scans yielded the highest peaks for ferrous iron. This might have something to do with their unique biochemistry and the fact that they need large quantities of iron. It is also typical for them to produce BMPs representative of highly oversaturated thermodynamically metastable/stable phases at the zone they inhabit in the OATZ. At the top of the chemocline MB primarily produce BMPs containing magnetite, a mixed valence iron oxide phase that is oversaturated in this part of the water column. This may be due to the appearance of both ferrous and ferric iron in the presence of oxygen. A similar situation is taking place below this point in the water column where greigite, another

thermodynamically metastable mixed valence phase, is also more oversaturated than many other iron sulfides.

4.5.1 Free energy calculations

At the top of the OATZ where Fe (II) and particulate iron (mainly in the (III) valence state) are present there is a large potential for Fe(II) oxidation via the following reaction at circumneutral pH:

$4Fe^{2+} + O_2\,(aq) + 10\,H_2O = 4Fe(OH)_3\,(s) + 8\,H^+ \quad \Delta G^o = -82.21$ kJ/mol $O_2(aq)$ (37)

A number of different bacteria, such as *Gallionella, Sphaerotilus-leptothrix*, and some organisms from the group γ-Proteobacteria have been recorded as taking advantage of this reaction across redox interfacial environments where diffusion limited transport leads to low DO (Emerson and Moyer, 1997; Emerson, 2000, 2001; Roden et al. unpublished). The consequences of bacteria utilizing this type of mechanism would be a slight drop in pH due to the production of 8 $H^+$ during the oxidation of Fe (II) and an increase in particulate Fe (III) in the form of ferrihydrite. This reaction is examined here because both of those trends occur over both sampling periods within the water column at the OATZ where the first influx of microbial populations is located. This would lead to a cycling of Fe as it is continually oxidized to ferrihydrite and then sinks to undergo reductive dissolution. Using the familiar expression:

$$\Delta G = RT \ln (Q/K) = \Delta G^o + RT \ln Q \qquad (38)$$

several different depths can be analyzed for the proficiency of this type of reaction. In order to do this the profile obtained from the 2005 sampling period without the sampler

will be used because it is a more complete and accurate profile. Using equation 38 the following expression is derived:

$$8\log\{H^+\} - \log\{O_2\} - 4\log\{Fe^{2+}\} = \log Q \quad (39)$$

using the substitution $-\log\{H^+\} = pH$, or rather $\log\{H^+\} = -pH$ (40)

$$-8\,pH - \log\{O_2\} - 4\log\{Fe^{2+}\} = \log Q \quad (39a)$$

Using the equilibrium state model values generated by REACT, log Q and subsequently the free energy of the reaction occurring at this part of the chemocline can be investigated. The values of concern generated by REACT for the depth of 3.26 m, the first depth at which ferrous iron is detected, are:

$pH = 7.29$ $\log\{Fe^{2+}\} = -5.4684$ $\log\{O_2\} = -49.1273$

where log {O2} is calculated from the $E_H$ data. It should be noted that the DO calculated is an unrealistic number that is an artifact from GWB using the $E_H$ of the system to calculate ferric iron species and concentrations. The software only allows the system to be governed by one redox varibable, i.e. $E_H$, pe, or DO. Since ferrous iron is out of redox equilibrium with DO across the oxygenated part of the chemocline it was necessary to input $E_H$ as the redox variable for GWB. This allows GWB to ignore equilibrium with DO so speciation calculations relevant to the actual state of the system can be performed. With this in mind it is necessary to use the original measured data for the DO (36.56 µmol/l) of the system in the free energy calculations. From this it follows that:

$$-8\,(7.29) - (-4.437) - -4(5.468) = \log Q$$

$$\text{or } \log Q = -32.011 \text{ for 1 mol } O_2\,(aq)$$

Thus substituting this value into a modified form of equation 39

$\Delta G = RT\ 2.303 \log (Q/K) = \Delta G^o + RT\ 2.303 \log Q$ (41)

$\Delta G = -82.21 + -182.75 = -264.96$ kJ/mol $O_2$ (aq)

This type of calculation can be done through the chemocline to approximate the energy available from the geochemistry of the system. Several other reactions were also analyzed in the context of energy availibility in the upper portion of the chemocline. These included the formation of free ferric iron, ferrihydrite, hematite, and magnetite (Fig.43). While all these reactions yeild sufficient amounts of energy based on the 20 kJ/mol minimum proposed by Schink (1997), the formation of magnitite is of particular interest because it has the second highest yeild, which is due to its very negative free energy of formation, and is very close to hematite in free energy. Formation of magnetite also had the highest standard free energy of any reaction examined, -1034.54 kJ/mol $O_2$ (aq) and routinely had free energies of ~-360-300 kJ/mol $O_2$ (aq) throughout the OATZ.

The oxidation of thiosulfate to sulfate is a viable reaction for microbial growth between the depths of 3.26 m and 3.65 m. Bacteria can utilize this reaction in the water column across this depth, but they may be competing with abiotic oxidation because pyrite and other iron sulfides are present from diffusion and intermediates formed from the polysulfide pathway.

$0.5\ S_2O_3^{2-} + O_2\ (aq) + 0.5\ H_2O = SO_4^{2-} + H^+ \quad \Delta G^o = -419.33$ kJ/mol $O_2$ (aq) (42)

At 3.41 m there is a maximum of free energy for this reaction corresponding to over -444 kJ/mol $O_2$ (aq) (Fig. 43). This is more free energy than any other reaction except for the oxidation of ferrous iron to ferric iron. At this depth oxidation of sulfite could also be occuring if thiosulfate disproportionation to elemental sulur and sulfite is happening.

Sulfite is another favorable metabalite that is oxidized very easily and has a high Gibbs standard free energy associted with it:

$2\ SO_3^{2-} + O_2\ (aq) = 2\ SO_4^{2-}$ $\Delta G^o = -528.1$ kJ/mol $O_2$ (aq) (43)

Toward the bottom of the OATZ, where small amounts of DO are still present and sulfide becomes measurable, oxidation of sulfide will occur according to the following:

$0.5\ HS^- + O_2\ (aq) = 0.5\ SO_4^{2-} + 0.5\ H^+$ $\Delta G^o = -394.90$ kJ/mol $O_2$ (aq) (44)

But incomplete oxidation to thiosulfate will be more prominent:

$HS^- + O_2\ (aq) = 0.5\ S_2O_3^{2-} + 0.5\ H_2O$ $\Delta G^o = -370.52$ kJ/mol $O_2$ (aq) (45)

Both of these reactions occur between 3.58 and 3.65 m where sulfide first becomes detectable while there is still DO present. For the complete oxidation of sulfide to sulfate $\Delta G = -384$ and -380 kJ/mol $O_2$ (aq) at 3.58 and 3.65 m. respectively. According to Oguz et al. (2001) who ascribed a DO concentration of 2 µM as the lower limit at which sulfide oxidation can efficiently take place, the overlap between DO and sulfide within the OATZ is well within the limits for this type of reaction to be taking place efficiently for microbial exploitation. DO does not drop below this value until 3.698 m and at 3.649 m DO is still at 4.37 µM. Free energy from oxidation of sulfide to thiosulfate rivals that of complete oxidation and is -340 and -370 kJ/mol $O_2$ (aq) at 3.58 and 3.65 m respectively .

The 7.01 cm layer between 3.58 and 3.65 m is a very important part of the chemocline because this is the only depth where ferrous iron, DO, and sulfide are all present at the same time (Figs. 18 and 19). It is also at this region in the chemocline that greigite, the most energetic of the mineral forming reactions, is predicted to be oversaturated. One reaction for the formation greigite is:

$6\ Fe^{2+} + 8\ HS^- + O_2\ (aq) = 2\ Greigite + 4\ H^+ + 2\ H_2O \quad \log K = 124.0212 \quad (46)$

Other than the formation of free ferric iron and thiosulfate oxidation, greigite formation is the most energetic process occuring across the chemocline (Fig. 43). Greigite formation requires sulfide to be present where there are low concentrations of oxidizing species. After formation in a weakly oxidizing region of the water column, greigite may be metastable for an indefinate period of time and may never even transform to pyrite if favorable conditions persist. This small layer of the chemocline is prone to facilitating complex oxidation processes involving elemental sulfur, polysulfides, and iron sulfides that are most likely being utilized by bacteria (Zopfi et al., 2001). For example it is known that FeS can be a growth substrate for $Fe^{2+}$ or $HS^-$ oxidizing bacteria and $NO_3^-$ reducing bacteria.

Below the OATZ, where DO is no longer detectable, anoxygenic phototrophic bacteria can oxidize $HS^-$, $Mn^{2+}$, and $Fe^{2+}$ in association with phototrophic reduction of $CO_2$ to form organic matter. These are important reactions because anoxygenated photosynthesis is also considered a mechanism for OATZ formation (Oguz et al. 2001). Anaerobic oxidation reactions favorable under these environmental conditions are:

$5\ Fe^{2+} + NO_3^- + 6\ H^+ = 5\ Fe^{3+} + .5\ N_2(aq) + 3H_2O \quad \Delta G^o = -244\ kJ/mol\ NO_3^- \quad (47)$

$HS^- + NO_3^- + H^+ + H_2O = SO_4^{2-} + NH^{4+} \quad \Delta G^o = -487\ kJ/mol\ NO_3^- \quad (48)$

With such a diversity of reactions viable for metabolism across the OATZ and into the sulfidic hypolimnion, there is sure to be a diversity of microorganisms utilizing the steep gradients and multiple pathways of oxidation and reduction to yield energy for

growth. As of yet the impact of these different bacteria and the pathways they are using have not been fully elucidated. This is especially true for the MB.

4.5.2 Limitations on microorganisms by analyte distribution and free energy

Often times one of the main sustaining factors for the creation of chemical gradients, such as those across the chemocline, is the diffusivity of analytes and theyr ability to remain constant so a relatively stratified system has the potential to develop and persist throughout the summer. The significance of this lies in the prospect for such systems to develop permanent zones of incomplete oxidation where analytes are continually cycling from reduced to oxidized states. This can happen at the top of the chemocline where ferric iron is undergoing reductive dissolution, or at the (DOSO) where incomplete oxidation of sulfide leads to intermediates such as thiosulfate, polysulfides, and sulfite.

Oxygen concentrations directly impact the ability of microbes to exploit redox reactions for metabolic needs. At high DO levels the kinetics of iron oxidation are so fast that microbes do not have time to utilize the analytes. When DO levels approach zero, the rate of iron oxidation drops dramatically, however the amount of energy from a thermodynamic point of view has not changed very much. This is illustrated in Figure 44 where the half-life of iron and the free energy for equation 37 are plotted against the concentration of DO. The rate equation used to construct the figure is:

$$\frac{-dFe(II)}{dt} = K*[Fe(II)]*[O_2(aq)]*[OH^-]^2 \qquad (49)$$

where K = 1.5 *10^16 $l^{-3}$ $mol^{-3}$ $min^{-3}$

Fixing the concentratons of iron and pH allow for a first order approximation of the kinetics. This is not too different than what is found in Salt Pond because of the way it reaches a state of psuedo equilibrium during the summer. This means concentrations of analytes across the chemocline will remain unchanged from one sampling period to the next. If the measusred values for DO, ferrous iron, and pH are substituted into equation 49 to find the rate of abiotic iron oxidation it is also calculating the minimum rate at which iron reduction is happening in order to keep the system in a metastable state. This is considered the minimum addition rate because across these depths microorganisms will be utilzing large quantities of iron relative to abiotic reactions meaning that if iron were only replaced at the rates of abiotic oxidation it would very quickly become devoid of iron.

The distribution of ferrous iron, DO, sulfide and incompletely oxidized species across the chemocline create two regions of favorable energetics for microorganisms. The first region is located at the top of the chemocline from 3.26 to 3.5 m and is devoid of sulfide. This is also the region where iron oxides such as magnetite are oversaturated. The second region extends from 3.5 to 3.7m and corresponds to the region where both sulfide and DO overlap as well as where the largest concentrations of ferrous iron and thiosulfate are present. The only difference in the potential energy there for bacteria is the additional reaction pathways availible with the presence of sulfide in the second region. The upper region will be characterized by microorganisms obtaining energy through iron oxidation and the oxidation of thiosulfate to sulfate while the deeper region will be characterized by oxidation of sulfide or maybe even formation of iron sulfides.

The upper region of the chemocline lacking sulfide is where magnetite is being formed by MB and likely precipitating out abiotically as well. Before it was shown that up to ~-360 kJ/mol $O_2$ (aq) can be obtained through the formation of magnetite in this system. Assuming 90% of the DO can be utilized by bacteria for the fomration of magnetite, then at the top of the chemocline ~-12 J/l are availible for microbes to utilize metabolically, which translates into 78.8 µg dry wt/l of primary biomass. If the bacteria in question at this depth are primarily MB (~3% dry wt iron) then 2.4 µg/l of iron are sequestured in living MB. Taking the average of the discrete depth calculations one can make an approximation of the maximum biomasss across the 3.26 and 3.5 m part of the chemocline. If it is assumed that only 50% of Salt Pond is deep enough for a chemocline to form, this translates into 1.44 kg dry wt biomass (or 65.5 g C of biomass) and 43.2 g iron (in the case of MB). Cycling of nutrients for this part of the system can be estimated based on MB having a life span of approxmately one day. Most of the nutrients will be recycled very quickly, however the iron sequestered by the MB may be permenantly removed from the system through burial. This occurs because the organelles containing the iron phases are resistant to degradation.

An analogous process is occuring at the DOSO where there are many species taking part in reactions of microbial relevance. Similarly, greigite can be fulfilling the role of a favorable energetic reaction in the lower layer. It should be noted that magnetite in the upper layer and greigite in the lower layer are not only some of the most energetic of the iron mineral forming there processes, but they are also the minerals being used by MB at those respective zones in the water column. Using the same thermodynamic

assumptions for greigite that were made for magnetite, it was calculated that there was -3.75 J/l availible to bacteria in this region, which translates to a primary biomass of 24.6 µg/l. This yeilds a primary production of 611 g dry wt for this portion of the chemocline (or 27.8 g C of biomass) and if the majority of the bacteria there are MB then there would be 18.3 g iron sequestered in the living MB.

The solubility indices as well as the phase stability diagrams show that the change in the types of minerals that are oversaturated through the chemocline are in part controlled by stable and metastable equilibrium. It also seems there is a direct correlation between the geochemistry at different layers in the water column with respect to the minerals that are oversaturated and the types of MB that reside there. Incomplete oxidation occurring in the chemocline and OATZ will directly affect the speciation and distribution of analytes so there will exist stability zones for thiosulfates, polysulfides, and elemental sulfur that create multiple chemical pathways for abiotic and biotic reactions. This will have a large impact on the free energy available to microorganisms, their productivity, and where they reside in the water column. Figures 41 and 42 portray the biogeochemical relationship between the microorganisms and the geochemical gradients they exploit.

**5. Summary and significance of the work**

The convenience associated with sampling Salt Pond and the similarity of this system to larger, less accessable systems such as the Carioco Basin, Framvaren Fjord, or the Black Sea has made it an important analogue for study and research that will aid investegatoins elsewhere. It is easier to put constraints on a smaller system like Salt

Pond, giving it the potential to provide better characterized analyses than other systems. This could be very valuable when examining pyritization, especially considering the role it plays in the biogeochemical cycling of iron, sulfide, oxygen, and carbon. The investigation of pyritization could also be extended to examine the kinetics and nucleation process of pyritization so that a more quantitative view could be taken when examining the process in situ. For instance, the unique kinetics of this process have been studied in the Black Sea and in Framvaren Fjord, though it is difficult to quantify the extent of pyritization in the water column in such large bodies of water. There are too many currents, upwelling zones, and other abiotic factors affecting the in situ meaasurement of pyritization. Abiotic processes are not the only ones at work in the biogeochemical cycling of iron and sulfur because contributions from microorgansims play a major role. For instance, MB creating BMPs have the potential to sequester large amounts of iron oxides and sulfides in the sediments below the area of the water column they inhabit.

Due to the complex nature of systems containing a permanently stratified water column and an OATZ, a variety of different experiments still need to be done on the abiotic as well as biotic components in order to better constrain biogeochemical cycling of chemical species and their effect on productivity and eutrophication. In the future, a more complete characterization of the water column should be done. Much of this can now be done *in situ* with solid state voltammetric electrodes. Particulate data needs to be obtained on the mineral phases that are precipitating directly out of the water column. In conjunction with this a new method needs to be developed that does not disturb the

chemocline to the extent the current sampler does so more representative fluid samples can be retrieved. Such data would enable the construction of a model to aid in determining the distribution of analytes within the system and place better constraints on the biotic and abiotic cycling of key elements. Microbial influences such as ligand production and subsequent complexation with different forms of iron could also be included in order to examine their impact on the bioavailability of analytes and free energy.

**ACKNOWLEDGMENTS**

I would like to thank my advisors who have supported my investigation of the geochemistry and thermodynamics of this system as well as NSF for support via grant # OCE-0241791. I also thank Sheri Simmons for the procurement of some of the data used in this paper.

## REFERENCES


Andrews, S.C., Robinson, A.K., Rodriguez-Quinones, F., 2003. Bacterial iron homeostasis. FEMS Microbiology Reviews 27, 215-237.

Balkwill, D.L., Maratea, D., Blakemore, R.P., 1980. Ultrastructure of a magnetic spirillum. Journal of Bacteriology 141, 1399-1408.

Barbequ, K., Rue, E.L., Bruland, W., Butler, A., 2001. Photochemical cycling of iron in the surface ocean mediated by microbial iron(III)-binding ligands. Nature 418, 889-892.

Bazylinski, D.A., Moskowitz, B.M., 1997. Microbial biomineralization of magnetic iron minerals: microbiology, magnetism and environmental significance. Geomicrobiology: Interactions Between Microbes and Minerals. In: Banfield, J.F., Nealson, K.H. (editors), Reviews in Mineralogy and Geochemistry vol. 35 Mineralogical Society of America, Washington, DC, 181-223.

Bazylinski, D.A., Schlezinger, D.R., Howes, B.H., Frankel, R.B., Epstein, S.S, 2000. Occurrence and distribution of diverse populations of magnetic protests in a chemically stratified coastal salt pond. Chemical Geology 169, 319-328.

Bazylinski, D and Frankel, R.B, 2004. Magnetosome formation in prokaryotes. Nature Reviews, Microbiology 2, 217-229.

Benning, L.G., Wilkin, R.T., Barnees, H.L., 2000. Reaction pathways in the Fe-S system below 100°C. Chemical Geology 167, 25-51.

Berner, R.A., 1964. Iron sulfphides formed from aqueous solution at low temperatures and atmospheric pressure. Journal of Geology 72, 293-306.

Berner, R.A., 1967. Thermodynamic stability of sedimentary iron sulfides. American Journal of Science 265, 773-785.

Berner R. A., 1970. Sedimentary pyrite formation. American Journal of Science 268, 1-23.

Berner, R. A. and Raiswell R., 1983. Burial of organic carbon and pyrite sulfur in sediments over Phanerozoic time: A new theory. Geochimica et Cosmochemica Acta 47, 855-862.

Berner, E.K. and Berner, R.A. The global water cycle. Prentice-Hall, New Jersey, 1987.

Blakemore, R.P., 1975. Magnetotactic Bacteria. Science 190, 377-379.

Brendel, P.J. and Luther III, G.W. 1995. Development of a gold amalgam voltammetric microelectrode for the determination of dissove Fe, Mn, $O_2$, and S(-II) in porewaters of marine and freshwater sediments. Environmental and Science Technology 29, 751 – 761.

Byrne, R.H and Kester, D.R., 1976a. A potentiometric study of ferric ion complexes in synthetic media and seawater. Marine Chemistry 4, 275-287.

Byrne, R.H and Kester, D.R., 1976b. Solubility of hydrous ferric oxide and iron speciation in seawater. Marine Chemistry 4, 255-74.

Calugay, R.J., Miyashita, H., Okamura, Y. and Matsunaga, T., 2003. Siderophore production by the magnetic bacterium Magnetospirillum magnet*icum* AMB-1. FEMS Mircrobiology Letters 218, 371-375.

Calugay, R.J., Okamura, Y., Wahyudi, A.T., Takeyama, H. and Matsunaga, T., 2004.

Siderophore production of a periplasmic transport binding protein kinase gene defective mutant of Magnetospirillum magneticum AMB-1. Biochemical and Biophysical Research Communications 323, 852-857.
Cape Cod Commission. Cape Cod atlas of tidally restricted salt marshes. Cape Cod Commission, Barnstable, Massachusetts. 2001.
Chen, K.Y. and Morris, J.C., 1972. Kineticsof oxidation of aqueous sulfide by $O_2$. Environmental Science and Technology 6 529 -537.
Cline, J.D., 1969. Spectrophotometric determination of hydrogen sulfide in natural waters. Limnology and Oceanography 14, 454-458.
Cunningham, K.M., Goldberg, M.C. and Weiner, E.R., 1985. Photodissolution of iron oxides in the presence of adsorbed alcohols. Photochemistry and Photobiology 41, 409.
Cutter, G.A. and Krahgorst, C.F., 1988. Sulfide in surface waters of the western atlantic ocean. Geophysical Research Letters 15, 1393-1396.
Davison, W., Buffle, J., DeVitre, R., 1998. Voltammetric characterization of a dissolved iron sulfide species by laboratory and field studies. Analytica Chimica Acta 377, 193-203.
Dekkers, M.J. and Schonen, M.A.A., 1994. An electrokinetic study of synthetic greigite and pyrrhotite. Geochimica et Cosmochimica Acta 58, 4147-4153.
Demitrack, A. A search for bacterial magnetite in the sediments of Eel Marsh, Woodsd Hole, Massachusetts. In (Eds. Kirschvink et al.) Magnetite Biomineralization and Magnetoreception in Organisms. Plenum Publishing. 1985.
Drobner, E., Huber, H.J., Wachterhauser, G., Rose, D., Stetter, K.O., 1990. Pyrite formation linked with hydrogen evolution under anaerobic conditions. Nature 246, 742-744.
Emerson, D. Microbial oxidation of Fe(II) and Mn(II) at circumneutral pH. In Environmental Metal Microbe Interactions (Ed. Lovley, D.R.). ASM Press Washington DC, pp 31-52. 2000.
Emerson, D., 2001. Bacterial iron oxidation at circumneutral pH. In Iron in the Natural Environment: Biogeochemistry, Microbial Diversity, and Bioremediation (Eds. Coates, J.D. and Zhang, C.). Kluver, pp. Submitted for publication.
Emerson, D. and Moyer, C., 1997. Isolation and characterization of novel lithotrophic iron-oxidizing bacteria that grow at circumneutral pH. Applied Environmental Microbiology 63, 4784-4792.
Emerson, S., Jacobs, L., Tebo, B. The behavior of trace metals in marine anoxic waters: solubilities at the oxygen-hydrogen sulfide interface. In Trace Metals in Seawater, Plenum Press, New York, USA, pp 579-608. 1983.
Frankel, R.B., Blakemore, R.P., 1980. Navigational compass in magnetic bacteria. Journal of Magnetism and Magnetic Materials 15-18, 1562-1564.
Frankel, R.B., Bazylinski, D.A., Johnson, M., Taylor, B.L., 1997. Magneto-aerotaxis in marine, coccoid bacteria. Journal of Biophysics 73, 994-1000.
Holland, H.D. The chemistry of the atmosphere and oceans. Wiley, NewYork. 1978.
Holland, H.D.. The Chemical Evolution of the Atmosphere and Oceans. Princeton University press. 1984.

Keller,M., Bloch, E., Wachtershauser, G., and Stetter, K.O., 1994. Formation of amide bonds without a condensation agent and implications for origin of life. Nature 368, 836-838.

Kostka, J.E., Luther III, G.W., 1994. Partitioning and speciation of solid phase Fe in saltmarsh sediments. Geochimica et Cosmochimica Acta 58, 1701-1711.

Landing, W., M., and Lewis, B.L. Thermodynamicmodeling of trace metal speciation in the Black Sea. In Black Sea Oceanography (Izadar, E. and Murray, F.W., eds). Kluwer Academic Press, Dordecht, Netherlands, pp.487. 1991.

Liang , L., McNabb, J.A., Paulk, J.M., Gu, B., and McCarthy, J.F., 1993, Kinetics of Fe(II) oxygenation at low partial pressure of oxygen in the presence of natural organic matter. Environmental Science and Technology 27, 1864-1870.

Luther G. W. III, 1987 Pyrite oxidation and reduction: Molecular orbital theory considerations. Geochimica et Cosmochimica Acta 51, 3193–3.

Luther III, G.W. and Tsamakis, E., 1989. Concentration and form of dissolved sulfide in the oxic water column of the ocean. Marine Chemistry 27, 165-177.

Luther G. W. III. The frontier-molecular-orbital theory approach in geochemical processes. In Aquatic Chemical Kinetics (ed. Stumm W.), pp. 173–198. John Wiley and Sons, New York. 1990.

Luther III, G.W., 1991. Pyrite synthesis via polysulphide compounds. Geochimica et Cosmochimica Acta 55, 2839-2849.

Luther III, G.W., Church, T.M. and Powell, D., 1991. Sulfur speciation and sulfide oxidation in the water column of the Black Sea. Deep Sea Research 38, 1121-1137.

Luther III, G.W., Kostka, J.E. Church, T.M., Sulzberger, B. and Stumm, W., 1992. Seasonal iron cycling in the salt marsh sedimentary environment: the importance of ligand complexes with Fe(II) and F(III) in the dissolution of Fe(III) minerals and pyrite respectively. Marine Chemistry 40, 81-103.

Luther III, G.W. and Ferdelman, T.G., 1993. Voltammetric characterization of iron(II) sulfide complexes in laboratory solutions and in marine waters and porewaters. Environmental Science and Technology 27, 1154-1163.

Luther III, G.W., Shellenbarger, P.A., Brendel, P.J., 1996. Dissolved organic Fe(III) and Fe(III) complexes in salt marsh porewaters. Geochimica et Cosmochimica Acta 60, 951-960.

Matsunaga, T. and Okamura, Y., 2003. Genes and proteins involved in bacterial magnetic particle formation. Trends in Microbiology 11, 536-541.

Morel, F.M.M., Hering, J.G. Principles and Applications of Aquatic Chemistry. Pub. John Wiley and Sons, Inc. New York, USA, pp. 79. 1993.

Morse, J.W., Millero, F.J., Cornwell, J.C., Ricard, D., 1987. The chemistry of the hydrogen sulfide and iron sulfide systems in natural waters. Earth Science Reviews 24, 1-42.

Moses, C. O., Nordstrom D. K., Herman J. S., and Mills A. L. 1987 Aqueous pyrite oxidation by dissolved oxygen and by ferric iron.Geochimica et Cosmochimica Acta 51, 1561–1571.

Moses C. O. and Herman J. S. (1991) Pyrite oxidation at circumneutral pH. Geochimica

et Cosmochimica 55, 471–482.
Muramoto J.A., Honjo, S., Fry, B. Hay, B.J., Howarth, R.W., and Cisne, J.L., 1991. Sulfur,iron and organic carbon fluxesin the Balck Sea: sulfur isotopic evidence for origin of sulfur fluxes. Deep-Sea Research 38, S1151 – S1187.
Oguz, T., Murray, J.W., Callahan, A.E., 2001. modeling redox cycling across the suboxic-anoxic intergace zone in the Black Sea. Deep-Sea Research I 48, 761-787.
O'Sullivan, D.W., Hanson, A.K. Jr., Kester, D.R., 1997. The distribution and redox chemistry of iron in the Pettaquamscutt estuary. Estuarine, Coastal and Shelf Science 45, 769-788.
Rickard, D., 1969. The chemistry of iron sulphide formation at low temperatures. Stockholm Contributions in Geology 20, 67-95.
Rickard, D., 1975. Kinetics and mechanism of pyrite formation at low temperatures. American Journal of Science 275, 636-652.
Rickard, D., 1989. Experimental conenctration-time curves for the iron(II) sulphide precipitation process in aqueous solutions and their interpretation. Chemical Geology 78, 315-324.
Rickard, D., 1997. Kinetics of pyrite formation by the $H_2S$ oxidation of iron (II) monosulfide in aqueous solutions between 25 and 125°C: The rate equation. Geochimica et Cosmochimica Acta 61, 115-134.
Rickard, D., and Luther III, G.W., 1997. Kinetics of pyrite formation by the $H_2S$ oxidation of iron (II) monosulfide in aqueous solutions between 25 and 125°C: The mechanism. Geochimica et Cosmochimica Acta 61 135-147.
Roden, E.E., Sobolev, D., Glazer, B., and Luther III, G.W. , unpublished article. New insights into the biogeochemical cycling of iron in circumneutral sedimentary environments, Potential for a rapid microscale bacterial Fe redox cycle at the aerobic-anaerobic interface.
Rue, E.L. and Bruland, K.W., 1995. Complexation of iron (III) by natural ligands in the central North Pacific as determined by a new competitive ligand equilibrium/adsorptive cathodic stripping voltammetric method. Marine Chemistry 50, 117 – 138.
Schink B., 1997. Energeticsof syntropic cooperation in methanogenic degradation. Microbiology and Molecular Biology Reviews, 61, 19-321.
Schlesinger, W.H. Biogeochemistry: An analysis of global change. Academic Press, San Diego, CA. 1991
Skei, J.M., 1988. Formation of framboidal iron sulfide int eh water of a permanently anoxic fjord – Framvaren, south Norway. Journal or Marine Chemistry 23, 345 – 352.
Simmons, S.L., Sievert, S.M., Frankel, R.B., Bazylinski, D.A., Edwards, K.J., 2004. Spatiotemporal distribution of marine magnetotactic bacteria in a seasonally stratified coastal salt pond. Applied and Environmental Microbiology 70, 6230-6239.
Stolz, J.F, 1992. Magnetotactic bacteria: biomineralization, ecology, sediment magnetism, environmental indicator. Cantena supplement 21, 133-145.

Sulzberger, B., Suter, D. Siffert, C., Banwart, S. and Stumm, W., 1989. Dissolution of Fe(III)(hydro)oxides in natural waters, laboratory assessment on the kinetics controlled by surface coordination. Marine Chemistry 28, 127-144.

Stookey, L. L. 1970. Ferrozine—a new spectrophotometric reagent for iron. Analytical Chemistry 42, 779-781

Sweeney, R. E. and Kaplan I. R. (1973) Pyrite framboid formation: laboratory synthesis and marine sediments. Economic Geology 68, 618-634.

Tessier, A., Campbell, P.G.C. Partitioning of trace metals in sediments. In Kramer, J.R., Allen, H.E. (editors), Metal Speciation, Theory, Analysis and Application. Lewis Publishers 183-199. 1988.

Unesco 1981. Unesco Technical Paper on Marine Science no. 38. Paris: Unesco.

Voillier, E., Inglett, P.W., Hunter, K., Roychoudhury, A.N., Van Cappellen, P., 2000. The Ferrozine method revisited: Fe(II) / Fe(III) determination in natural waters. Applied Geochemistry 15, 785-790.

Wada, H., 1977. The synthesis of greigite from a polysulfide solution at about 100 °C. Bulletin of the Chemical Society of Japan 50, 2615-2617.

Wang, Q. and Morse, J.M., 1996. Pyrite formation under conditions approximating those in anoxic sediments: I. Pathway and morphology. Marine Chemistry 52, 99-121.

Wakeham, S.G., Howes, B.L., Dacey, J.W.H., Schwarzenbach, R.P., Zeyer, J., 1987. Biogeochemistry of dimethylsulphide in a seasonally stratified coastal salt pond. Geochimica et Cosmochimica Acta 51, 1675-1684.

Wilkin, R.T., 1995. Size distribution in sediments, synthesis, and formation mechanism of framboidal pyrite. Ph.D. dissertation, Pennsylvania State University.

Wilken, R.T. and Barnes, H.L., 1996. Pyrite formation by reactions of iron monosulfides with dissolved inorganic and organic sulfur species. Geochimica et Cosmochimica Acta 60, 4167-4179.

Wilken, R.T. and Barnes, H.L., 1997. Formation processes of framboidal pyrite. Geochimica et Cosmochimica Acta 61, 323-339.

Williamson, M.A. and Rimstidt, J.D., 1992. Correlation between structures and thermodynamic properties of aqueous sulfur species. Geochimica et Cosmochimica Acta 56, 3867 – 3880.

Witter, A.E., Lewis, B.L., Luther III, G.W. 2000. Iron speciation in the Arabian Sea. Deep-Sea Research Part II 47, 1517 – 1539.

Xu, Y. and Schoonen, MA.A., 1995. The stability of thiosulfate in the presence of pyrite in low-temperature aqueous solutions. Geochemica et Cosmochemica Acta 59, 4605 – 4622.

Zopfi, J., Ferdelman, T.G., Jorgensen, B.B., Teske, A., Thamdrup, B. Influence of water column dynamics on sulfide oxidation and other major biogeochemical processes in the chemocline of Mariager Fjord (Denmark). Marine Chemistry 74, 29-51.

Table 1: Configuration used for voltammetric sampling and calibrations.

| Parameter | Program Entry |
|---|---|
| Technique | Cyclic Voltammetry |
| Scanned Channel | Current |
| Run Type | Sample |
| CV Potential | -0.050 V |
| Vertex 1 | n/a |
| Vertex 2 | n/a |
| Final Potential | -1.800 V |
| Holding Potential | 0.000 V |
| Pulse Height | n/a |
| IR Compensation | OFF |
| Average Step Size | 0.0018 V |
| Scan Rate | 1000.00 mV/S |
| Square Wave Frequency | n/a |
| Line Sync | OFF |
| Line Frequencey | n/a |
| Chronoamp T1 | n/a |
| Chronoamp2 | n/a |
| Sampling Time | 1.750E-3 s |
| Points | 1999 |
| Scan Time | 3.498 + 0s |
| Current Range | 1, 10 or 100 μA |
| I/E Filter | OFF |
| Dummy Cell | OFF |
| Working Electrode | Solid |
| Drop Test | n/a |
| Degas | OFF |
| Stir | OFF |
| Conditioning | ON, Degas OFF, Stir OFF |
| Potential 1 | -0.050 V For 2s |
| Stripping | OFF |
| Equilibration | OFF |
| Potential At Experiment End | Holding Potential |
| Cell At Experiment End | OFF |
| Pre Acquisition Trigger Out | OFF |
| Acquisition Trigger Out | OFF |
| Post Acquisition Trigger Out | OFF |
| Moving Average | OFF |
| Aux 1 | OFF |

Table 2: Measured YSI data for the 8-11-2004 sampling period from Salt Pond entered into REACT.

| Depth (m) | O2 (mg/L) | T °C | pH | Sulfide (µM) | TDFe (µM) | Dfe2 (µM) |
|---|---|---|---|---|---|---|
| 0.00 | 7.32 | 24.70 | | | | |
| 0.30 | 7.70 | 24.80 | 7.69 | | | |
| 0.61 | 7.58 | 24.80 | 7.81 | | | |
| 0.91 | 7.71 | 24.70 | 7.99 | | | |
| 1.22 | 7.21 | 24.60 | 8.07 | | | |
| 1.52 | 7.38 | 24.70 | | | | |
| 1.83 | 7.44 | 24.60 | 8.93 | | | |
| 2.13 | 7.51 | 24.50 | 8.75 | | | |
| 2.44 | 2.80 | 24.40 | 8.61 | | | |
| 2.59 | 1.68 | 24.60 | 8.24 | | | |
| 2.74 | 1.36 | 24.40 | 8.23 | | | |
| 2.90 | 0.98 | 24.10 | 8.27 | | | |
| 3.05 | 0.19 | 23.50 | 7.87 | | 2.64 | 2.66 |
| 3.20 | 0.08 | 23.50 | 7.53 | 193.73 | 3.30 | 0.95 |
| 3.35 | | | 7.33 | 443.58 | 2.80 | 2.29 |
| 3.51 | | | 7.11 | 550.43 | 2.30 | 1.56 |
| 3.81 | | | 7.03 | 556.52 | 1.97 | 1.19 |
| 4.11 | | | 7.04 | 567.90 | 1.97 | 0.46 |
| 4.42 | | | 7.01 | 506.55 | 1.64 | 0.59 |

Table 3: Major ion concentrations calculated from conservative mixing for the 8-11-04 sampling period from Salt Pond entered into REACT.

| Major Ion Concentrations from Conservative Mixing Calculations (mM) | | | | | | | |
|---|---|---|---|---|---|---|---|
| **Depth (m)** | **$Cl^-$** | **$Na^+$** | **$SO_4^{2-}$** | **$Mg^{2+}$** | **$K^+$** | **$Ca^{2+}$** | **$HCO_3^-$** |
| 0.3048 | 368.476 | 315.566 | 19.015 | 35.872 | 6.878 | 6.878 | 1.605 |
| 0.6096 | 382.528 | 327.600 | 19.740 | 37.240 | 7.140 | 7.140 | 1.666 |
| 0.9144 | 385.651 | 330.274 | 19.901 | 37.544 | 7.198 | 7.198 | 1.680 |
| 1.2192 | 390.335 | 334.286 | 20.143 | 38.000 | 7.286 | 7.286 | 1.700 |
| 1.524 | 391.896 | 335.623 | 20.223 | 38.152 | 7.315 | 7.315 | 1.707 |
| 1.8288 | 396.580 | 339.634 | 20.465 | 38.608 | 7.402 | 7.402 | 1.727 |
| 2.1336 | 398.141 | 340.971 | 20.546 | 38.760 | 7.431 | 7.431 | 1.734 |
| 2.4384 | 435.613 | 373.063 | 22.479 | 42.408 | 8.131 | 8.131 | 1.897 |
| 2.5908 | 443.420 | 379.749 | 22.882 | 43.168 | 8.277 | 8.277 | 1.931 |
| 2.7432 | 448.104 | 383.760 | 23.124 | 43.624 | 8.364 | 8.364 | 1.952 |
| 2.8956 | 451.227 | 386.434 | 23.285 | 43.928 | 8.422 | 8.422 | 1.965 |
| 3.048 | 455.911 | 390.446 | 23.527 | 44.384 | 8.510 | 8.510 | 1.986 |
| 3.2004 | 459.033 | 393.120 | 23.688 | 44.688 | 8.568 | 8.568 | 1.999 |
| 3.3528 | 459.033 | 393.120 | 23.688 | 44.688 | 8.568 | 8.568 | 1.999 |
| 3.5052 | 459.033 | 393.120 | 23.688 | 44.688 | 8.568 | 8.568 | 1.999 |
| 3.81 | 459.033 | 393.120 | 23.688 | 44.688 | 8.568 | 8.568 | 1.999 |
| 4.1148 | 459.033 | 393.120 | 23.688 | 44.688 | 8.568 | 8.568 | 1.999 |
| 4.4196 | 459.033 | 393.120 | 23.688 | 44.688 | 8.568 | 8.568 | 1.999 |

Table 4: Measured YSI data from the 9-22-05 sampling period at Salt Pond with the sampler. Salinity, DO charge and precent DO were not entered into REACT, while the others were.

| Depth m | DO % | DO Conc mg/L | ORP mV | DO Charge | pH | Temp C | Salinity ppt |
|---|---|---|---|---|---|---|---|
| 3.127 | 12.620 | 0.908 | -173.600 | 35.400 | 7.296 | 23.768 | 28.264 |
| 3.249 | 18.022 | 1.296 | -24.444 | 34.778 | 7.309 | 23.854 | 28.151 |
| 3.313 | 7.450 | 0.535 | -221.250 | 34.250 | 7.225 | 23.560 | 28.365 |
| 3.350 | 11.530 | 0.828 | -28.100 | 34.300 | 7.274 | 23.715 | 28.251 |
| 3.420 | 7.438 | 0.538 | -84.000 | 34.000 | 7.258 | 23.613 | 28.316 |
| 3.496 | 0.310 | 0.024 | -285.600 | 33.100 | 7.018 | 23.253 | 28.525 |
| 3.560 | bdt | bdt | -339.200 | 35.100 | 6.854 | 22.953 | 28.731 |

bdt= below detection limit

Table 5: Measured YSI data from the 9-22-05 sampling period at Salt Pond without the sampler. Salinity, specific conductivity, and DO charge were not entered into REACT while the rest were.

| Depth m | DO % | ORP mV | DO Charge | DO Conc mg/L | pH | Salinity ppt | SpCond mS/cm | Temp C |
|---|---|---|---|---|---|---|---|---|
| 0.196 | 101.100 | 139.000 | 49.000 | 7.460 | 7.740 | 24.530 | 38.560 | 23.460 |
| 0.317 | 101.200 | 136.000 | 49.000 | 7.480 | 7.740 | 24.590 | 38.640 | 23.390 |
| 0.940 | 101.300 | 135.000 | 49.000 | 7.510 | 7.750 | 24.580 | 38.620 | 23.220 |
| 1.220 | 101.400 | 134.000 | 48.000 | 7.530 | 7.760 | 24.610 | 38.660 | 23.160 |
| 1.523 | 102.000 | 134.000 | 49.000 | 7.580 | 7.760 | 24.590 | 38.630 | 23.100 |
| 1.863 | 93.800 | 135.000 | 49.000 | 6.930 | 7.700 | 24.690 | 38.790 | 23.380 |
| 2.765 | 65.400 | 132.000 | 46.000 | 4.700 | 7.560 | 27.340 | 42.530 | 24.070 |
| 3.269 | 16.200 | 119.000 | 42.000 | 1.170 | 7.290 | 27.910 | 43.320 | 23.840 |
| 3.352 | 9.100 | 107.000 | 41.000 | 0.660 | 7.260 | 28.080 | 43.560 | 23.730 |
| 3.438 | 5.500 | 64.000 | 41.000 | 0.400 | 7.260 | 28.230 | 43.760 | 23.570 |
| 3.493 | 3.700 | 30.000 | 41.000 | 0.270 | 7.270 | 28.280 | 43.830 | 23.490 |
| 3.552 | 2.800 | -3.000 | 40.000 | 0.200 | 7.290 | 28.370 | 43.950 | 23.390 |
| 3.576 | 4.300 | 0.000 | 40.000 | 0.310 | 7.300 | 28.350 | 43.920 | 23.370 |
| 3.649 | 1.900 | -147.000 | 40.000 | 0.140 | 7.270 | 28.470 | 44.080 | 23.150 |
| 3.698 | bdt | -249.000 | 39.000 | bdt | 6.860 | 28.540 | 44.180 | 22.900 |
| 3.763 | bdt | -285.000 | 39.000 | bdt | 6.750 | 28.620 | 44.280 | 22.610 |
| 3.831 | bdt | -319.000 | 38.000 | bdt | 6.740 | 28.740 | 44.440 | 22.460 |
| 3.972 | bdt | -341.000 | 38.000 | bdt | 6.720 | 28.840 | 44.570 | 21.720 |
| 3.975 | bdt | -345.000 | 39.000 | bdt | 6.720 | 28.870 | 44.610 | 21.670 |
| 4.121 | bdt | -354.000 | 41.000 | bdt | 6.710 | 29.030 | 44.820 | 21.210 |
| 4.154 | bdt | -357.000 | 41.000 | bdt | 6.710 | 28.920 | 44.660 | 21.090 |

bdt= below detection limit

Table 6: Major ion concentrations calculated from conservative mixing for the 9-22-05 sampling period at Salt Pond with the sampler entered into REACT.

| Depth | Major Ion Concentrations from Conservative Mixing Calculations (mM) | | | | | | |
|---|---|---|---|---|---|---|---|
| m | $Na^+$ | $Cl^-$ | $SO_4^{2-}$ | $Mg^{2+}$ | $K^+$ | $Ca^{2+}$ | $HCO_3^-$ |
| 3.127 | 377.93 | 441.297 | 22.773 | 42.961 | 8.237 | 8.237 | 1.922 |
| 3.249 | 376.421 | 439.534 | 22.682 | 42.79 | 8.204 | 8.204 | 1.914 |
| 3.313 | 379.281 | 442.874 | 22.854 | 43.115 | 8.266 | 8.266 | 1.929 |
| 3.35 | 377.756 | 441.094 | 22.762 | 42.942 | 8.233 | 8.233 | 1.921 |
| 3.42 | 378.629 | 442.112 | 22.815 | 43.041 | 8.252 | 8.252 | 1.926 |
| 3.496 | 381.42 | 445.372 | 22.983 | 43.358 | 8.313 | 8.313 | 1.94 |
| 3.56 | 384.175 | 448.588 | 23.149 | 43.671 | 8.373 | 8.373 | 1.954 |

Table 7: Major ion concentrations calculated from conservative mixing for the 9-22-05 sampling period without the sampler entered into REACT.

| Depth | Major Ion Calculations from Conservative Mixing Calculations (mM) | | | | | | |
|---|---|---|---|---|---|---|---|
| (m) | $Na^+$ | $Cl^-$ | $SO_4^{2+}$ | $Mg^{2+}$ | $K^+$ | $Ca^{2+}$ | $HCO_3^-$ |
| 0.3048 | 328.803 | 383.933 | 19.813 | 37.377 | 7.166 | 7.166 | 1.672 |
| 0.9598152 | 328.67 | 383.777 | 19.804 | 37.362 | 7.163 | 7.163 | 1.671 |
| 1.2137136 | 329.071 | 384.245 | 19.829 | 37.407 | 7.172 | 7.172 | 1.673 |
| 1.5243048 | 328.803 | 383.933 | 19.813 | 37.377 | 7.166 | 7.166 | 1.672 |
| 1.860804 | 330.141 | 385.494 | 19.893 | 37.529 | 7.195 | 7.195 | 1.679 |
| 2.7486864 | 365.575 | 426.87 | 22.028 | 41.557 | 7.968 | 7.968 | 1.859 |
| 3.2570928 | 373.197 | 435.77 | 22.487 | 42.423 | 8.134 | 8.134 | 1.898 |
| 3.4082736 | 377.475 | 440.766 | 22.745 | 42.91 | 8.227 | 8.227 | 1.92 |
| 3.5012376 | 378.144 | 441.546 | 22.786 | 42.986 | 8.242 | 8.242 | 1.923 |
| 3.575304 | 379.08 | 442.639 | 22.842 | 43.092 | 8.262 | 8.262 | 1.928 |
| 3.645408 | 380.685 | 444.513 | 22.939 | 43.274 | 8.297 | 8.297 | 1.936 |
| 3.694176 | 381.621 | 445.606 | 22.995 | 43.381 | 8.317 | 8.317 | 1.941 |
| 3.761232 | 382.69 | 446.855 | 23.06 | 43.502 | 8.341 | 8.341 | 1.946 |
| 3.831336 | 384.295 | 448.729 | 23.156 | 43.685 | 8.376 | 8.376 | 1.954 |
| 3.971544 | 385.632 | 450.29 | 23.237 | 43.837 | 8.405 | 8.405 | 1.961 |
| 3.9736776 | 386.033 | 450.758 | 23.261 | 43.882 | 8.414 | 8.414 | 1.963 |
| 4.1535096 | 388.173 | 453.257 | 23.39 | 44.126 | 8.46 | 8.46 | 1.974 |

Table 8 : Data measured using cyclic voltammetry for the 9-11-2005 sampling period at Salt Pond with the sampler; sulfide, thiosulfate, and ferrous iron were entered into REACT.

| Depth (m) | Concentration based on 9-30-05 Calibration Curves in μM | | | | | | |
|---|---|---|---|---|---|---|---|
| | Sulfide | Sulfide/100 | Thiosulfate | Ferrous Iron | Iron Monosulfide | Elemental Sulfur | Polysulfide |
| 3.127 | 22.589 | 0.226 | 0.000 | 0.000 | n | y | n |
| 3.249 | | | 0.000 | 0.000 | y | n | n |
| 3.313 | | | 4.766 | 16.502 | y | y | n |
| 3.350 | | | | | y | y | n |
| 3.420 | 83.346 | 0.833 | 3.262 | 23.937 | y | y | y |
| 3.496 | 1985.371 | 19.854 | 0.000 | 26.914 | n | y | y |
| 3.560 | 2818.435 | 28.184 | 0.000 | 0.000 | y | y | y |

Table 9. Data measured using cyclic voltammetry for the 9-11-2005 sampling period at Salt Pond without the sampler; sulfide, thiosulfate, and ferrous iron were entered into REACT.

| Depth (m) | Concentration based on 9-30-05 Calibration Curves in μM | | | | | | | |
|---|---|---|---|---|---|---|---|---|
| | sulfide | Sulfide/100 | thiosulfate | ferrous iron | iron monosulfide | Fe(III)-complexes | elemental sulfur | Polysulfide |
| 0.000 | 0.000 | 0.000 | 0.000 | 0.000 | y | y | n | n |
| 0.305 | 0.000 | 0.000 | 0.000 | 0.000 | y | y | n | n |
| 0.610 | 0.000 | 0.000 | 0.000 | 0.000 | y | n | n | n |
| 0.960 | 0.000 | 0.000 | 0.000 | 0.000 | y | y | n | n |
| 1.214 | 0.000 | 0.000 | 0.000 | 0.000 | y | y | n | n |
| 1.524 | 0.000 | 0.000 | 0.000 | 0.000 | y | n | n | n |
| 1.861 | 0.000 | 0.000 | 0.000 | 0.000 | y | n | n | n |
| 2.153 | 0.000 | 0.000 | 0.000 | 0.000 | y | n | n | n |
| 2.441 | 0.000 | 0.000 | 0.000 | 0.000 | y | n | y | n |
| 2.749 | 0.000 | 0.000 | 0.000 | 0.000 | y | n | y | n |
| 3.061 | 0.000 | 0.000 | 0.000 | 4.815 | y | n | y | n |
| 3.154 | 0.000 | 0.000 | 0.000 | 5.844 | y | n | y | n |
| 3.215 | 0.000 | 0.000 | 0.000 | 8.289 | y | n | y | n |
| 3.257 | 0.000 | 0.000 | 2.436 | 18.095 | y | n | y | n |
| 3.324 | 0.000 | 0.000 | 3.594 | 28.543 | y | n | y | y |
| 3.408 | 0.000 | 0.000 | 2.817 | 28.642 | y | n | y | y |
| 3.501 | 0.000 | 0.000 | 6.196 | 32.272 | y | n | y | y |
| 3.575 | 456.681 | 4.567 | 5.013 | 30.049 | y | n | y | y |
| 3.645 | 112.010 | 1.120 | 6.279 | 13.556 | y | n | y | y |
| 3.694 | 207.314 | 2.073 | 0.000 | 0.000 | n | n | y | y |
| 3.761 | 588.020 | 5.880 | 0.000 | 0.000 | n | n | y | y |
| 3.831 | 1236.586 | 12.366 | 0.000 | 0.000 | n | n | y | y |
| 3.972 | 1921.759 | 19.218 | 0.000 | 0.000 | y | n | y | y |
| 3.974 | 1163.169 | 11.632 | 0.000 | 0.000 | n | n | y | y |
| 4.011 | | | 0.000 | 0.000 | n | n | y | y |
| 4.154 | 3091.126 | 30.911 | 0.000 | 0.000 | n | n | y | y |

## FIGURE CAPTIONS

Figure 1: Salt Pond, Falmouth, Massachusetts shown relative to Cape Cod and other coastal features.

Figure 2: Voltammetric scan number 149 from 9-22-2005 at a depth of 3.83 m. The scan was done at a scan range of 10 μA and followed the parameters listed in Table 1. The sulfide, polysulfide, and elemental sulfur peaks are indicated on the votlammogram.

Figure 3: Vertical profiles of temperature (°C), salinity (ppt), and sigma (s, t, p) for the 8-11-2004 sampling period.

Figure 4: Vertical profiles of temperature (°C), salinity (ppt), and sigma (s, t, p) for the 9-22-2005 sampling period.

Figure 5: Vertical profiles of sulfide and DO for the 8-11-2004 sampling period.

Figure 6: Dissolved oxygen plotted against depth for the 9-22-2005 sampling period.

Figure 7: Vertical profile of $E_H$ for the 9-22-2005 sampling period at Salt Pond. The area most conforming to the change in slope has been outlined as the chemocline.

Figure 8: Plot of sulfide and dissolved oxygen (DO) against depth for the 9-22-2005 sampling period at Salt Pond. These measurements represent data collected with the YSI and electrodes attached to the sampler. The dissolved oxygen and sulfide overlap (DOSO) has been highlighted.

Figure 9: Plot of sulfide and dissolved oxygen (DO) against depth for the 9-22-2005 sampling period at Salt Pond. These measurements represent data collected with the YSI and electrodes free from the sampler. The dissolved oxygen and sulfide overlap (DOSO) has been highlighted.

Figure 10: Plot of dissolved iron species, total sulfide and dissolved oxygen against depth for the 8-11-2004 sampling period at Salt Pond. TDFe refers to the total dissolved iron, DFe3 refers to dissolved iron (III), and DFe2 refers to dissolved iron (II).

Figure 11: Chemical profiles of thiosulfate, ferrous iron and sulfide against depth for the 9-22-2005 sampling period at Salt Pond. This data was collected with the electrodes mounted to the sampler.

Figure 12: Chemical profiles of thiosulfate, ferrous iron and sulfide against depth for the 9-22-2005 sampling period at Salt Pond. This data was collected while the electrodes were free from the sampler.

Figure 13: Plot of dissolved iron versus depth for the 8-11-2004 sampling period. TDFe refers to the total dissolved iron, DFe3 refers to dissolved iron (III), and DFe2 refers to dissolved iron (II).

Figure 14: Iron profiles for the 9-22-2005 sampling period using both the Ferrozine method and voltammetry to analyze the system. Voltammetry measurements are in bold italic font. The numerous FZ measurements near 3.3 m are analogous to one sample at that depth since the sampler does not have the resolution required to make measurements on a scale of less than ~20 cm. It should also be noted that while there is a measurement for dissolved iron at 3.22 m there is not a total iron measurement there. This causes an artifact in the plot by creating the appearance that there is more dissolved iron than total iron at that depth.

Figure 15: Voltammogram of scan number 8 done on the surface from the 9-22-2005 sampling period. The arrow on the left is pointing to a low, broad FeS peak while the slight max on the right is in the vicinity of iron (III) organocomplexes.

Figure 16: Chemical profiles of voltammetry for the 9-22-2005 sampling period with and without the electrodes mounted to the sampler. Analytes in bold in the legend are the measurements taken with the electrodes mounted to the sampler.

Figure 17: Voltamogram of scan number 129 at a depth of 3.65 m at the bottom chemocline for the 9-22-2005 sampling period with the electrodes free from the sampler. There is a small iron and iron sulfide peak with a relatively strong sulfilde peak and a very small thiosulfate peak (from left to right across the scan).

Figure 18: Depth profiles of thiosulfate, ferrous iron, sulfide, and DO across the dissolved oxygen and sulfide overlap for the 9-22-2005 sampling period with the electrodes mounted to the sampler.

Figure 19: Depth profiles of thiosulfate, ferrous iron, sulfide, and DO across the dissolved oxygen and sulfide overlap for the 9-22-2005 sampling period with the electrodes free from the sampler.

Figure 20: Simple Schematic depicting the various pathways and relationships between different sulfur species. Dashed lines refer to minor processes in the cycle.

Figure21: Plot of the fractional abundance of different iron species for the 8-11-2004 sampling period as the chemocline is traversed.

Figure 22: Plot of the fractional abundance of different iron species for the 9-22-2005 sampling period as the chemocline is traversed with the sampler.

Figure 23: Plot of the fractional abundance of different iron species for the 9-22-2005 sampling period as the chemocline is traversed without the sampler.

Figure 24: Plot of log concentration versus depth for the 8-11-2004 sampling period.

Figure 25: Plot of log concentration versus depth for the 9-22-2005 sampling period demonstrating what large effects a small concentration of sulfide can have.

Figure 26: Plot of log concentration versus depth for the 9-22-2005 sampling period. Note the large difference between these measurements versus the ones with the sampler and the effects these measurements can have on the perceived state of the system.

Figure 27: Saturation indices plotted against depth for the 8-11-2004 sampling period.

Figure 28: Saturation indices plotted against depth for the 9-22-2005 sampling period with the sampler.

Figure 29: Saturation indices plotted against depth for the 9-22-2005 sampling period without the sampler.

Figure 30: $E_H$/pH diagram for the 8-11-2004 sampling period showing the most thermodynamically stable phases at 3.05 m.. A circle has been drawn around the area that is most probably like what would be seen in Salt Pond based on measurements and calculated estimates of $E_H$ from the 2005 year. The data supports the premise that magnetite is the most thermodynamically stable intermediate phase at this depth. Input parameters can be found in Appendix 4.

Figure 31: $E_H$/pH diagram for the 8-11-2004 sampling period showing the most thermodynamically stable phases at 3.20 m.. A circle has been drawn around the area that is most probably like what would be seen in Salt Pond based on measurements and calculated estimates of $E_H$ from the 2005 year. The data supports the premise that greigite is the most thermodynamically stable intermediate phase at this depth. Input parameters can be found in Appendix 4.

Figure 32: $E_H$/pH diagram for the 9-22-2005 sampling period at a depth of 3.31 m. The data used to construct this diagram was retrieved while the electrodes were mounted to the sampler. A small circle has been drawn onto the diagram representing the conditions at Salt Pond. Input parameters can be found in Appendix 5.

Figure 33: $E_H$/pH diagram for the 9-22-2005 sampling period at a depth of 3.42 m. The data used to construct this diagram was retrieved while the electrodes were mounted to the sampler. A small circle has been drawn onto the diagram representing the conditions at Salt Pond. Input parameters can be found in Appendix 5.

Figure 34: $E_H$/pH diagram for the 9-22-2005 sampling period at a depth of 3.50 m. The data used to construct this diagram was retrieved while the electrodes were mounted to the sampler. A small circle has been drawn onto the diagram representing the conditions at Salt Pond. Input parameters can be found in Appendix 5.

Figure 35: $E_H$/pH diagram for the 9-22-2005 sampling period at a depth of 3.26 m. The data used to construct this diagram was retrieved while the electrodes were free from the sampler. A small circle has been drawn onto the diagram representing the conditions at Salt Pond. Input parameters can be found in Appendix 6.

Figure 36: $E_H$/pH diagram for the 9-22-2005 sampling period at a depth of 3.41 m. The data used to construct this diagram was retrieved while the electrodes were free from the sampler. A small circle has been drawn onto the diagram representing the conditions at Salt Pond. Input parameters can be found in Appendix 6.

Figure 37: $E_H$/pH diagram for the 9-22-2005 sampling period at a depth of 3.50 m. The data used to construct this diagram was retrieved while the electrodes were free from the sampler. A small circle has been drawn onto the diagram representing the conditions at Salt Pond. Input parameters can be found inAppendix 6.

Figure 38: $E_H$/pH diagram for the 9-22-2005 sampling period at a depth of 3.58 m. The data used to construct this diagram was retrieved while the electrodes were free from the sampler. A small circle has been drawn onto the diagram representing the conditions at Salt Pond. Input parameters can be found in Appendix 6.

Figure 39: $E_H$/pH diagram for the 9-22-2005 sampling period at a depth of 3.65 m. The data used to construct this diagram was retrieved while the electrodes were free from the sampler. A small circle has been drawn onto the diagram representing the conditions at Salt Pond. Input parameters can be found in Appendix 6.

Figures 40: Schematic of MB distribution in Sat Pond illustrating locations of magnetite and greigite-producing MB relative to the stratified water column chemistry profile. From Simmons et al. 2004

Figure 41: Plot of protist number versus depth and $E_H$. Note how there is a maximum directly in the middle of the dissolved oxygen and sulfide overlap zone where there is also the highest concentration of ferrous iron and thiosulfate. This is the area with the greatest amount of disequilibrium and where a microbial community will experience the greatest free energy yield from the metabolic pathways they use to generate energy.

Figure 42: Plot of MB versus depth. There are two separate populations seen in the plot with the upper ppulation corresponding to a high in thiosulfate and a large increase in iron at a point where there is very little sulfide. The populaiton occuring at greater depth corresponds to an increase in sulfide and iron, but a decrease in DO and thiosulfate.

Figure 43: Plot comparing different redox reactions at the depths sampled through the chemocline for the 9-22-2005 sampling period with the electrodes free from the sampler. The iron oxide with the highest free energy yeild is magnetite, while the sulfide reactoin wit the highest free energy yeild is greigite.

Figure 44: Plot displaying the relation between DO, ferrous iron oxidation, and Gibbs free energy for the reaction at different DO concentrations. The pH was held at 7 and ferrous iron was held at 35 μM.

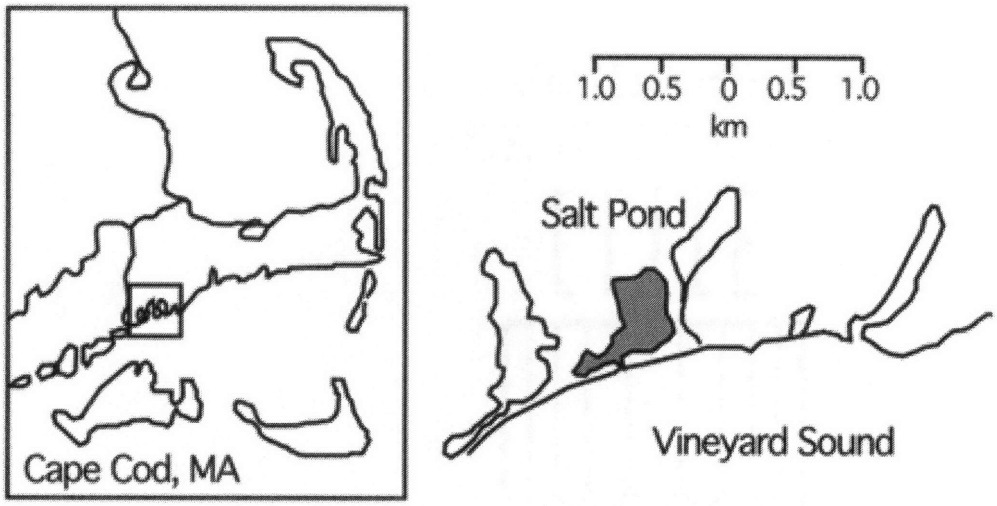


Figure 1 – P.A. Canovas III

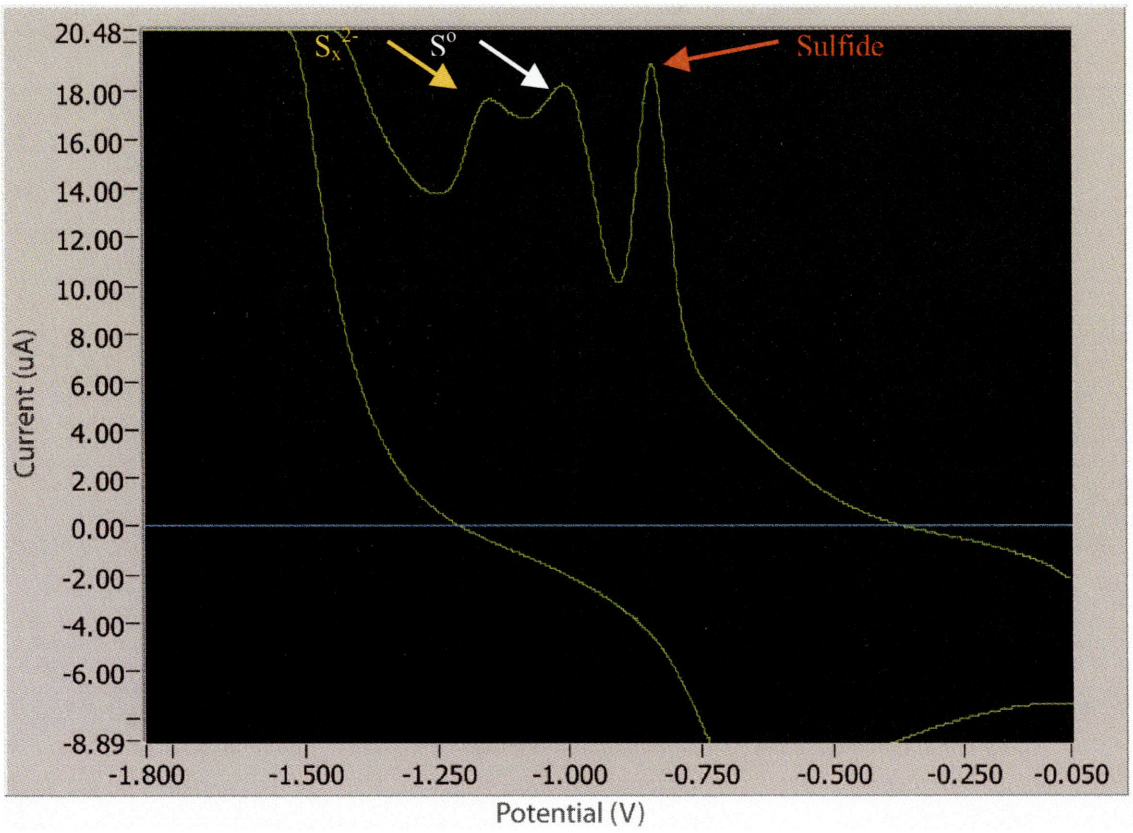


Figure 2 – P.A. Canovas III

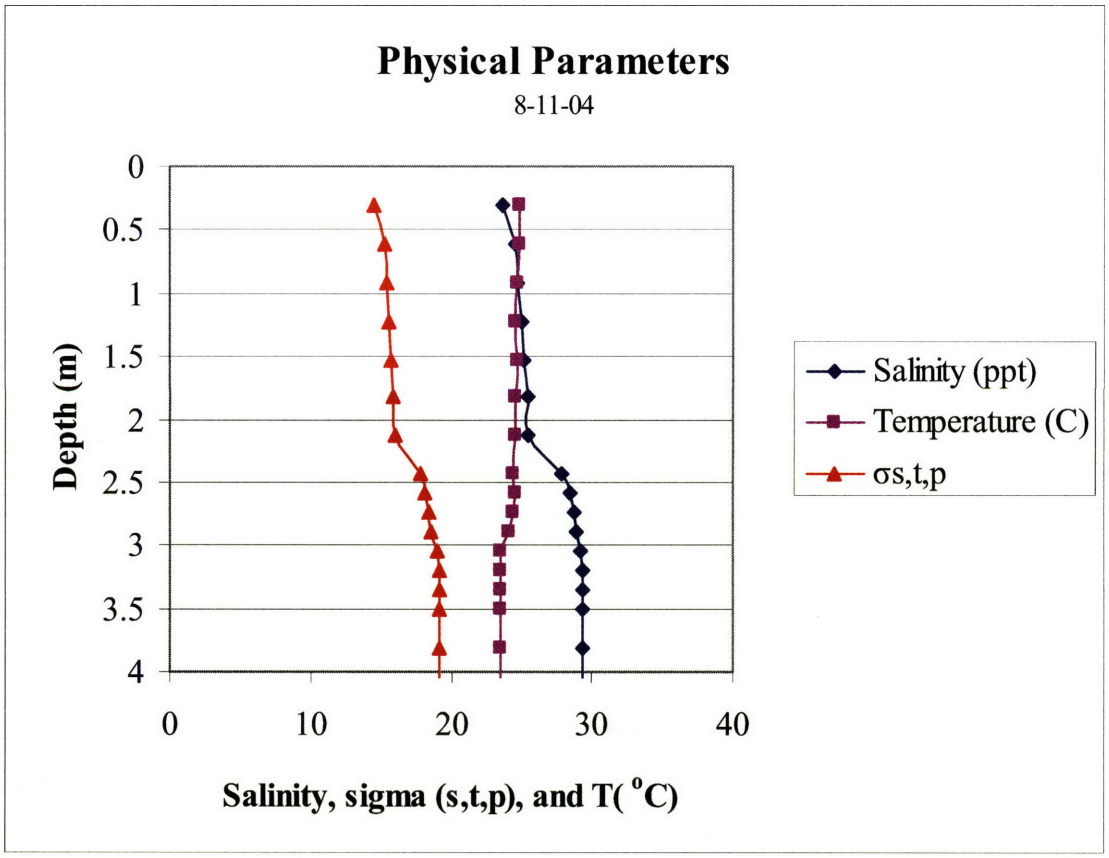


Figure 3-P.A. Canovas III

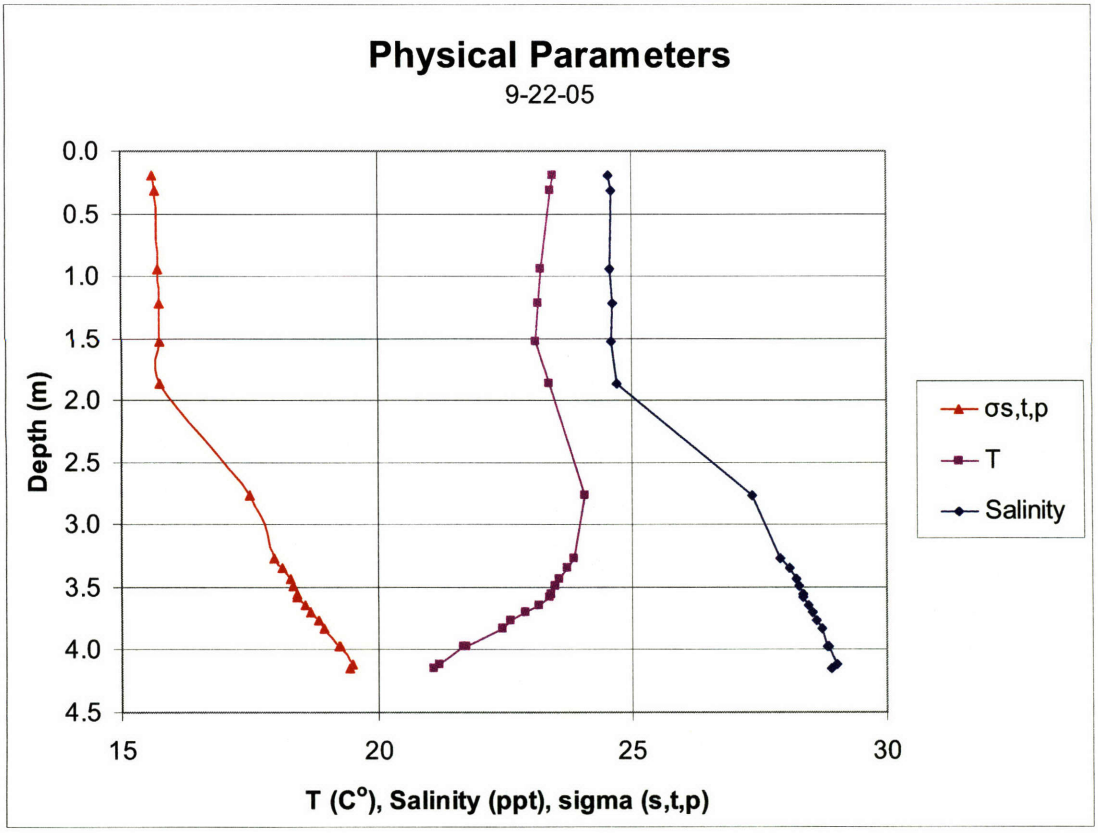


Figure 4.-P.A. Canovas III

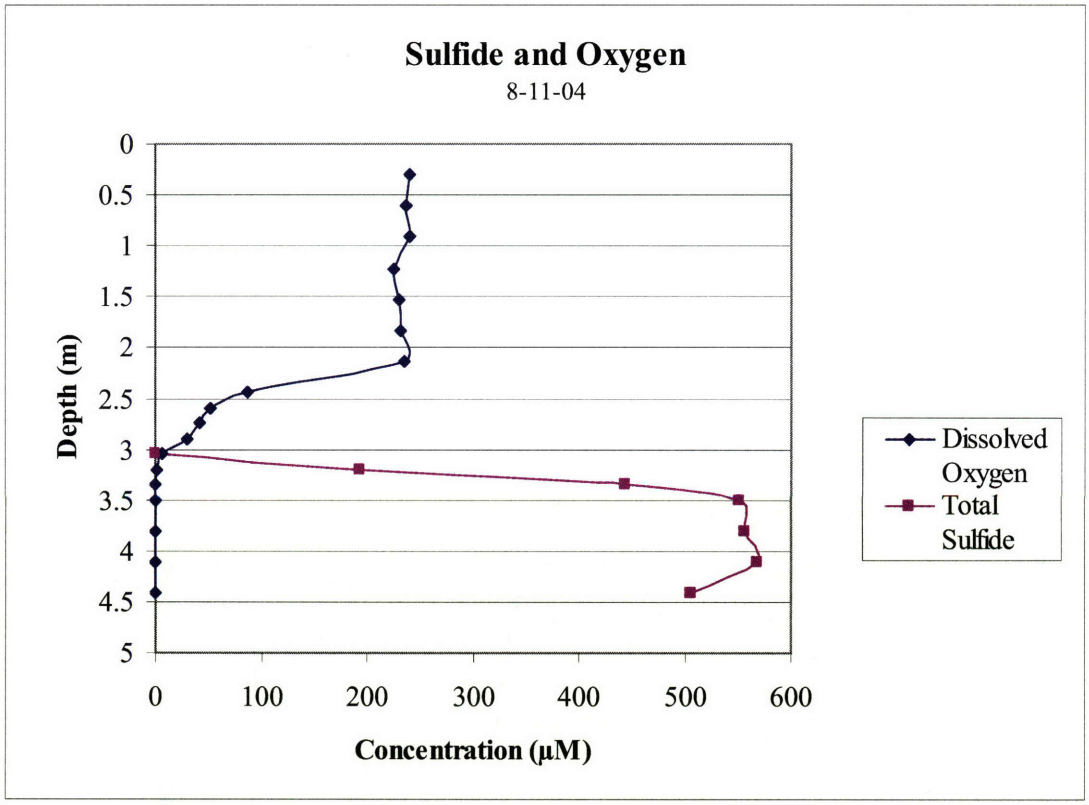


Figure 5- P.A. Canovas III

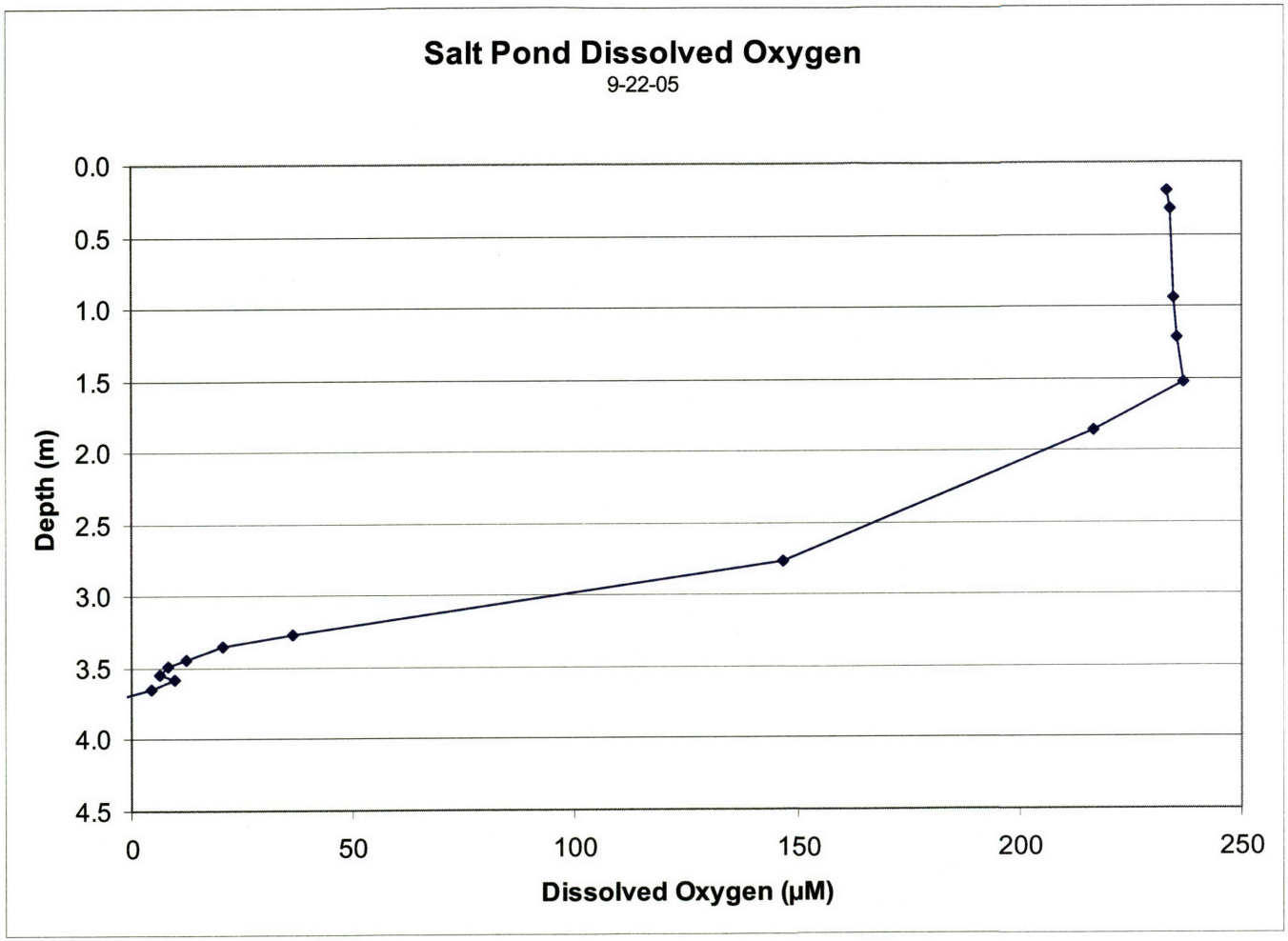


Figure 6 – P.A.Canovas III

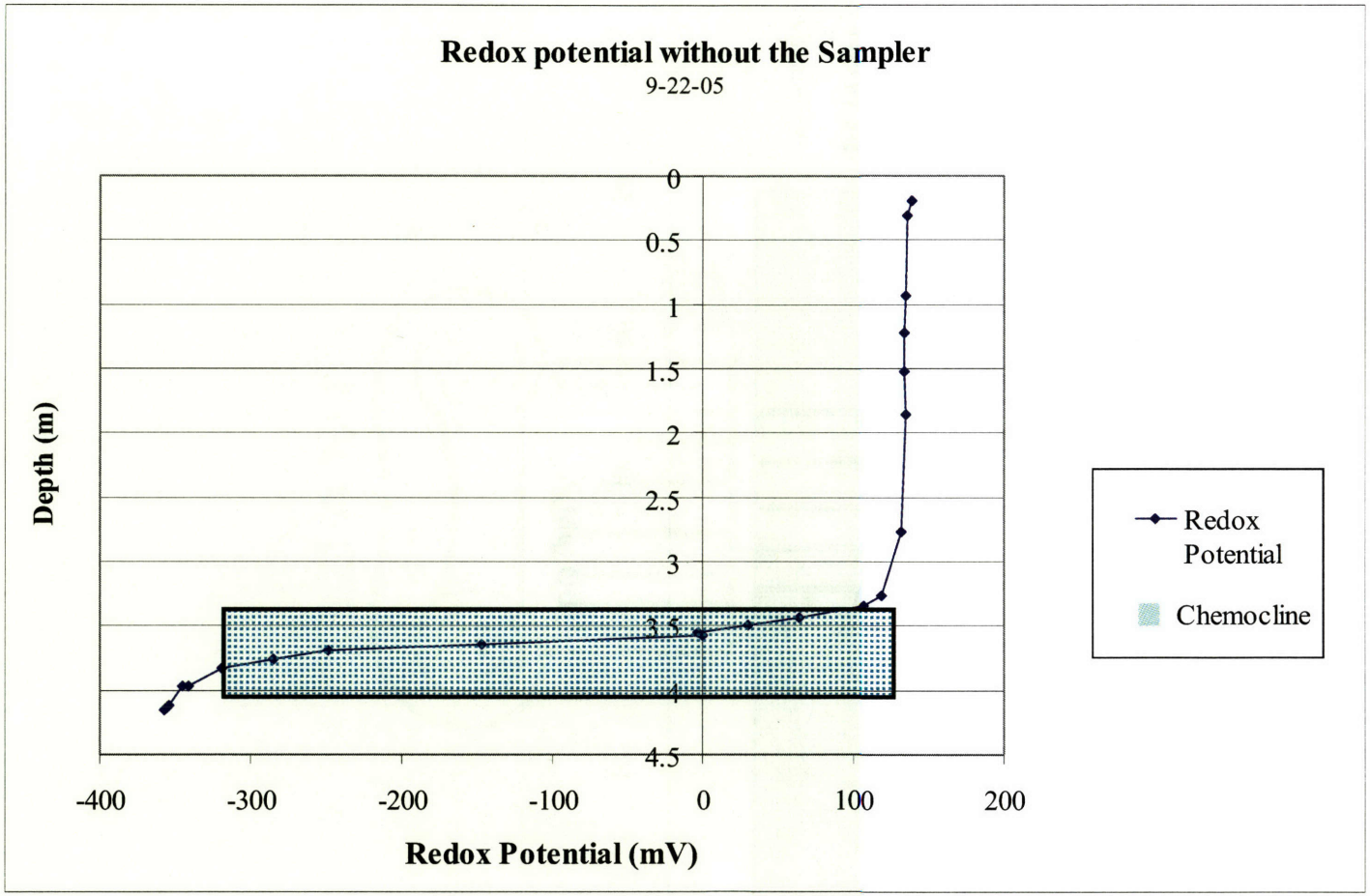


Figure 7 – P.A. Canovas III

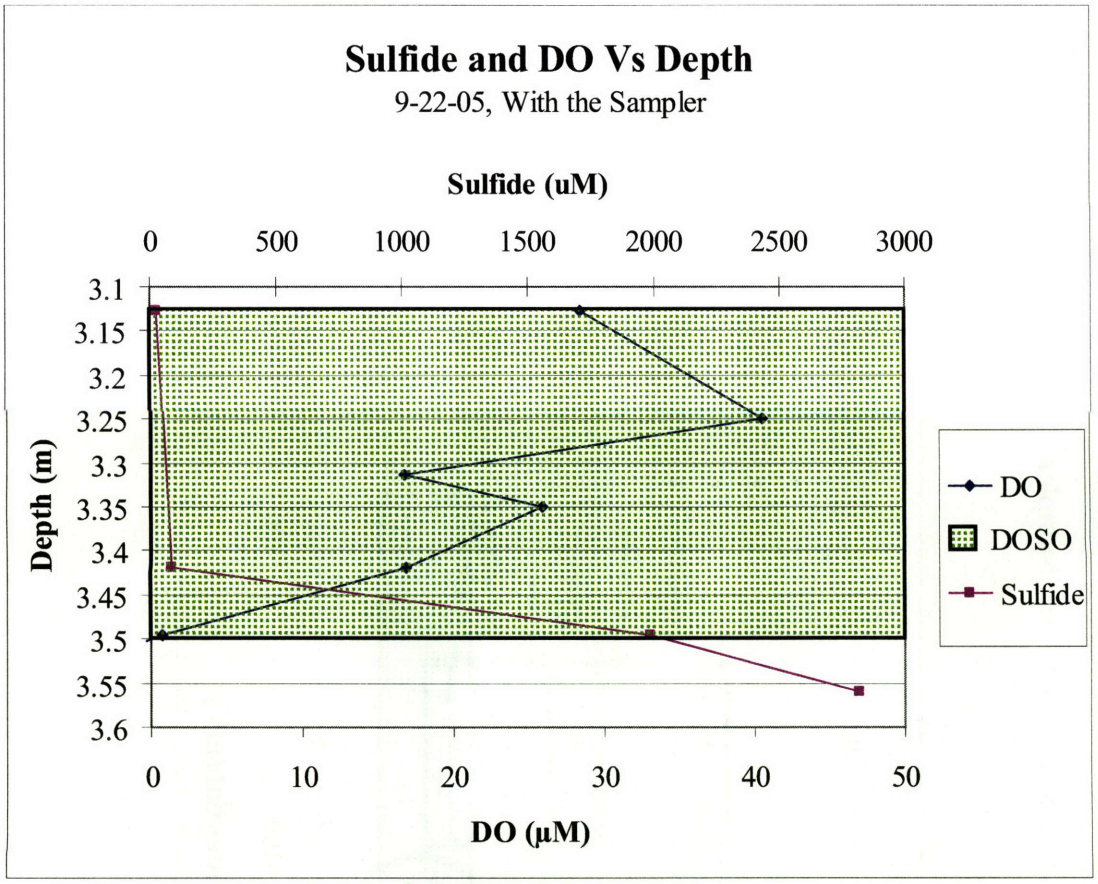


Figure 8 – P.A. Canovas III

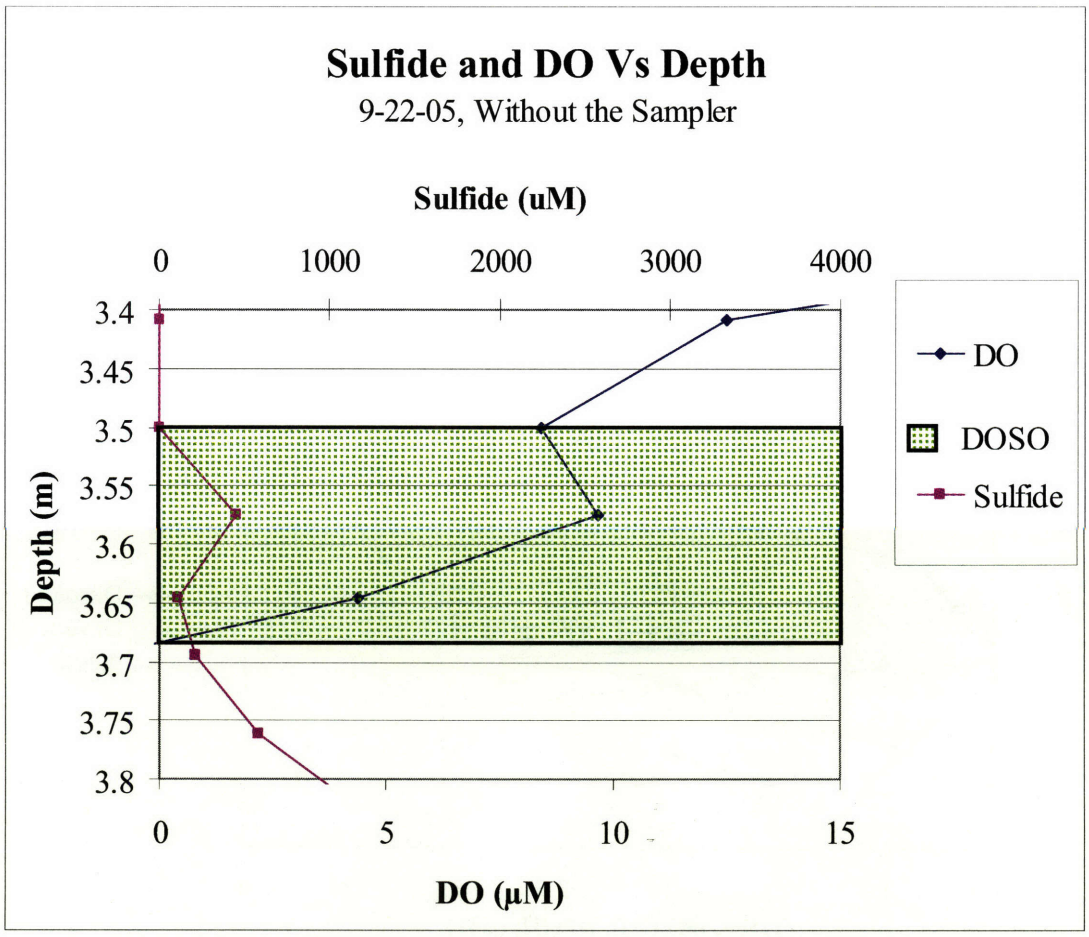


Figure 9 – P.A. Canovas III

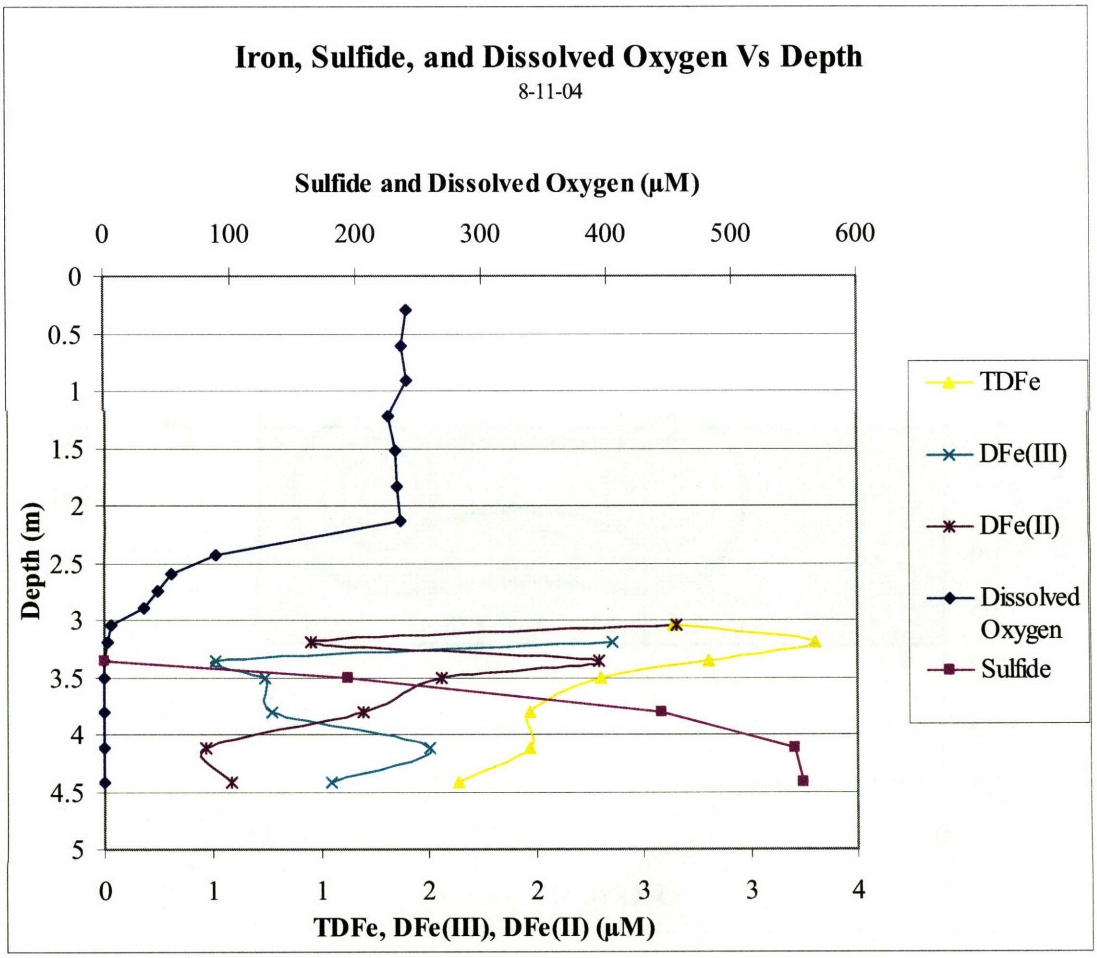


Figure 10 – P.A. Canovas III

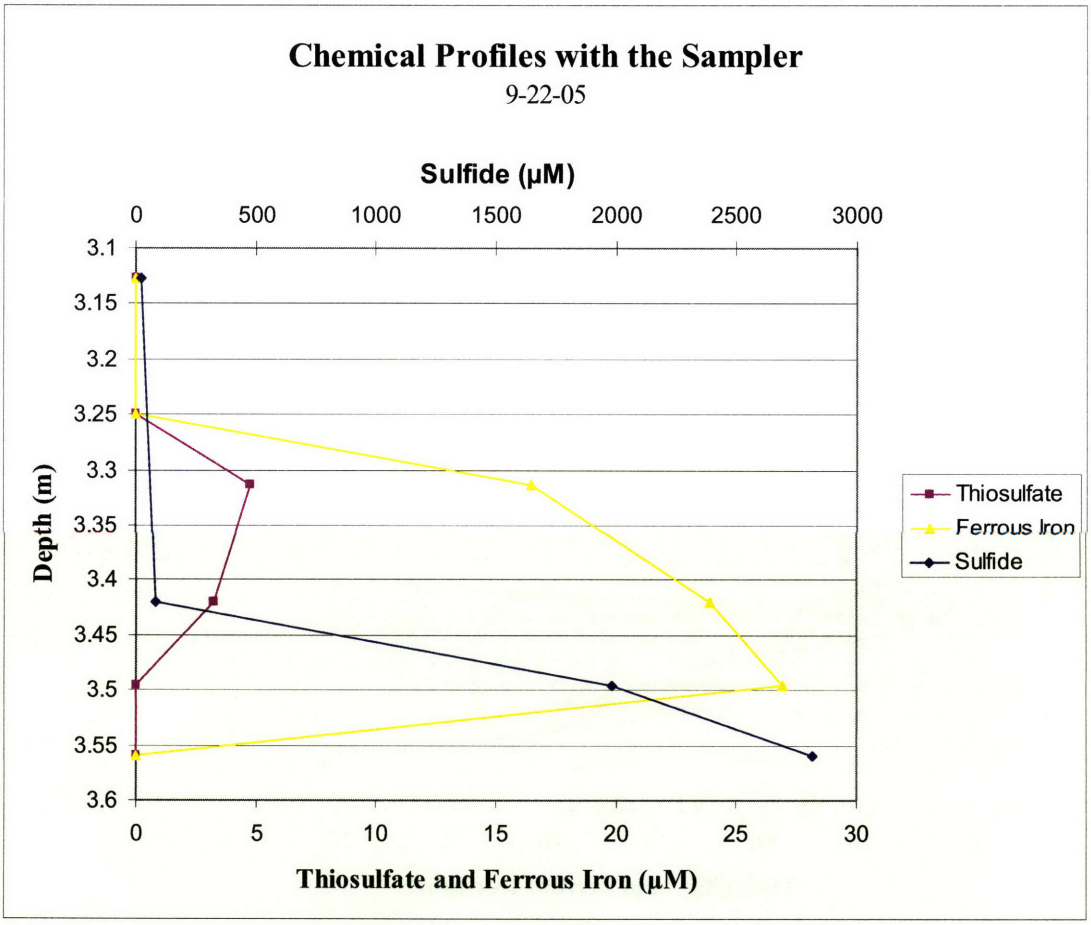


Figure 11 – P.A. Canovas III

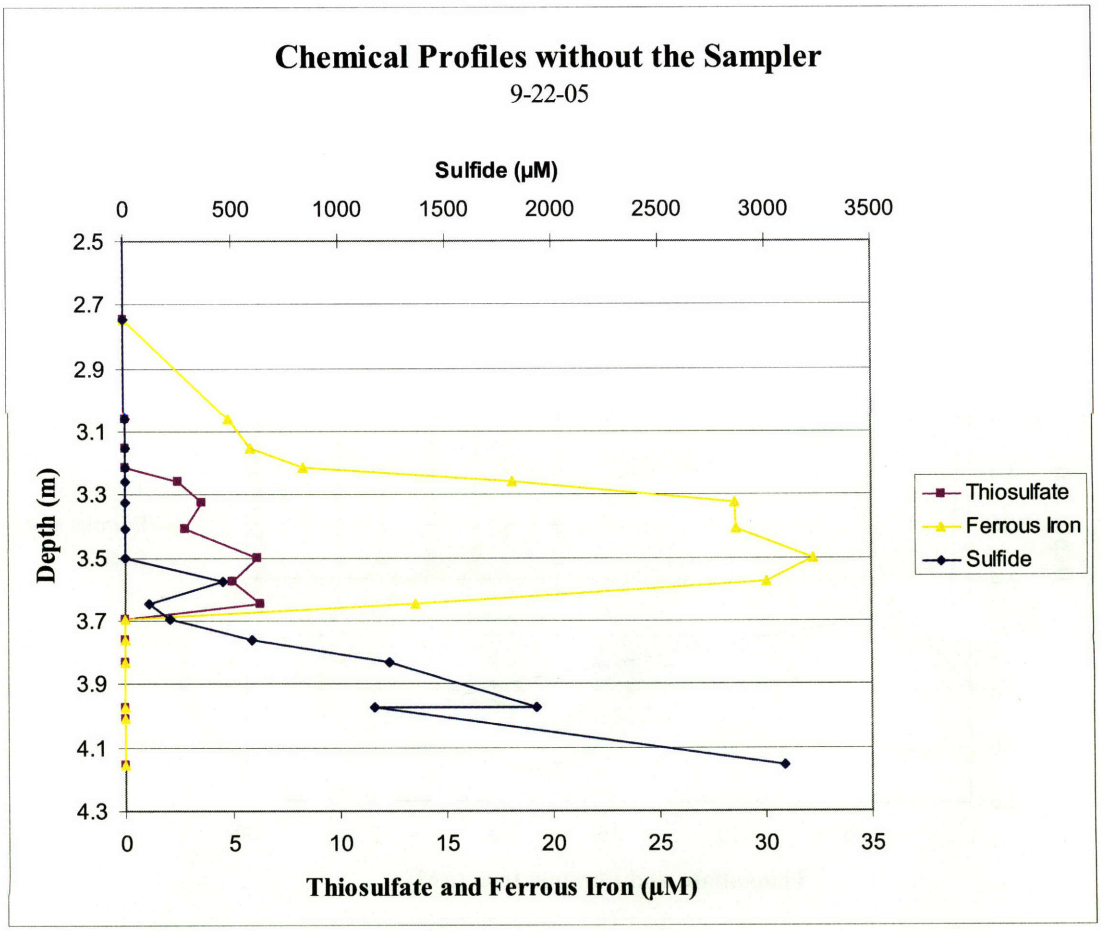


Figure 12 – P.A. Canovas III

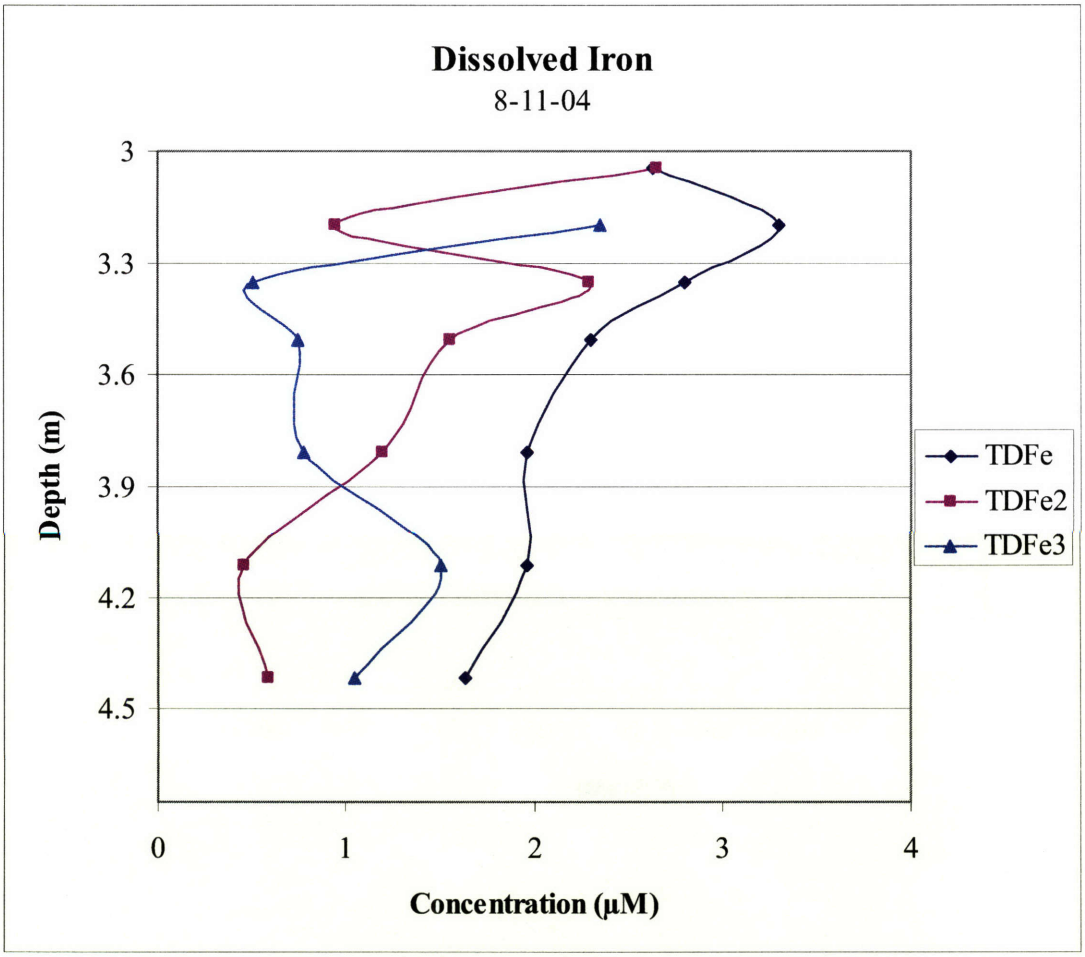


Figure 13 – P.A. Canovas III

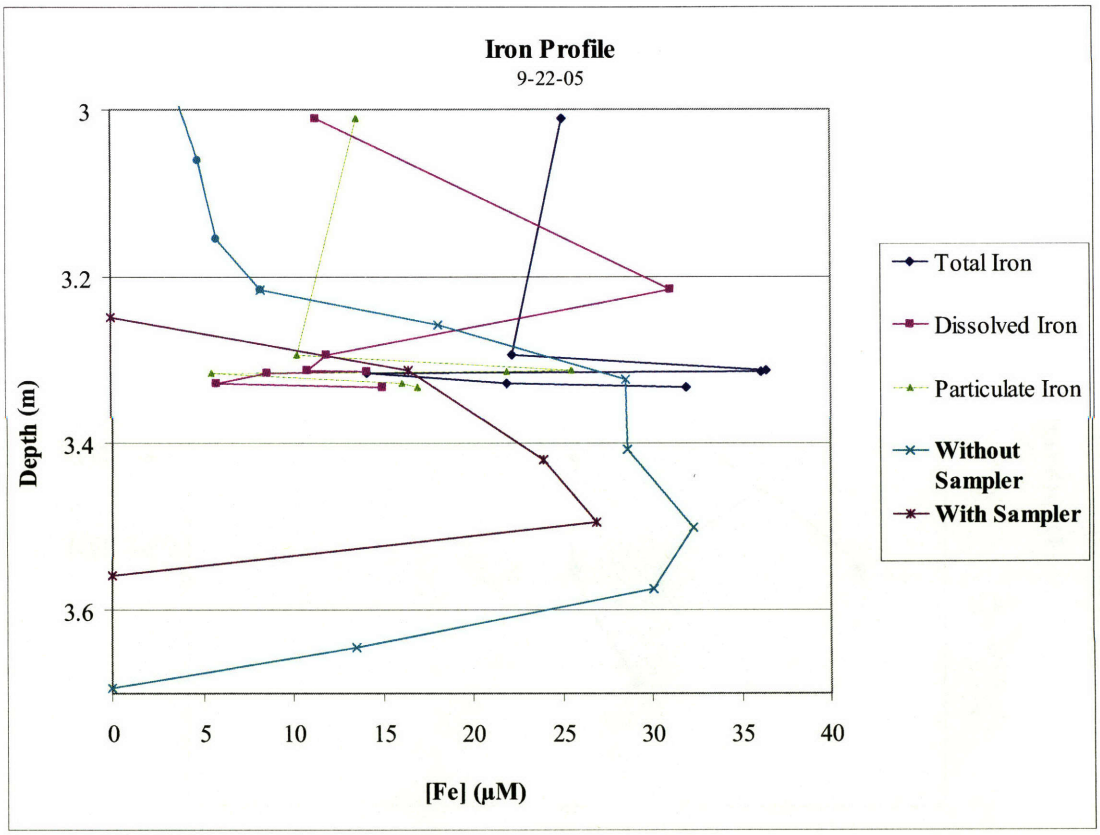


Figure 14 – P.A. Canovas III

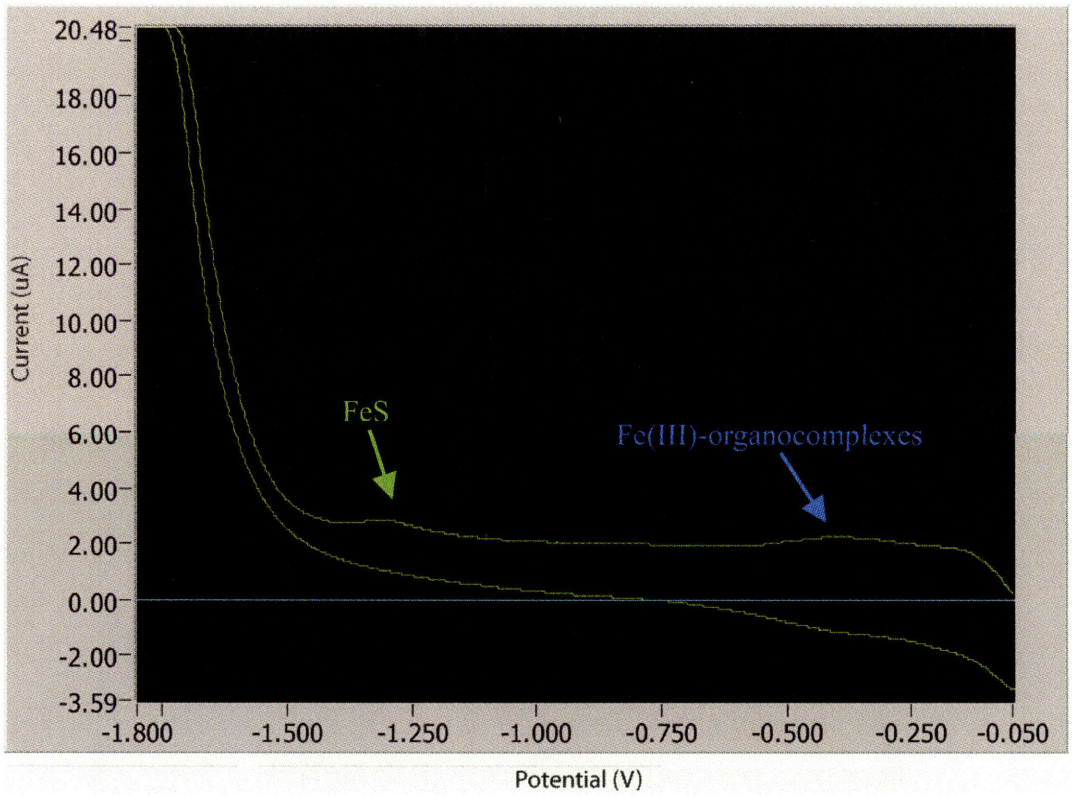


Figure 15 – P.A. Canovas III

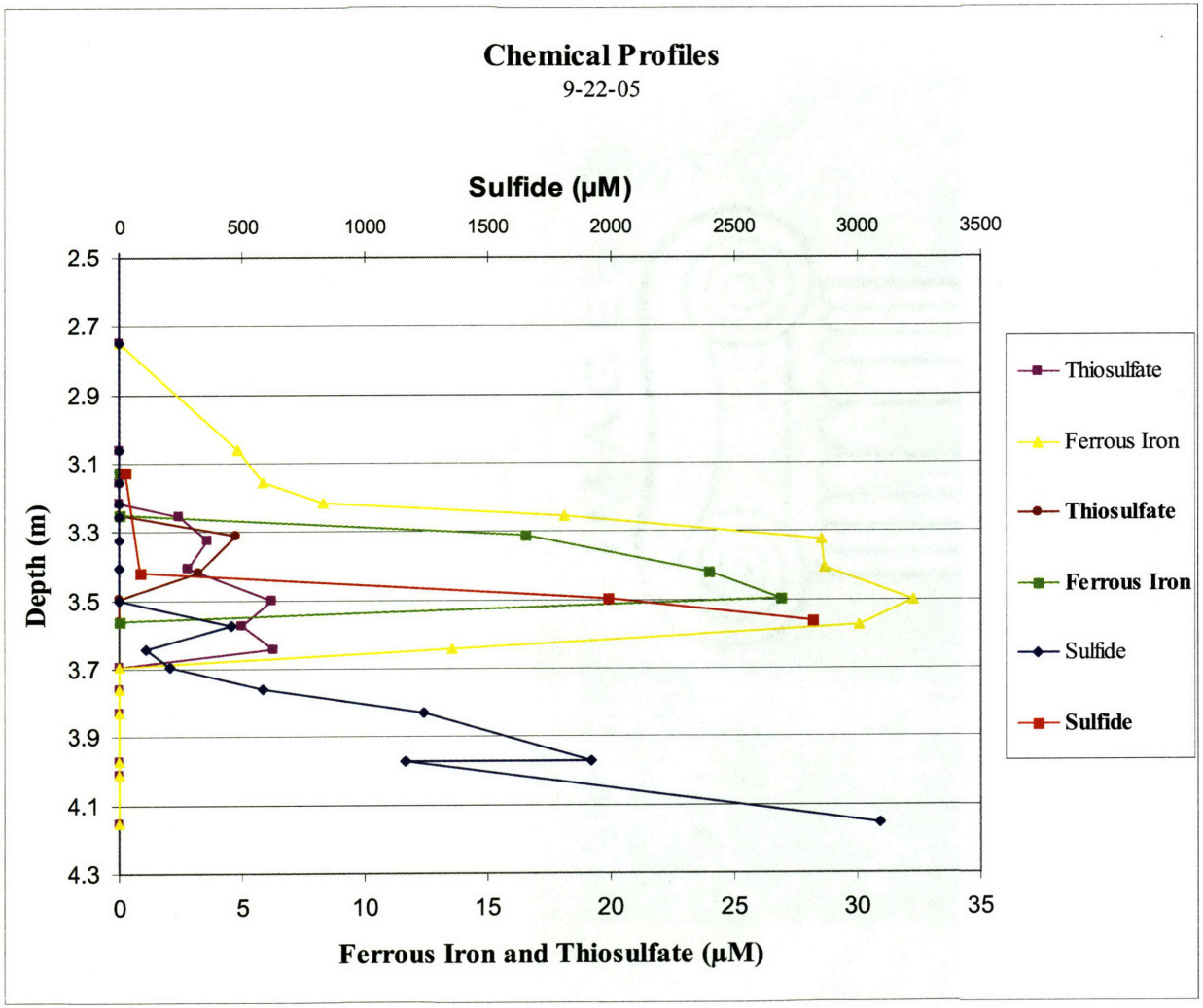


Figure 16 – P.A. Canovas III

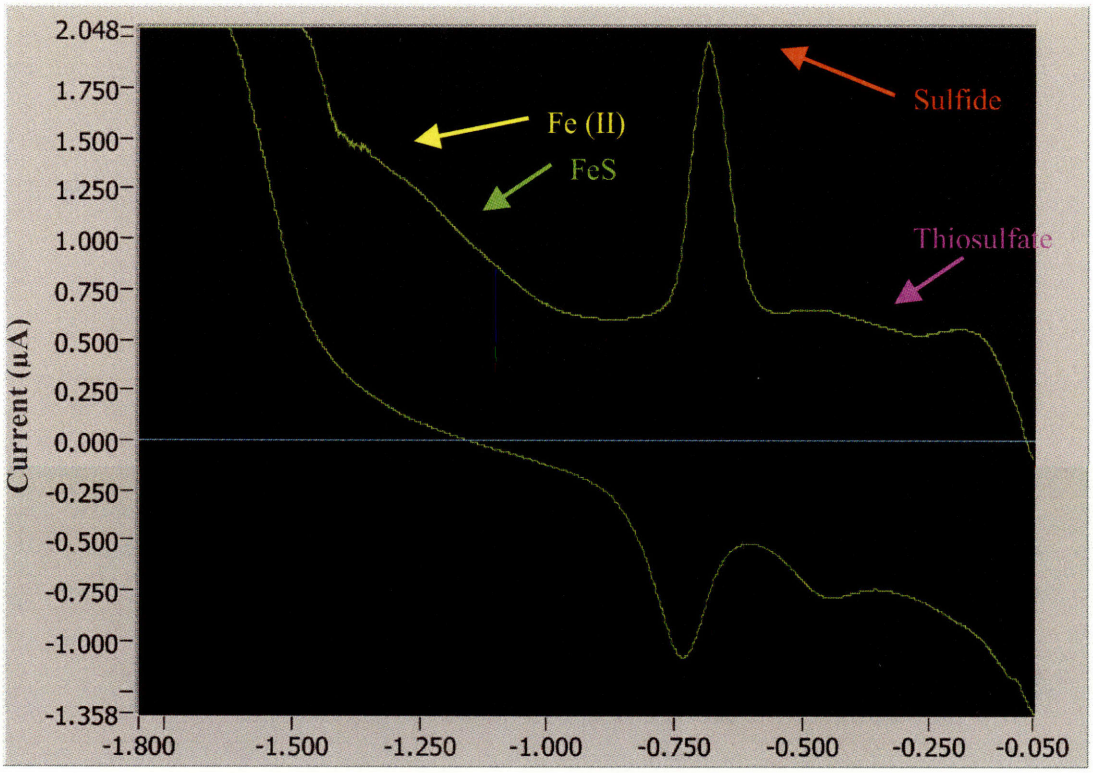


Figure 17 – P.A. Canovas III

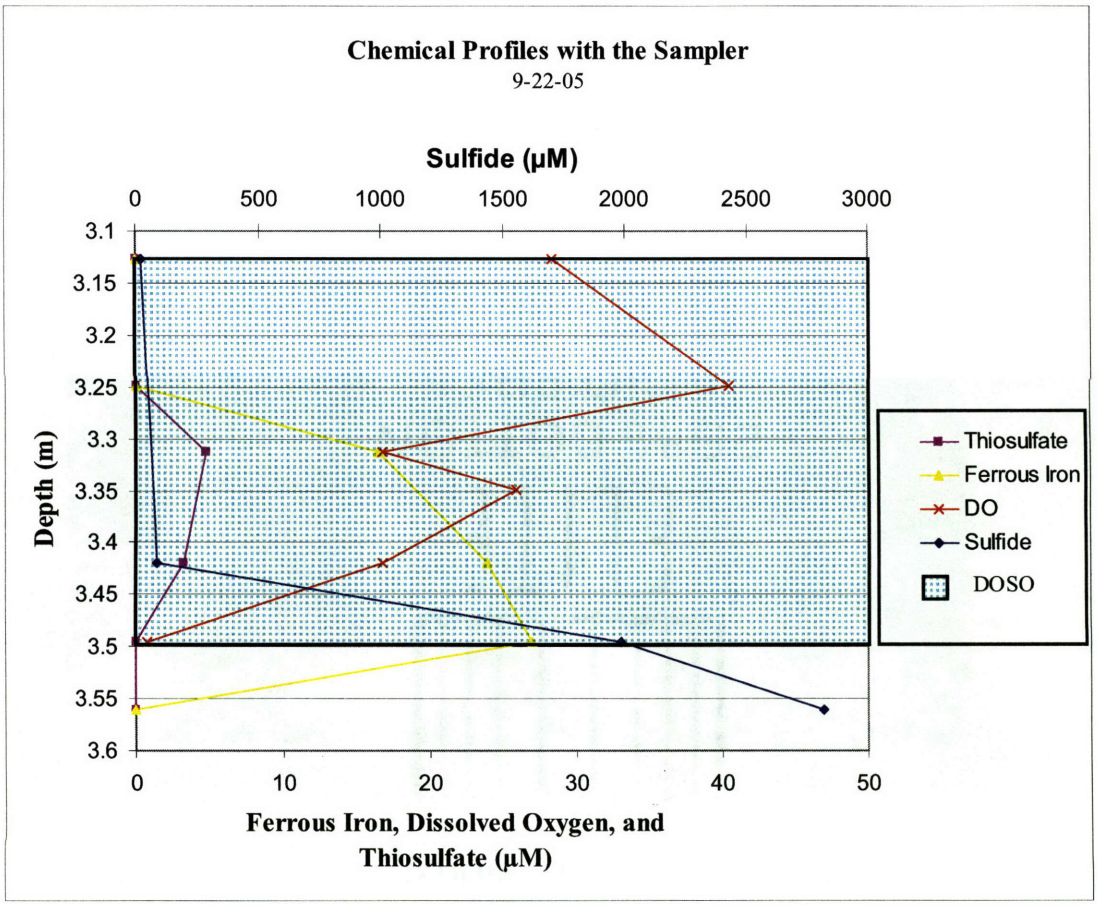


Figure 18 – P.A. Canovas III

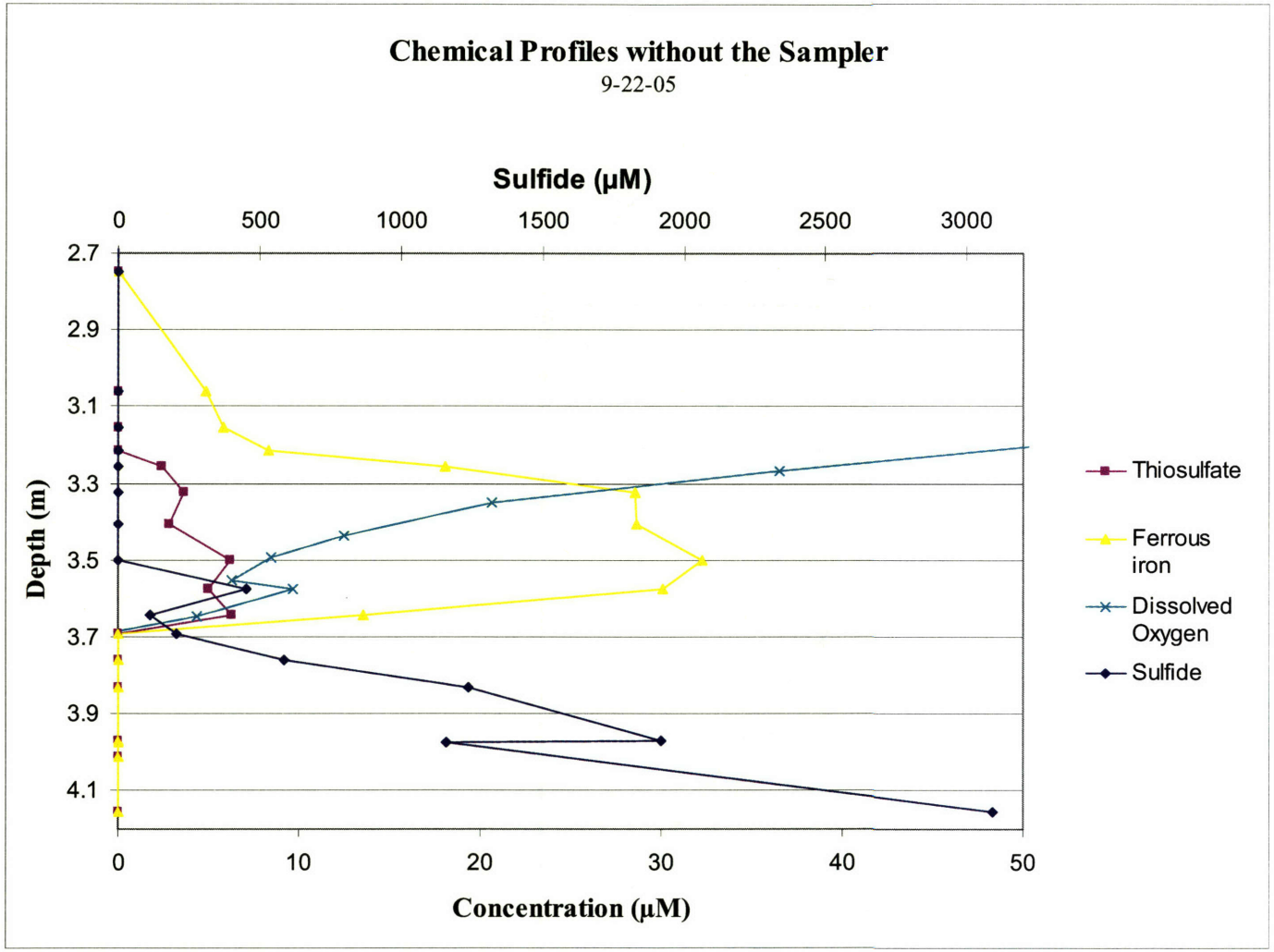


Figure 19 – P.A. Canovas III

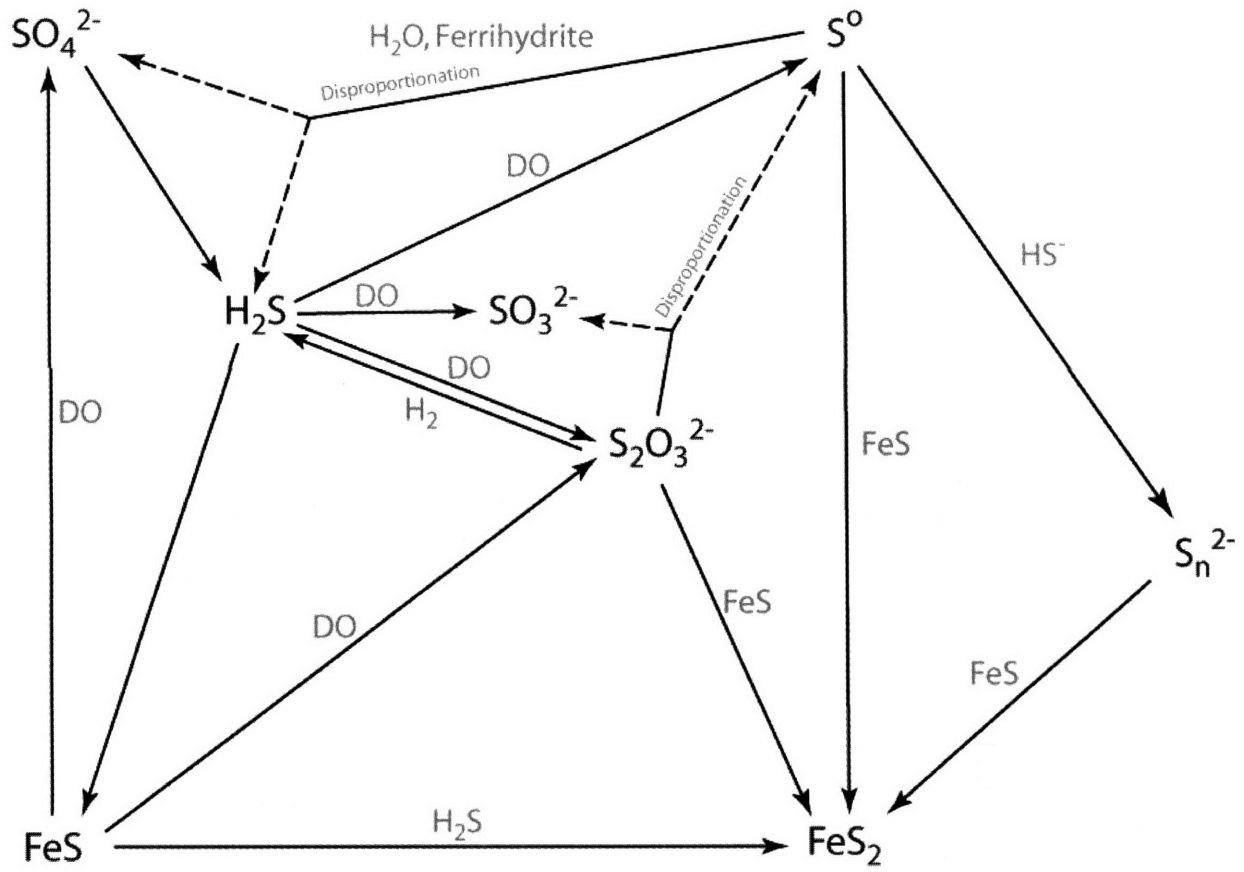


Figure 20 – P.A. Canovas III

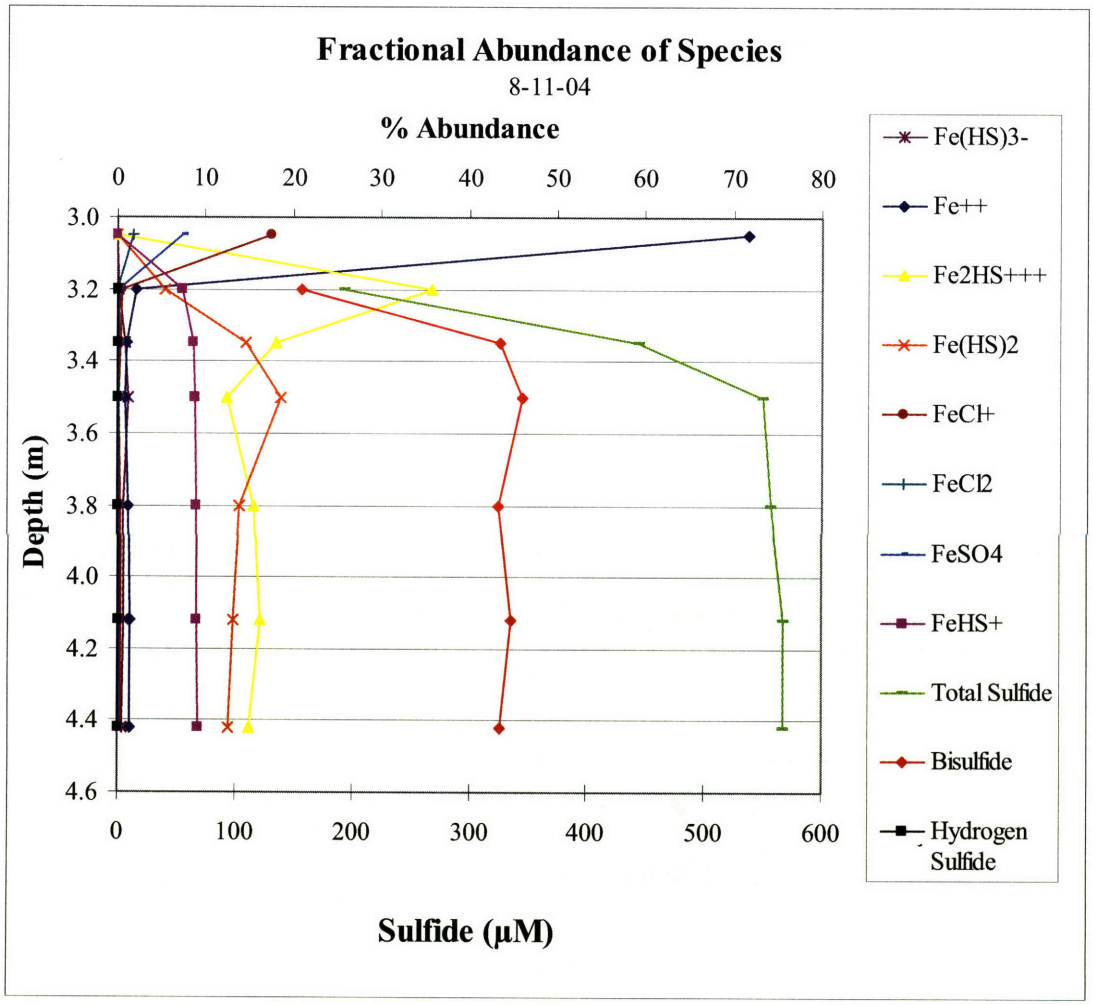


Figure 21 – P.A. Canovas III

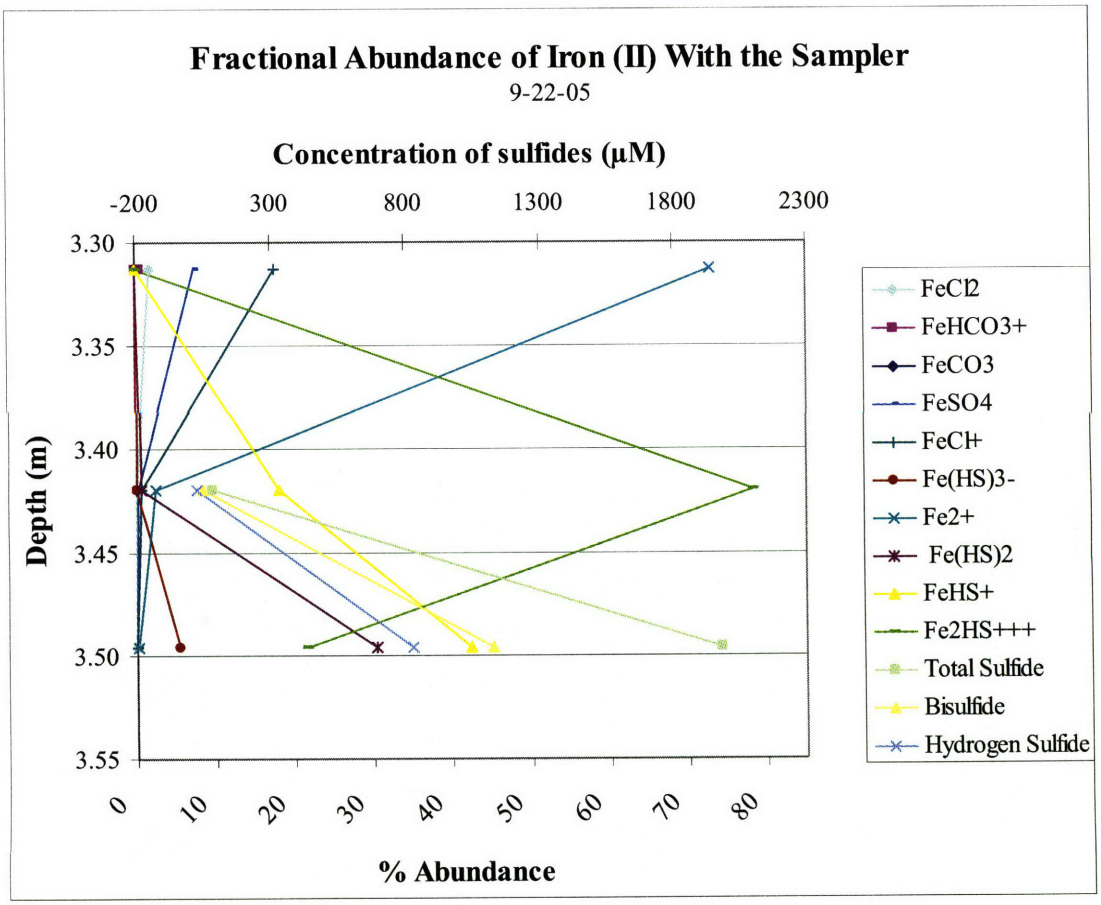


Figure 22 – P.A. Canovas III

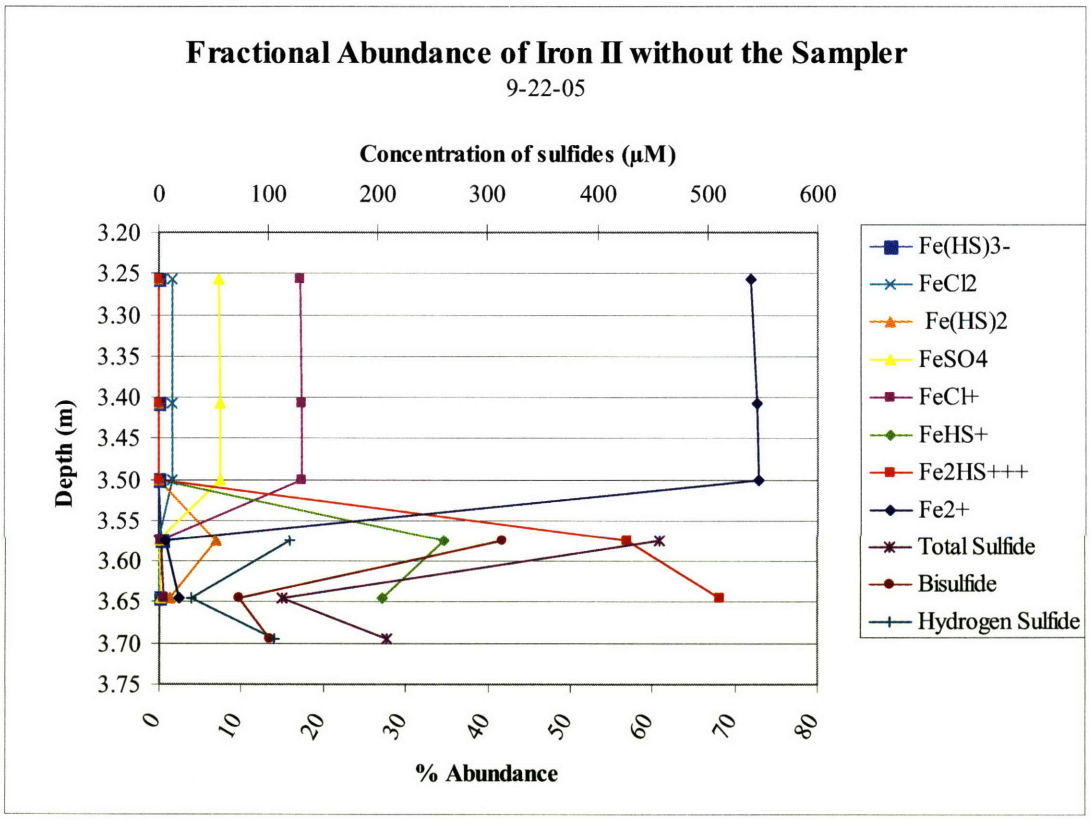


Figure 23 – P.A. Canovas III

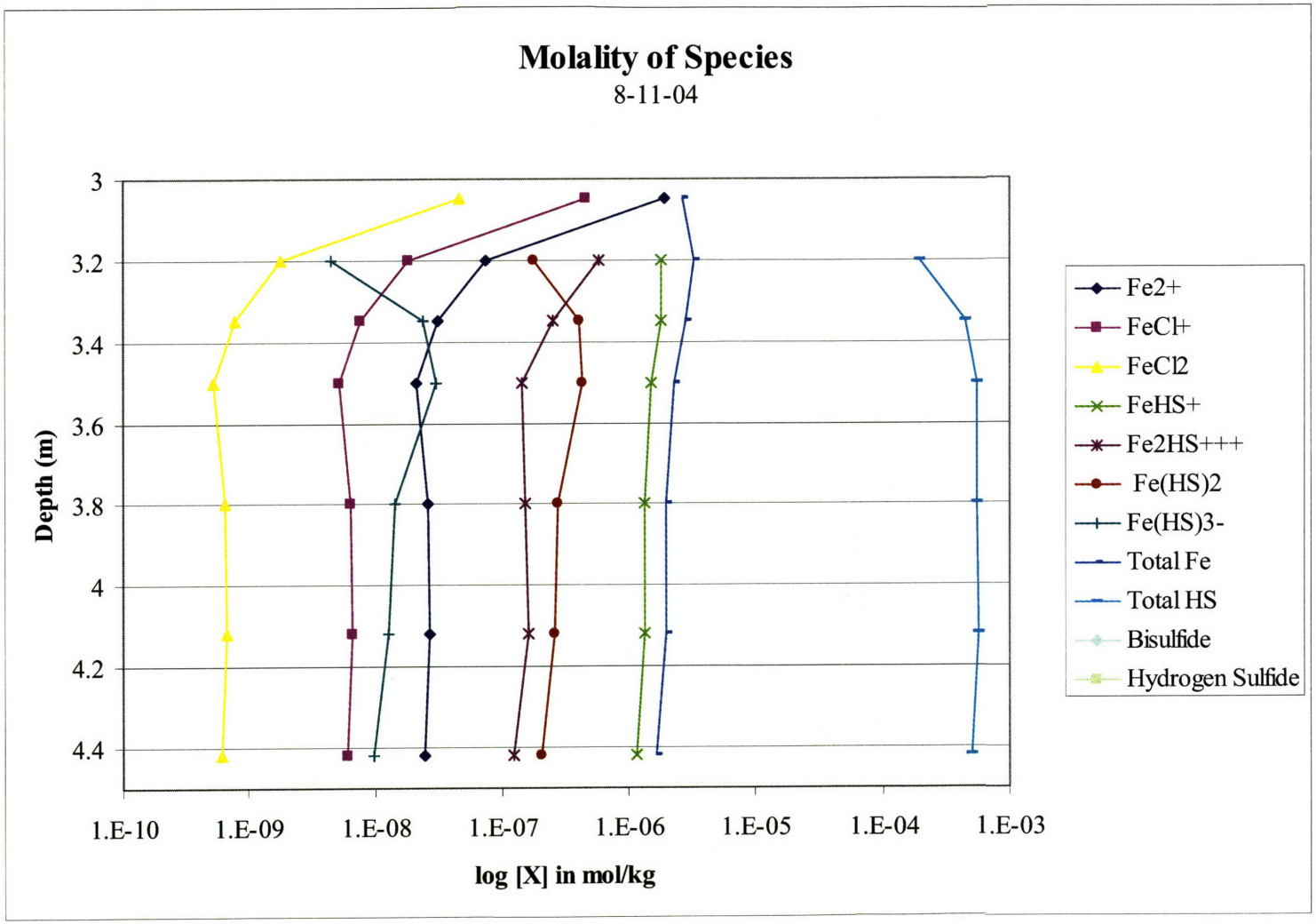


Figure 24 – P.A. Canovas III

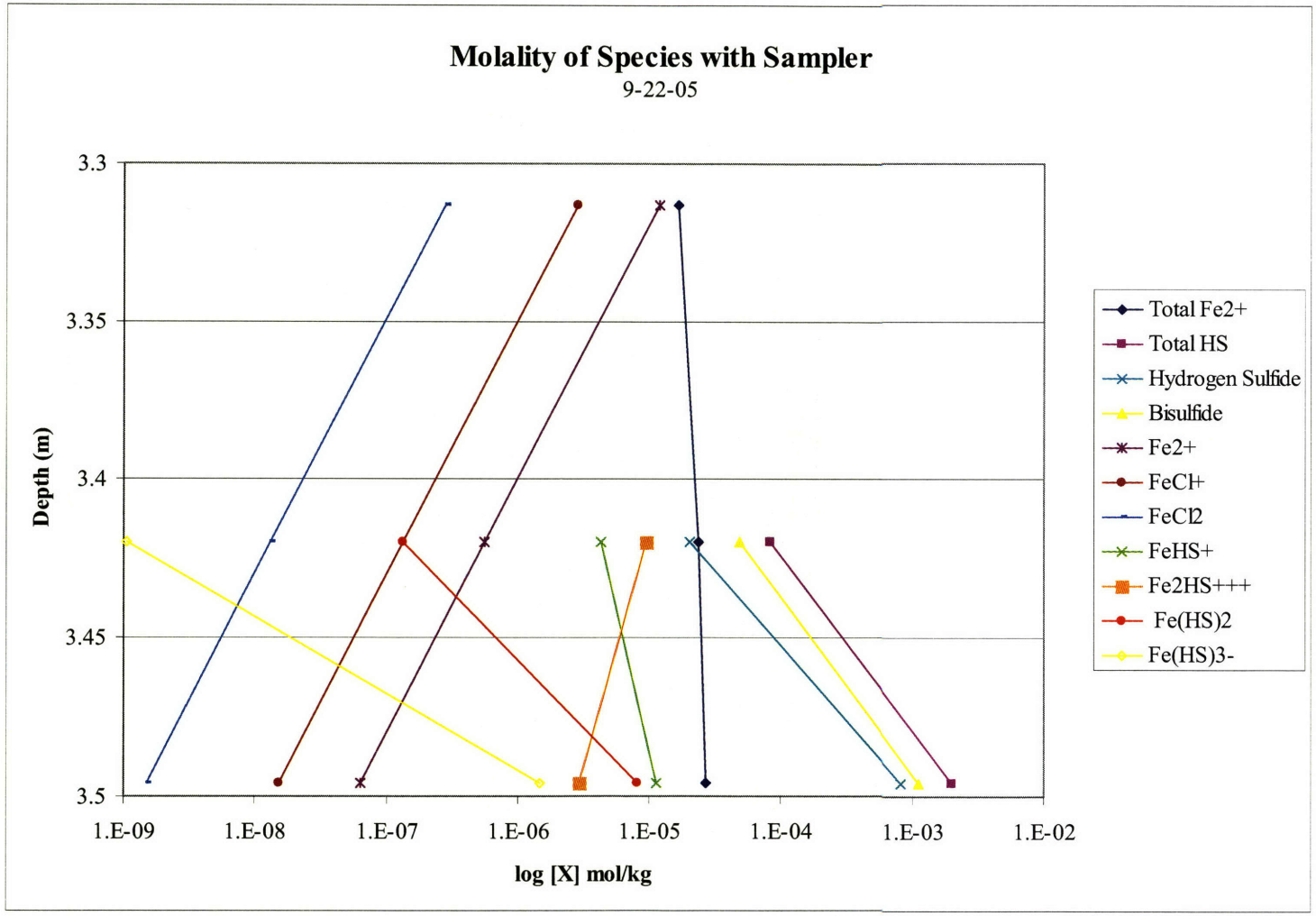


Figure 25 – P.A. Canovas III

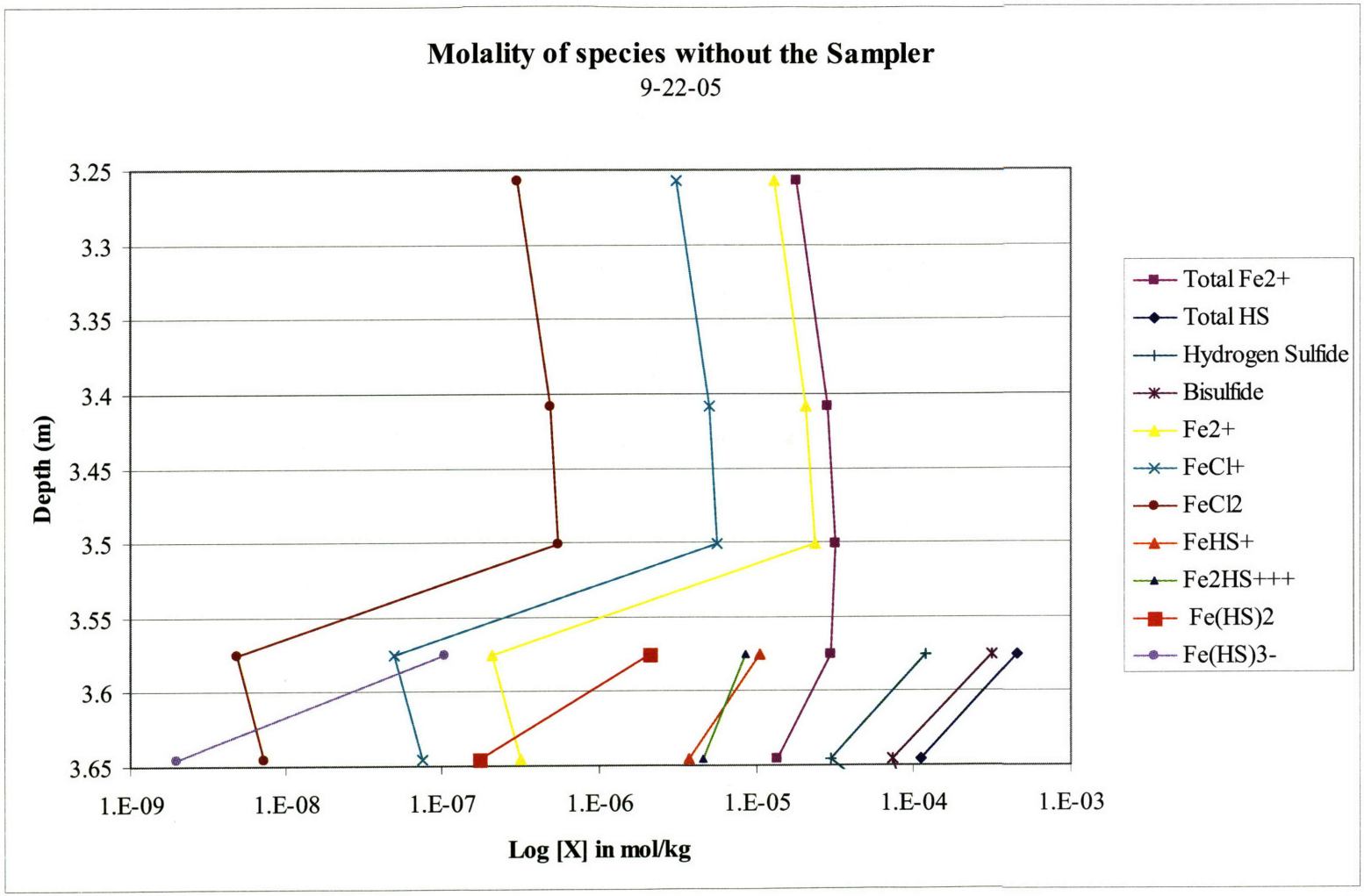


Figure 26 – P.A. Canovas III

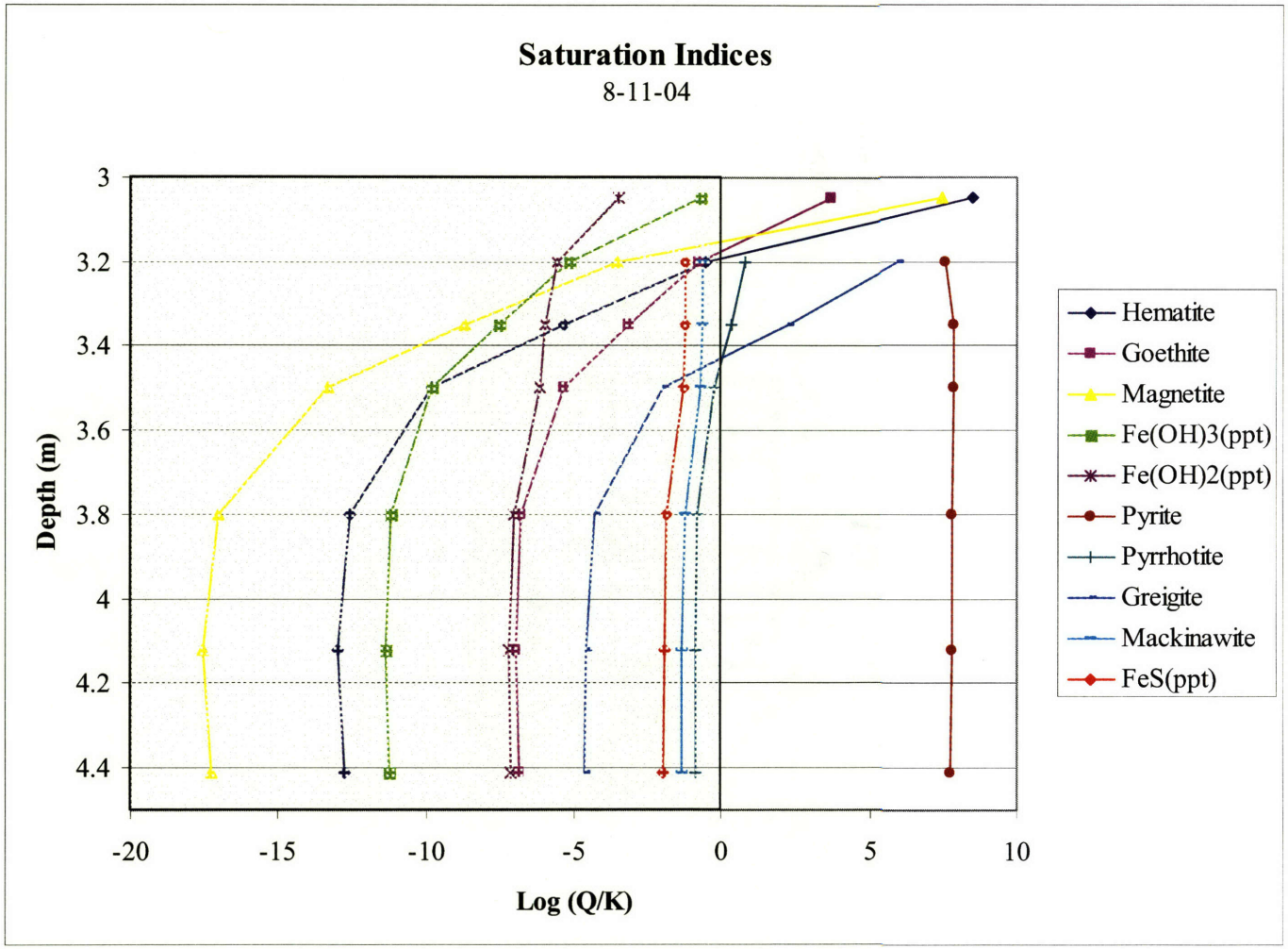


Figure 27 – P.A. Canovas III

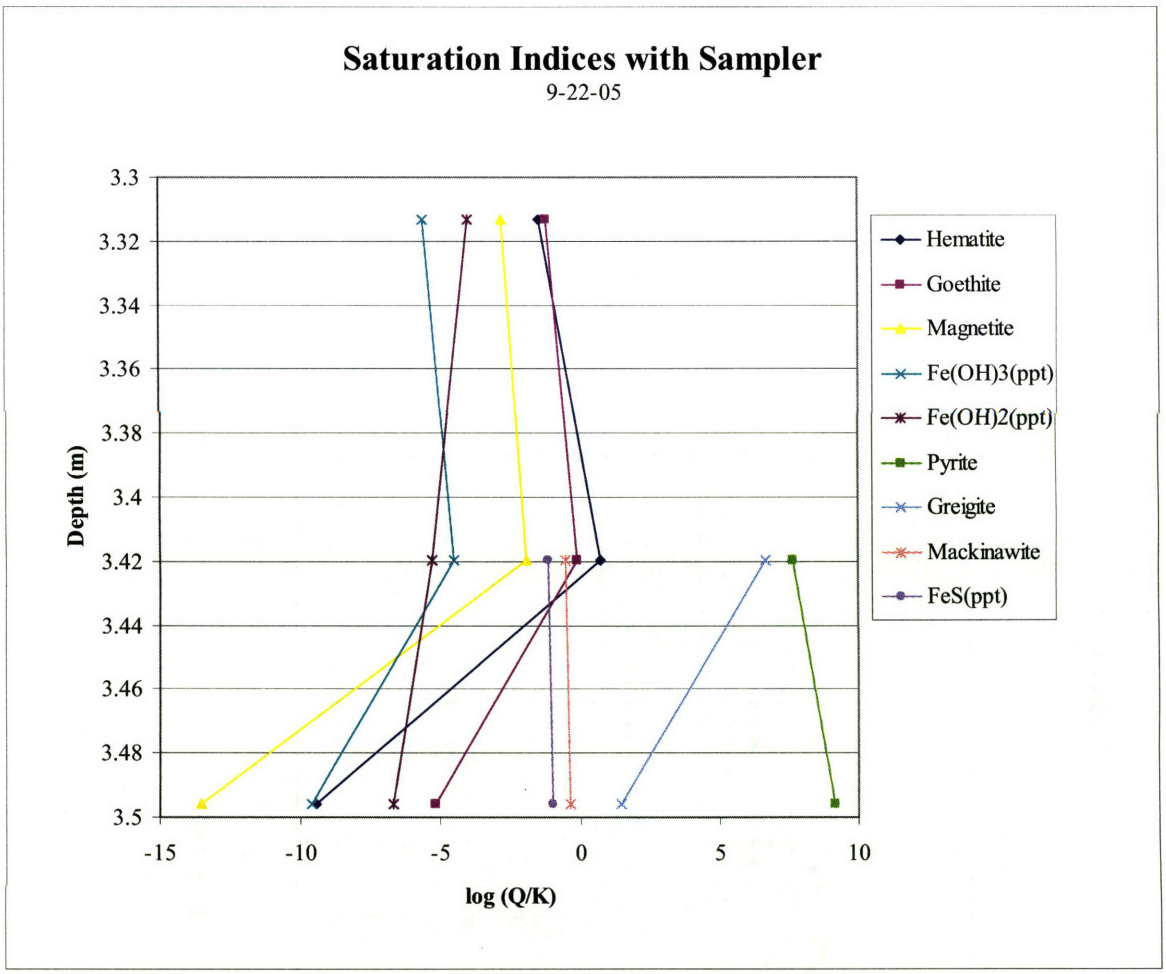


Figure 28 – P.A. Canovas III

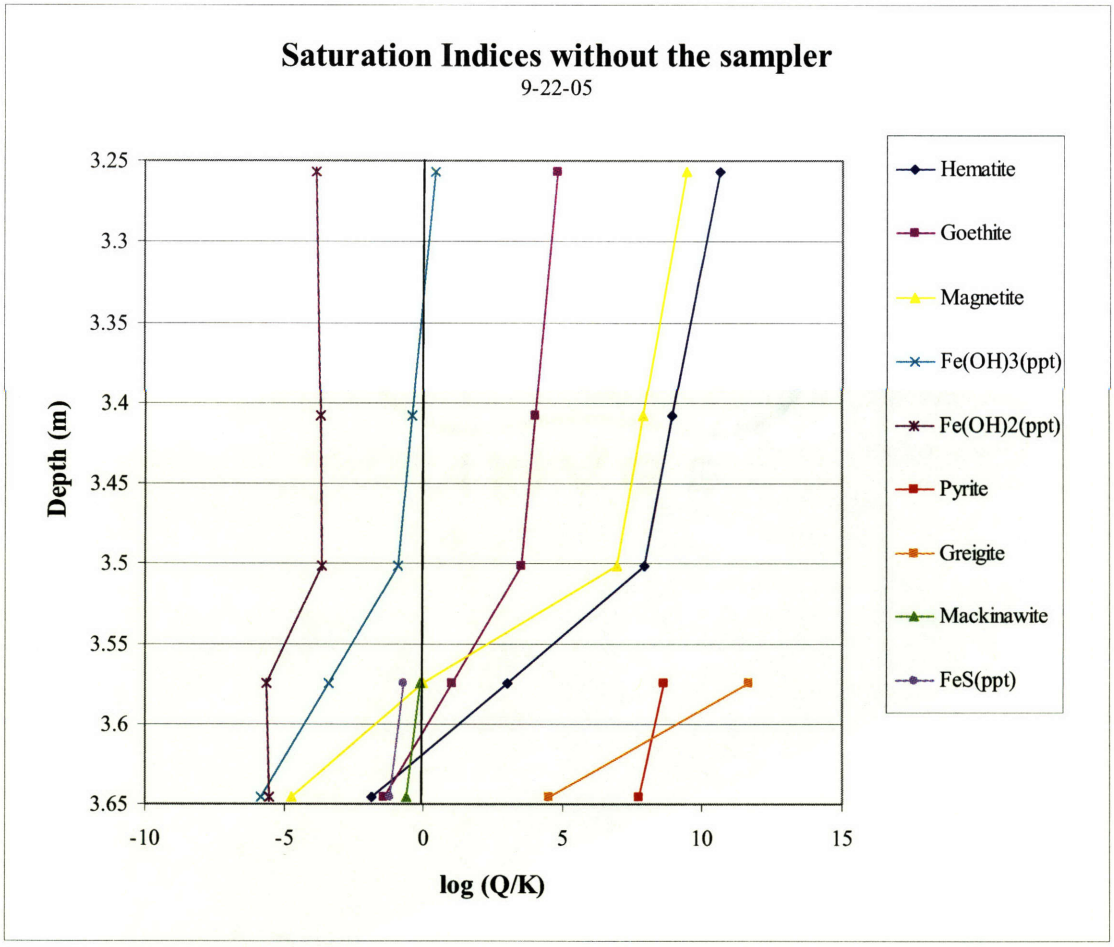


Figure 29 – P.A. Canovas III

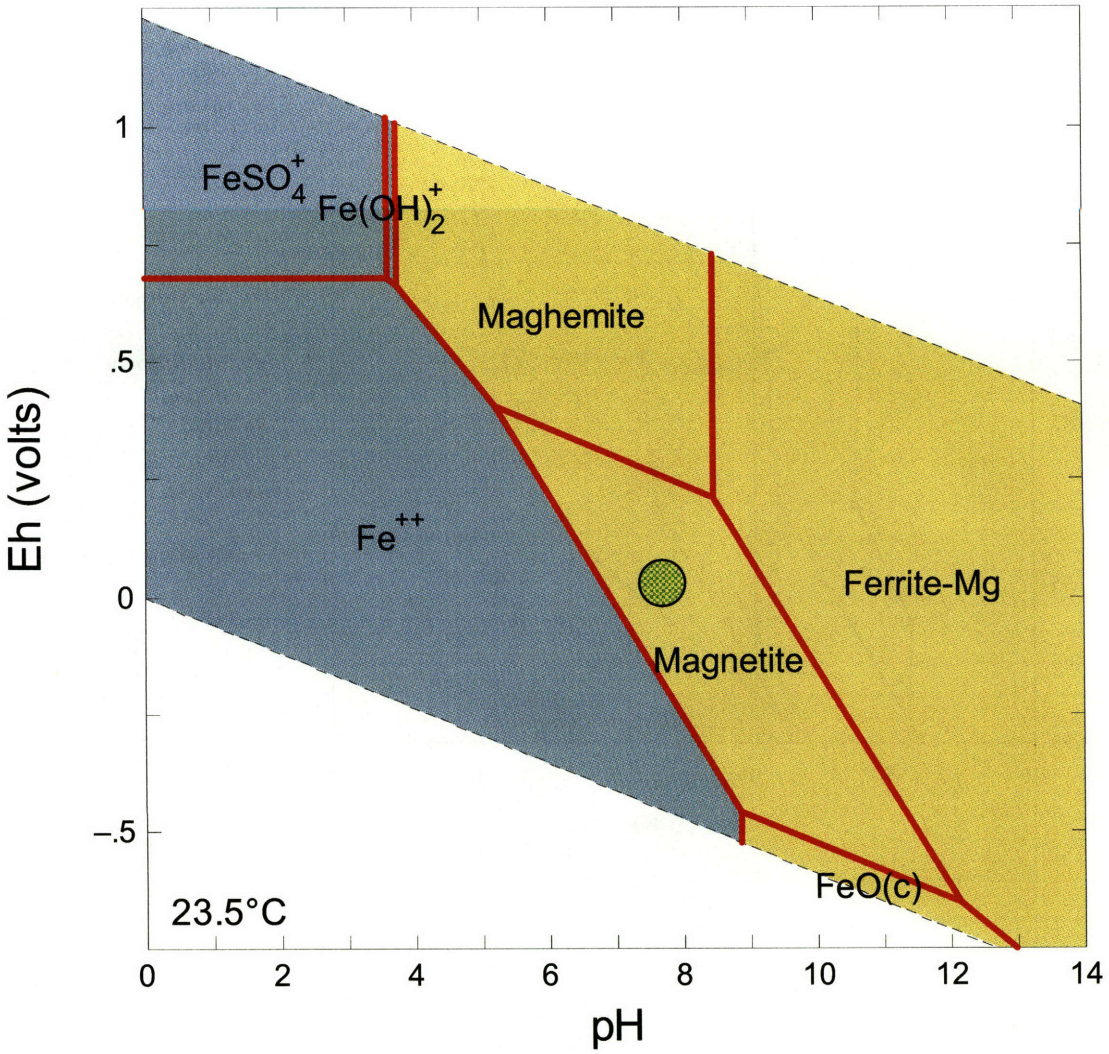


Figure 30 – P.A. Canovas III

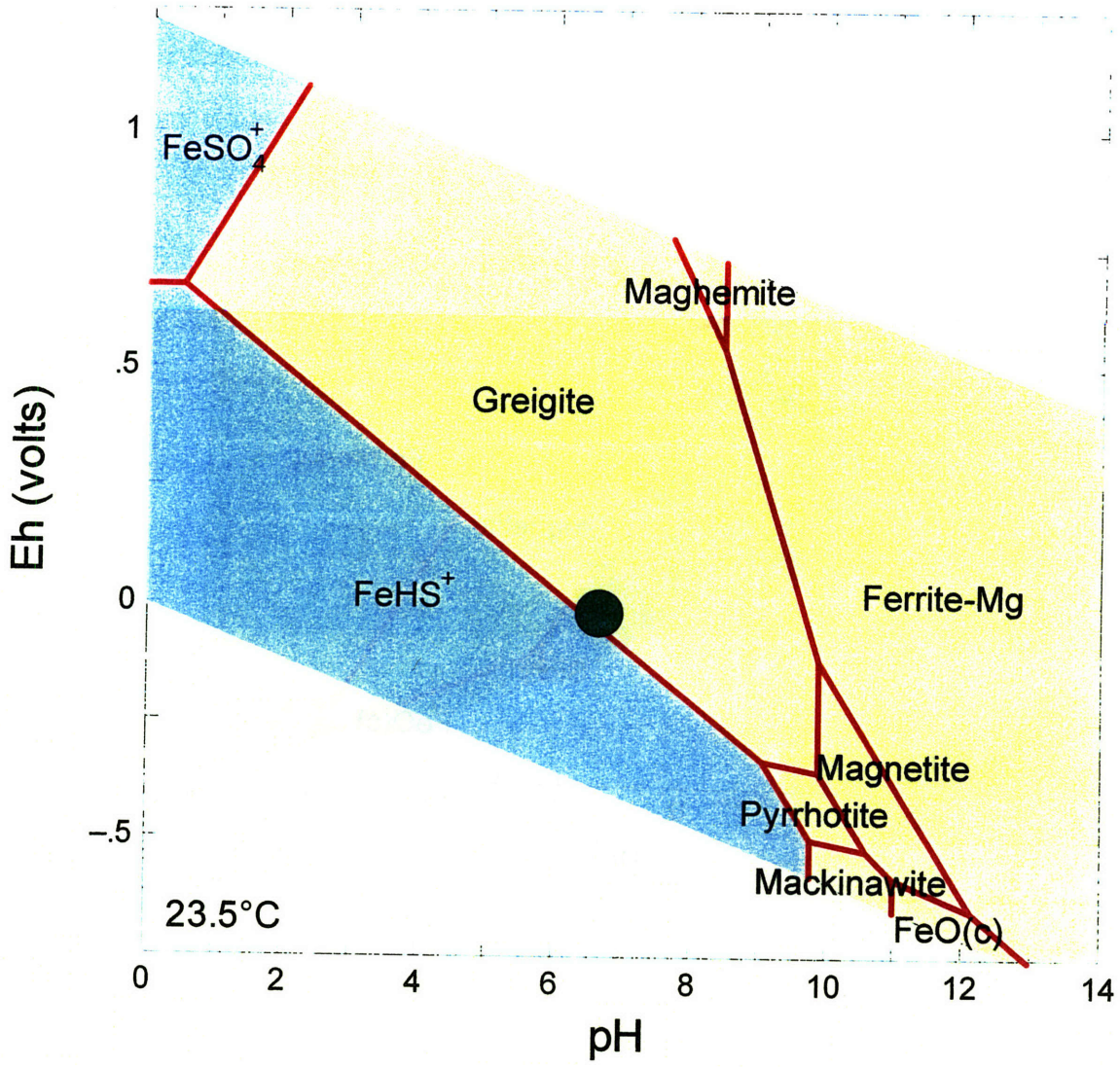


Figure 31– P.A. Canovas III

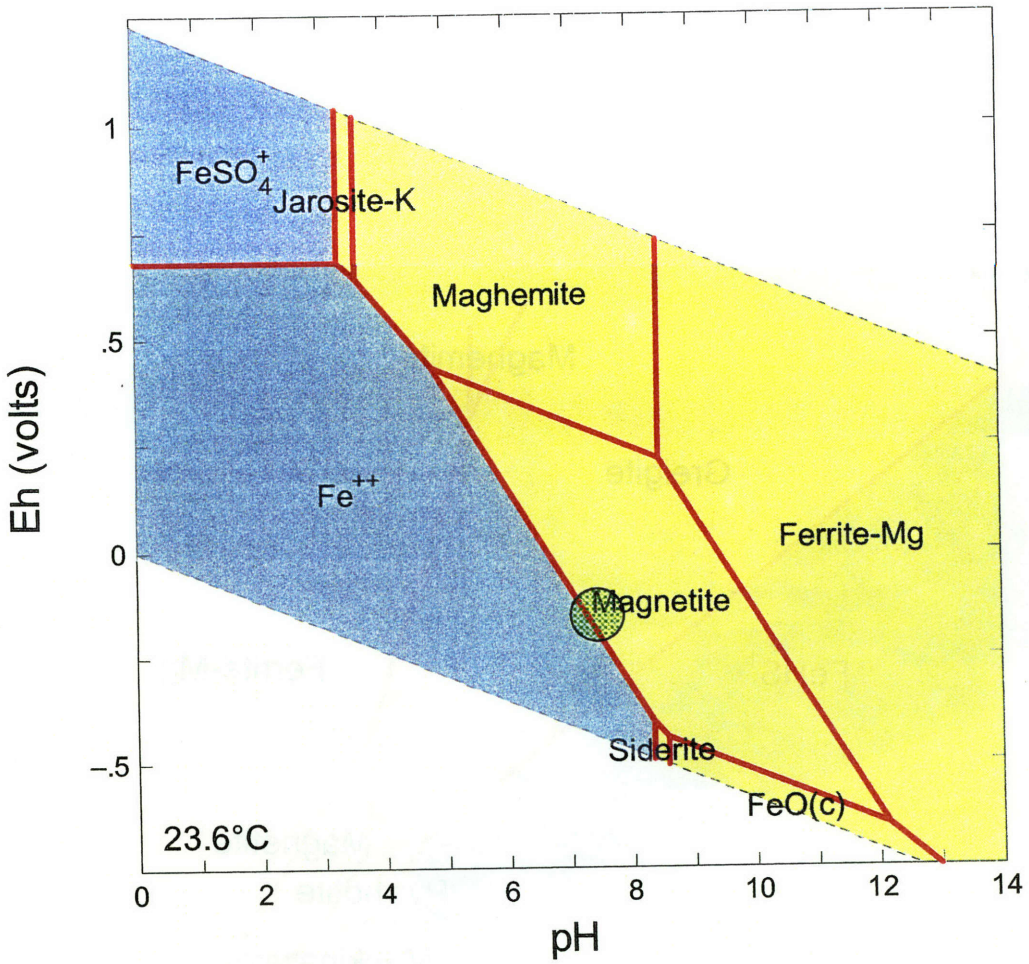


Figure 32 – P.A. Canovas III

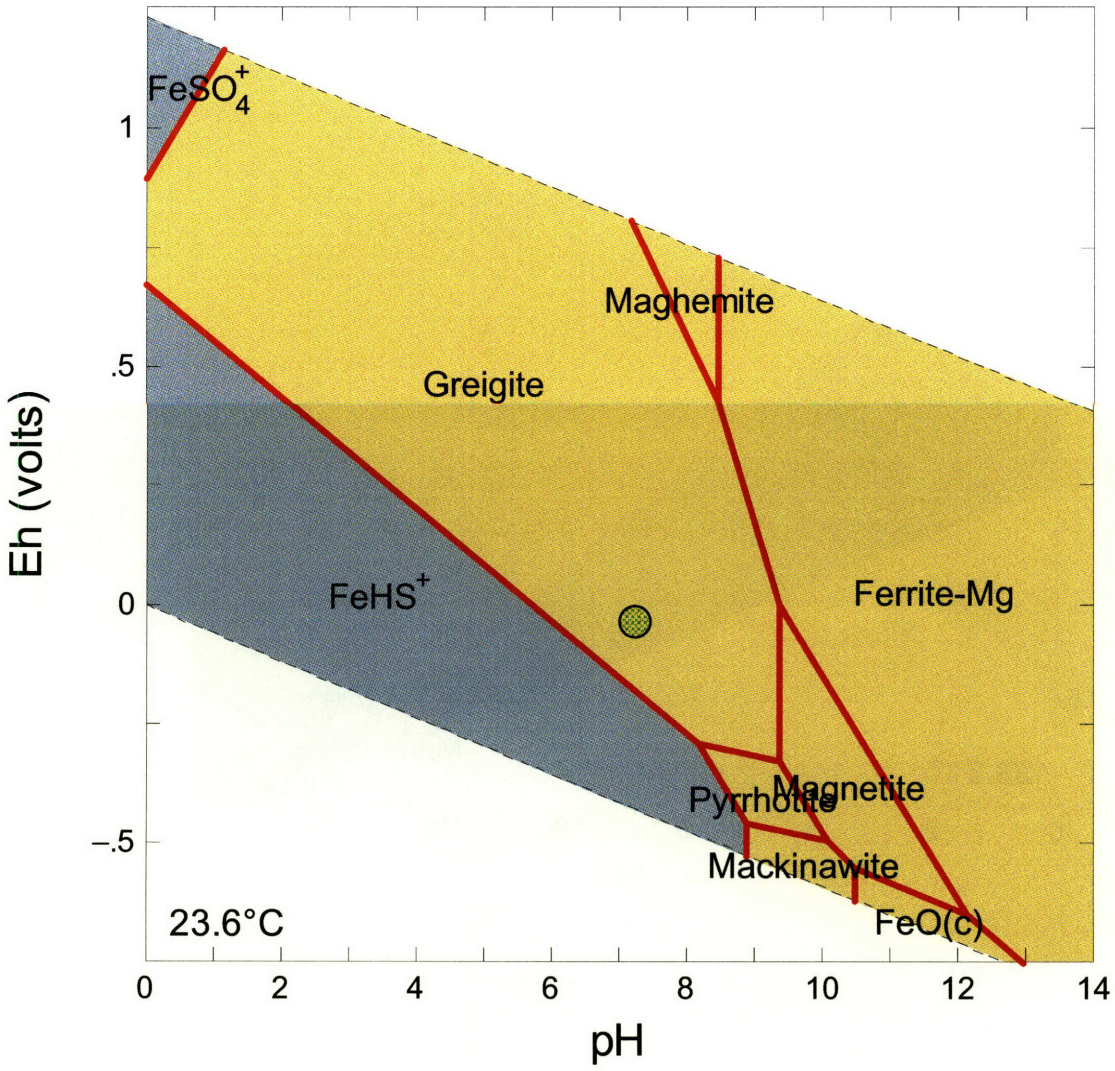


Figure 33 – P.A. Canovas III

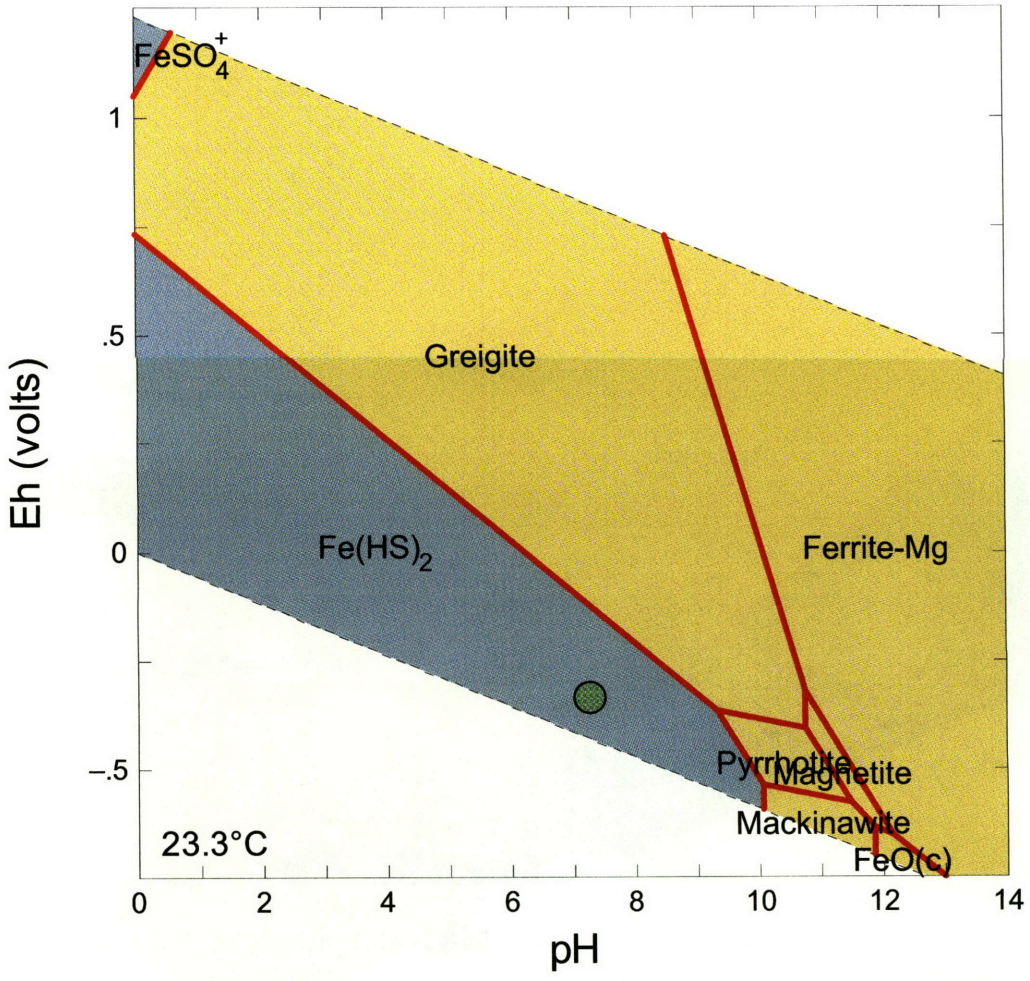


Figure 34 – P.A. Canovas III

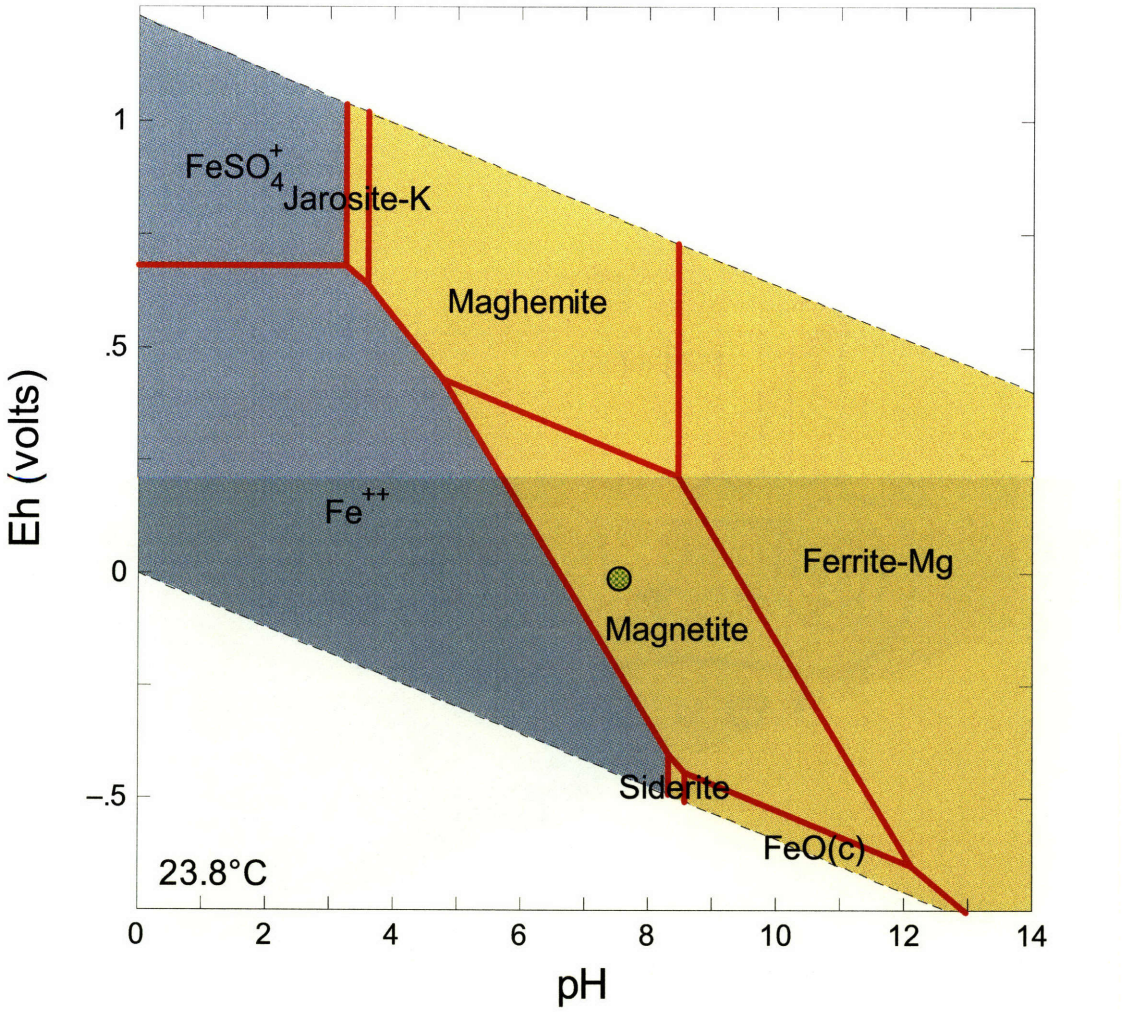


Figure 35– P.A. Canovas III

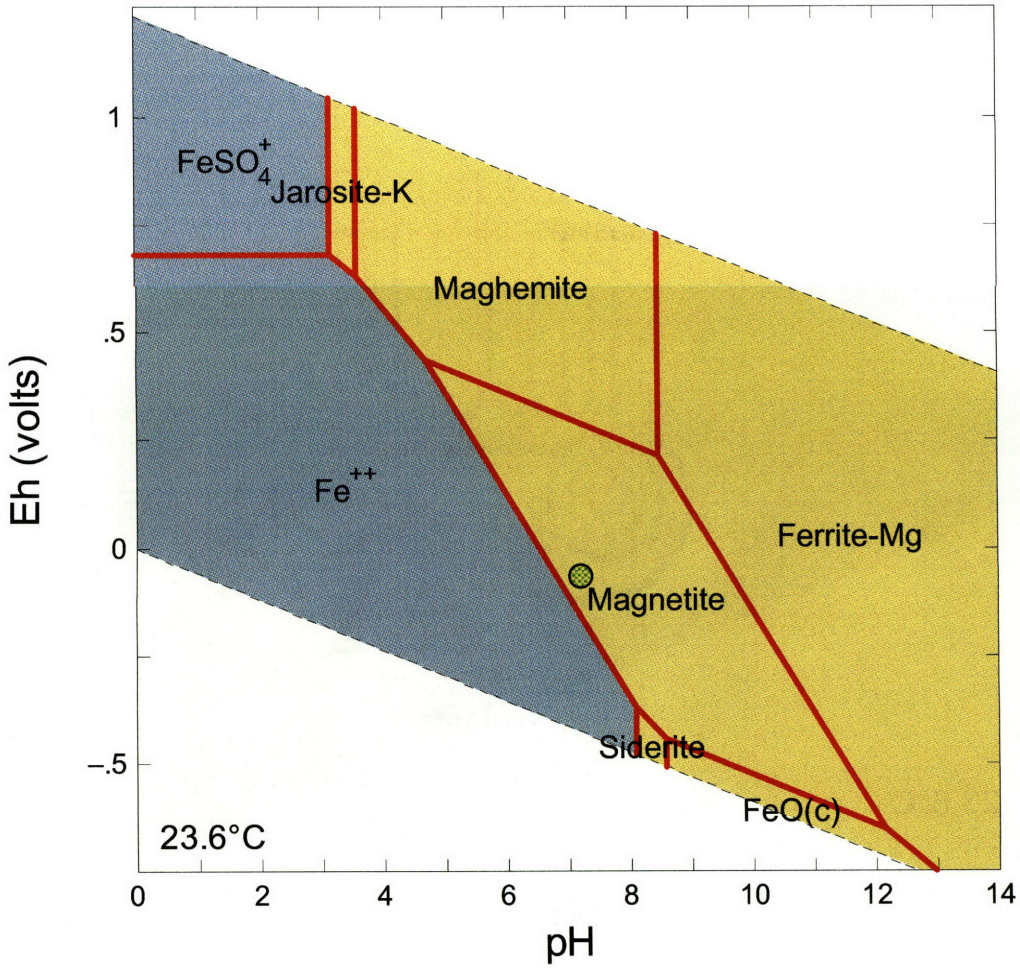


Figure 36 – P.A. Canovas III

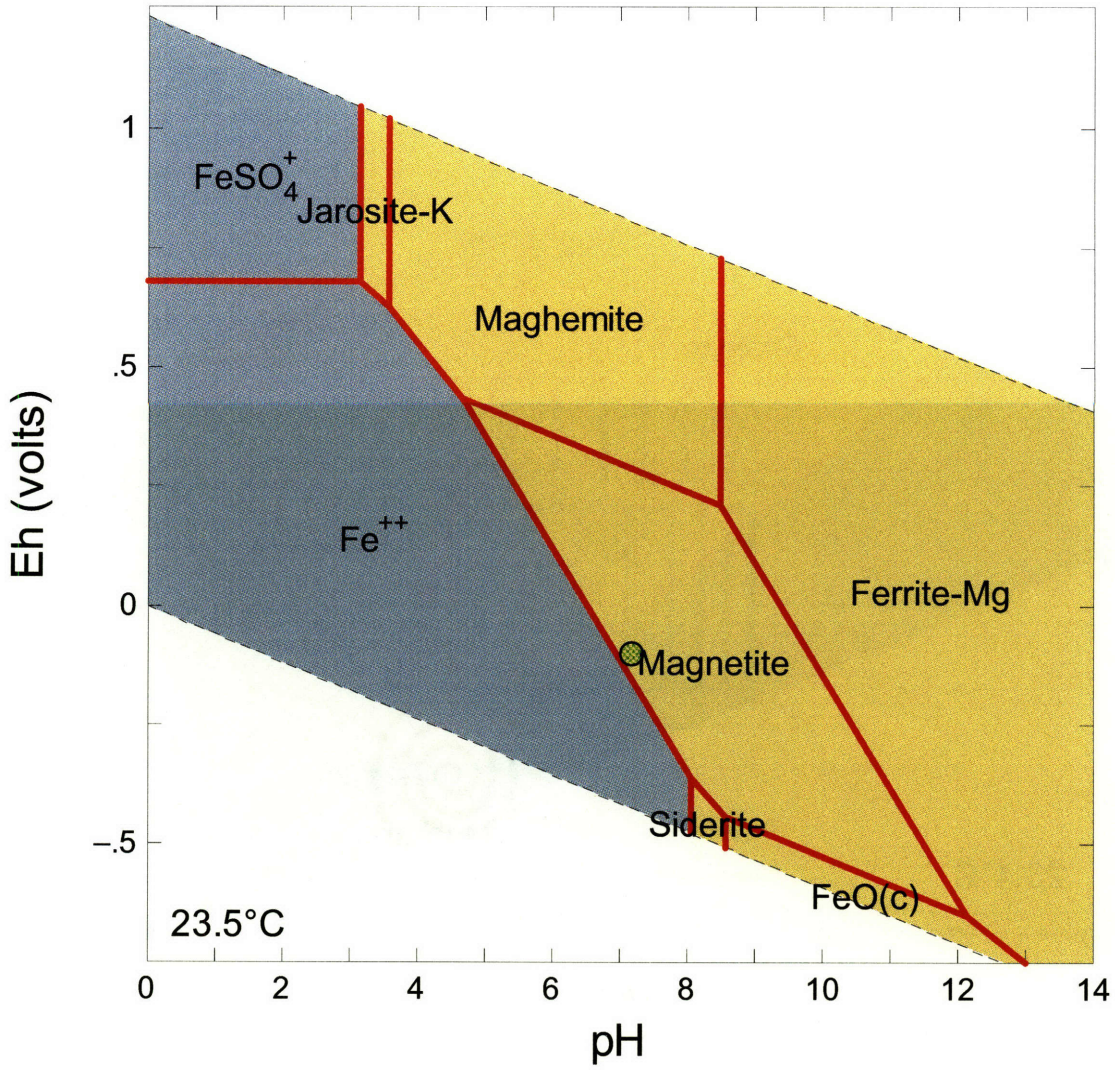


Figure 37 – P.A. Canovas III

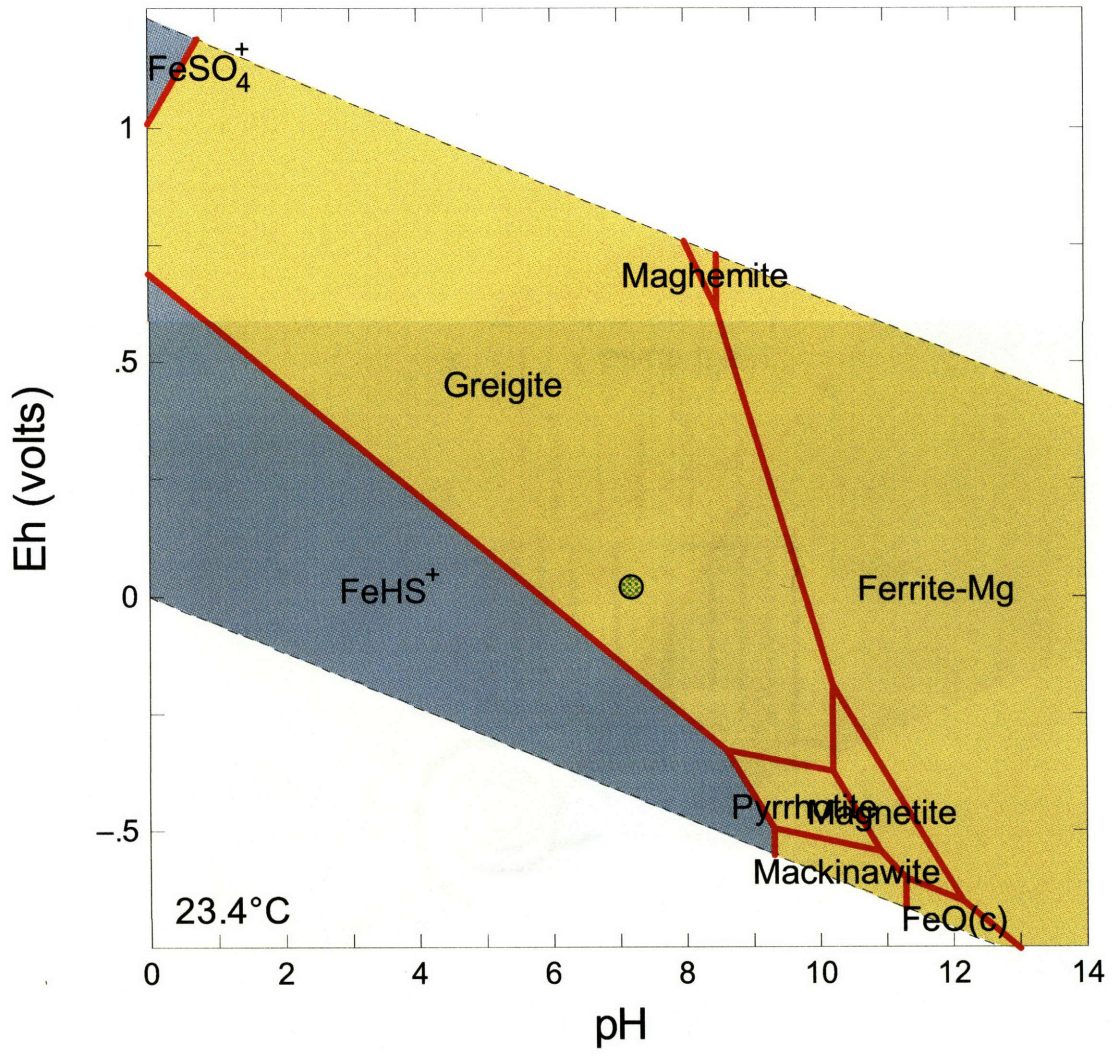


Figure 38 – P.A. Canovas III

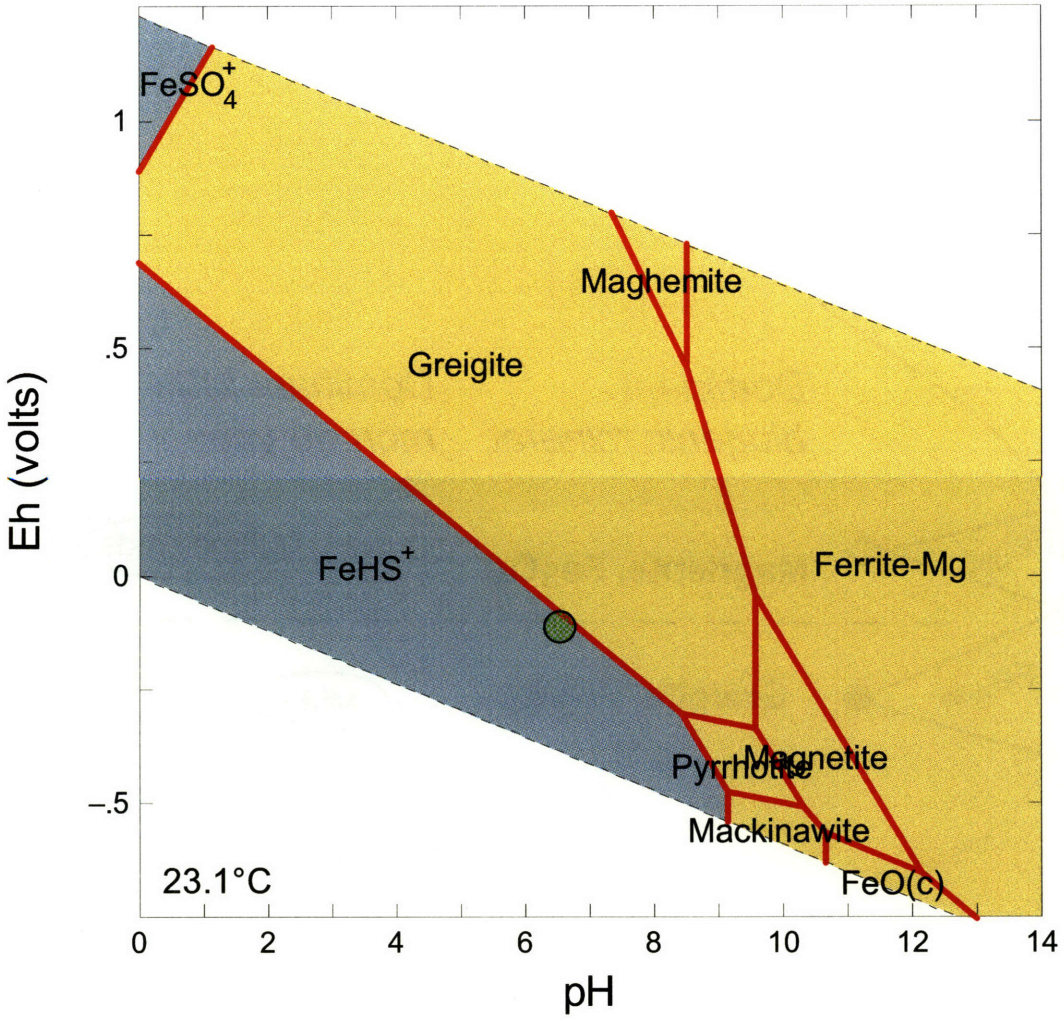


Figure 39 – P.A. Canovas III

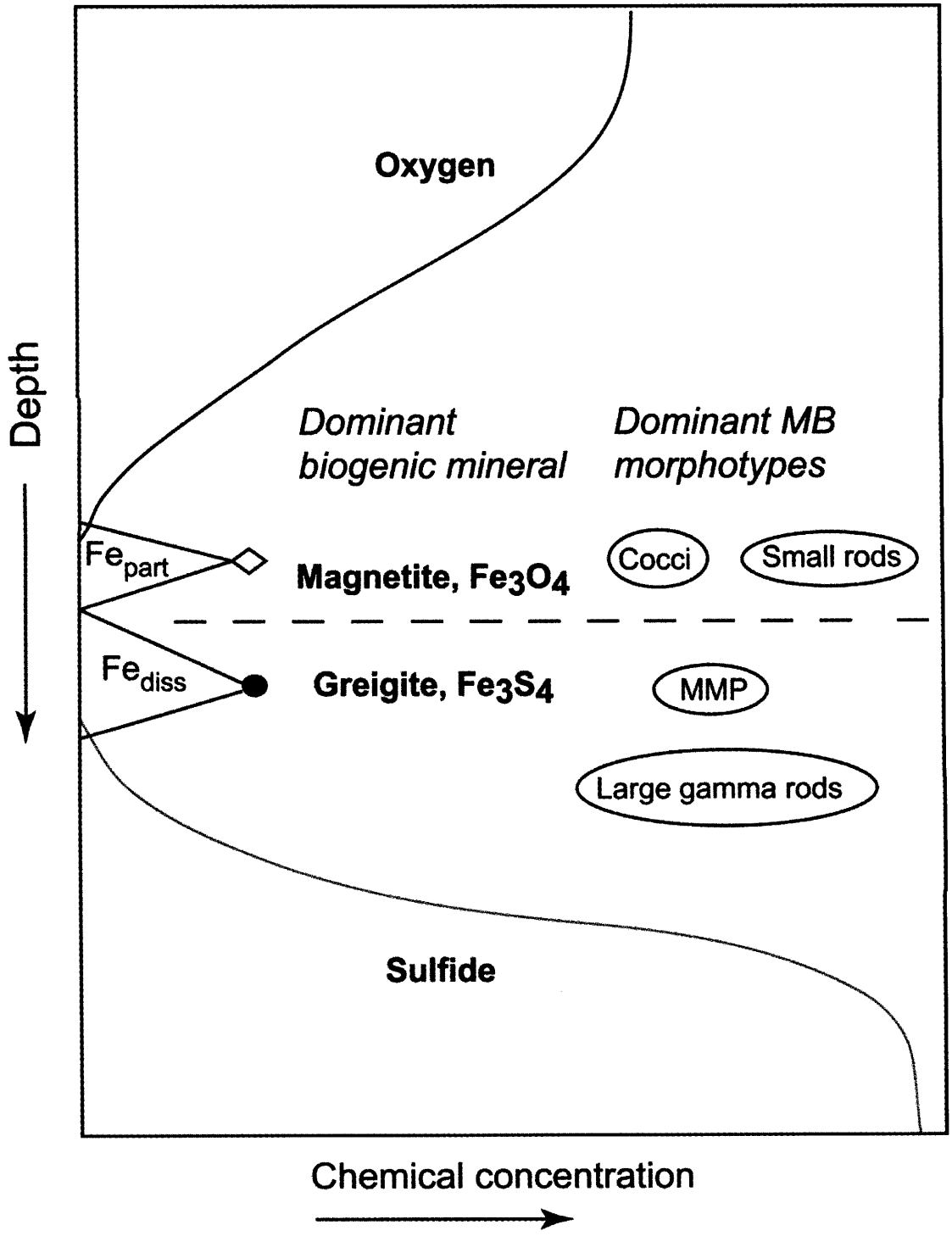


Figure 40 – P.A. Canovas III

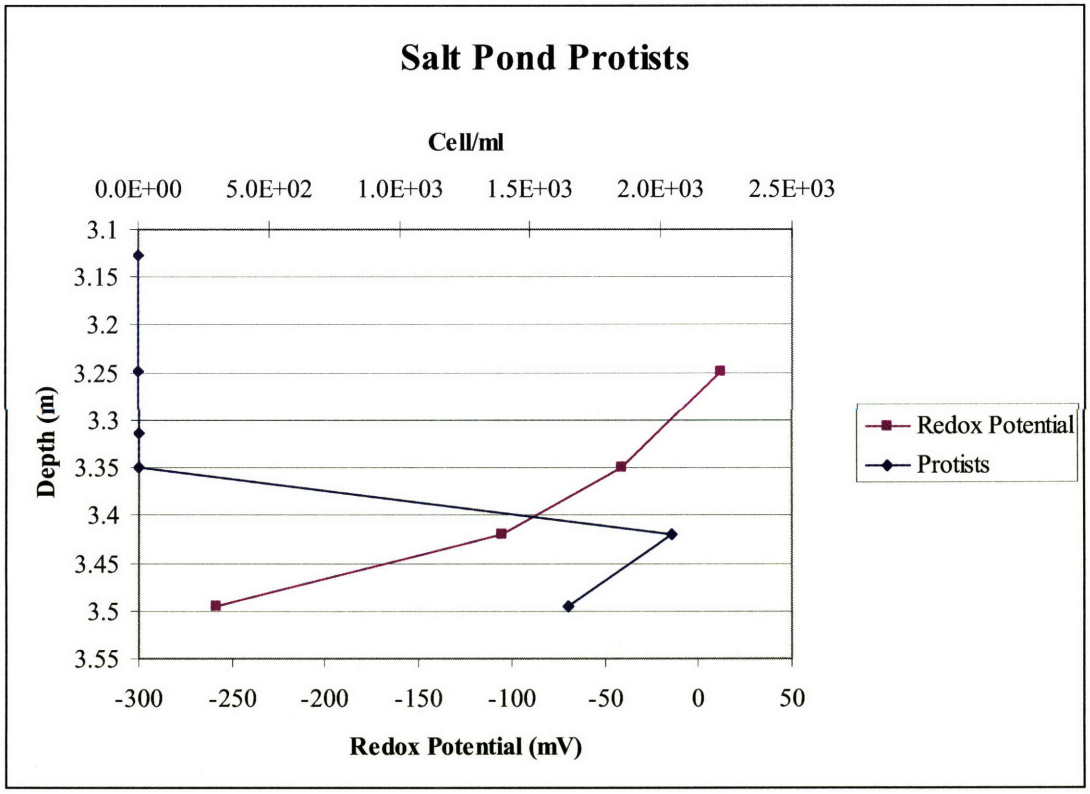


Figure 41 – P.A. Canovas III

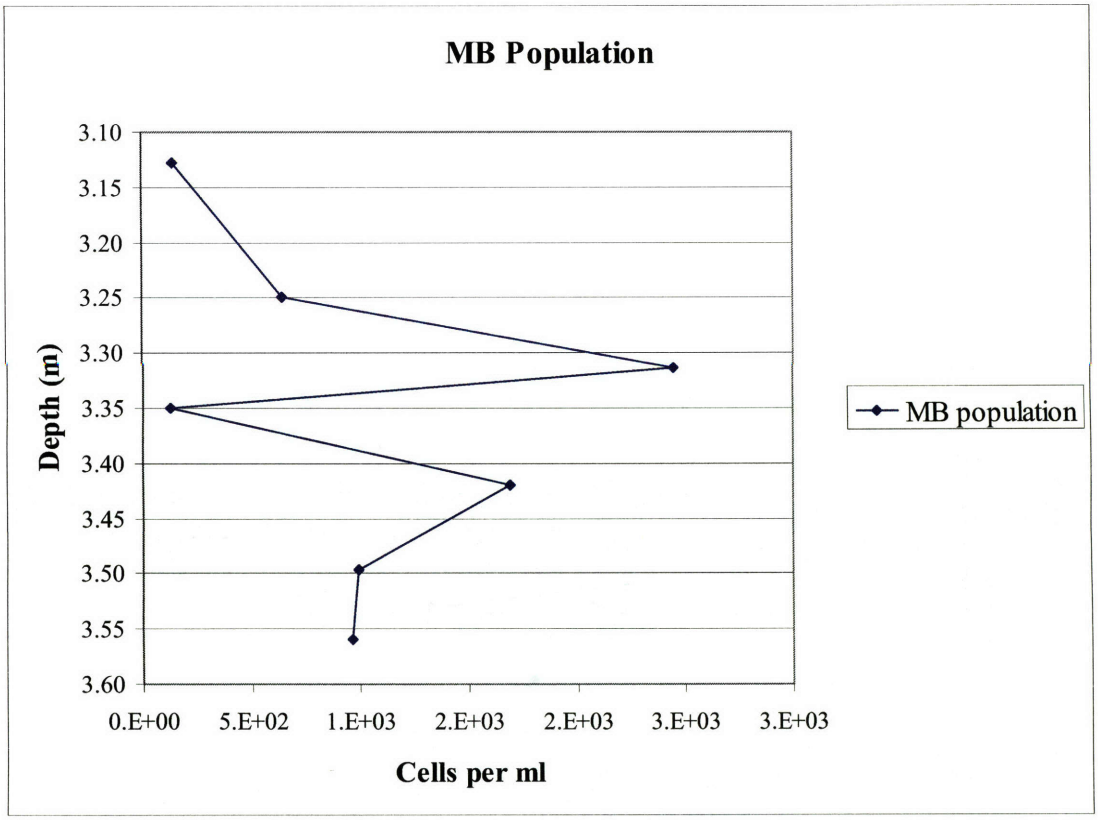


Figure 42 – P.A. Canovas III

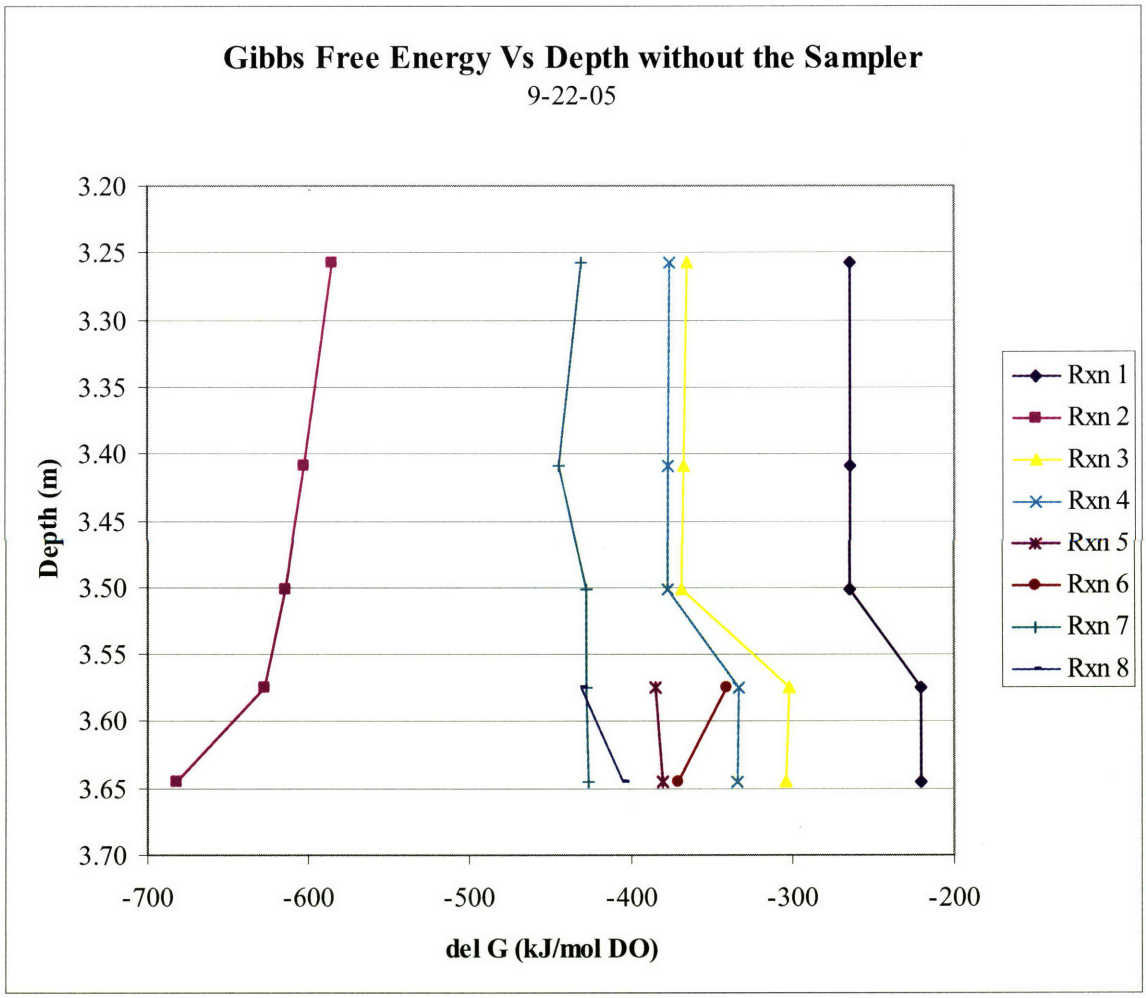


| | | |
|---|---|---|
| Rxn 1: | $4Fe^{2+} + O_2(aq) + 10\,H_2O = 4Fe(OH)_3 + 8\,H^+$ | log K = 14.4 |
| Rxn 2 : | $4\,Fe^{2+} + 4\,H^+ + O_2(aq) = 4\,Fe^{3+} + 2\,H_2O$ | log K = 33.95 |
| Rxn 3 : | $6\,Fe^{2+} + O_2(aq) + 12\,OH^- = Fe_3O_4 + 6\,H_2O$ | log K = 181.21 |
| Rxn 4: | $4\,Fe^{2+} + 4\,OH^- + O_2(aq) = 2\,Fe_2O_3 + 4\,H^+$ | log K = 89.81 |
| Rxn 5: | $0.5\,HS^- + O_2(aq) = 0.5\,SO_4^{2-} + 0.5\,H^+$ | log K = 69.17 |
| Rxn 6: | $HS^- + O_2(aq) = 0.5\,S_2O_3^{2-} + 0.5\,H_2O$ | log K = 64.9 |
| Rxn 7: | $0.5\,S_2O_3^{2-} + 0.5\,H_2O + O_2(aq) = SO_4^{2-} + H^+$ | log K = 73.45 |
| Rxn 8: | $6\,Fe^{2+} + 8\,HS^- + O_2(aq) = 2\,Fe_3S_4 + 4\,H^+ + 2\,H_2O$ | log K = 124.0212 |

Figure 43 – P.A. Canovas III

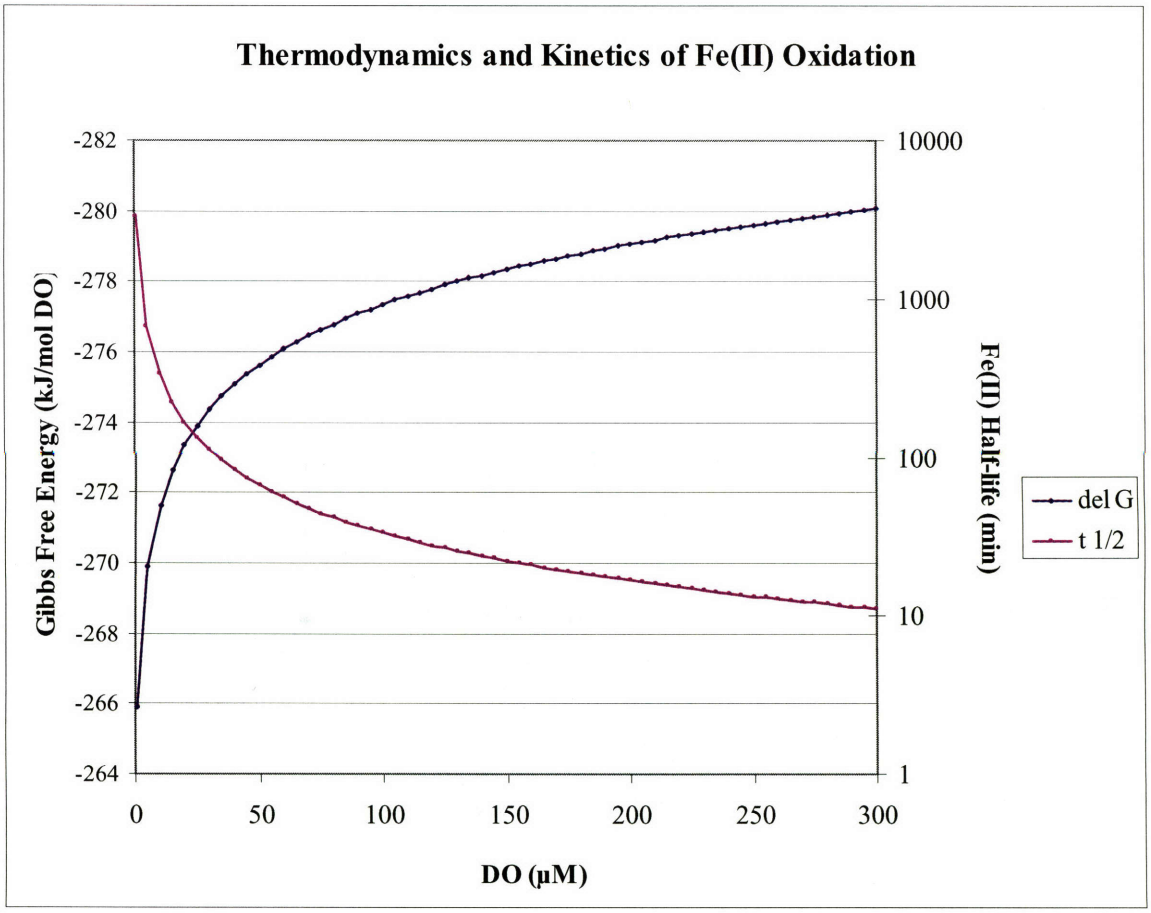


Figure 44 – P.A. Canovas III

## Appendix 1:GWB REACT Input Files for 8-11-2005 Sampling Period

**Depth: 3.05 m**

data = "C:\Program Files\Gwb\Gtdata\unfinished thermo_dat_modified5.dat" verify
temperature = 23.5
decouple HS-
swap e- for O2(aq)
1 kg free H2O
Eh = 0
pH = 7.87
total mmolar Na+ = 390.4457
balance on Cl-
total mmolar Cl- = 454.6857
total mmolar Mg++ = 44.384
total mmolar K+ = 8.5097
total mmolar Ca++ = 8.5097
total mmolar HCO3- = 1.9856
total mmolar SO4-- = 23.526
total umolar Fe++ = 2.64

suppress S2O3--
extrapolate
tables
printout species = long minerals = long basis = short reactions = short
plot = character

**Depth: 3.2 m**

data = "C:\Program Files\Gwb\Gtdata\unfinished thermo_dat_modified5.dat" verify
temperature = 23.5
decouple HS-
swap e- for O2(aq)
1 kg free H2O
Eh = -.119389
pH = 7.53
total mmolar Na+ = 393.12
balance on Cl-
total mmolar Cl- = 457.8
total mmolar Mg++ = 44.688
total mmolar K+ = 8.568
total mmolar Ca++ = 8.568
total mmolar HCO3- = 1.9992
total mmolar SO4-- = 23.688
total umolar Fe++ = 3.3

total umolar HS- = 193.72

suppress S2O3--
extrapolate
tables
printout species = long minerals = long basis = short reactions = short
plot = character

**Depth: 3.35 m**
data = "C:\Program Files\Gwb\Gtdata\unfinished thermo_dat_modified5.dat" verify
temperature = 23.5
decouple HS-
swap e- for O2(aq)
1 kg free H2O
pH = 7.53
total mmolar Na+ = 393.12
balance on Cl-
total mmolar Cl- = 457.8
total mmolar Mg++ = 44.688
total mmolar K+ = 8.568
total mmolar Ca++ = 8.568
total mmolar HCO3- = 1.9992
total mmolar SO4-- = 23.688
total umolar Fe++ = 2.8
Eh = -.239
total umolar HS- = 443.5818

suppress S2O3--
extrapolate
tables
printout species = long minerals = long basis = short reactions = short
plot = character

**Depth: 3.5 m**
data = "C:\Program Files\Gwb\Gtdata\unfinished thermo_dat_modified5.dat" verify
temperature = 23.5
decouple HS-
swap e- for O2(aq)
1 kg free H2O
pH = 7.53
total mmolar Na+ = 393.12

balance on Cl-
total mmolar Cl- = 457.8
total mmolar Mg++ = 44.688
total mmolar K+ = 8.568
total mmolar Ca++ = 8.568
total mmolar HCO3- = 1.9992
total mmolar SO4-- = 23.688
total umolar Fe++ = 2.3
Eh = -.359
total umolar HS- = 550.43

suppress S2O3--
extrapolate
tables
printout species = long minerals = long basis = short reactions = short
plot = character

**Depth: 3.81 m**
data = "C:\Program Files\Gwb\Gtdata\unfinished thermo_dat_modified5.dat" verify
temperature = 23.5
decouple HS-
swap e- for O2(aq)
1 kg free H2O
pH = 7.033
total mmolar Na+ = 393.12
balance on Cl-
total mmolar Cl- = 457.8
total mmolar Mg++ = 44.688
total mmolar K+ = 8.568
total mmolar Ca++ = 8.568
total mmolar HCO3- = 1.9992
total mmolar SO4-- = 23.688
total umolar Fe++ = 1.97
Eh = -.359
total umolar HS- = 556.5242

suppress S2O3--
extrapolate
tables
printout species = long minerals = long basis = short reactions = short
plot = character

**Depth: 4.11 m**
data = "C:\Program Files\Gwb\Gtdata\unfinished thermo_dat_modified5.dat" verify
temperature = 23.5
decouple HS-
swap e- for O2(aq)
1 kg free H2O
pH = 6.96
total mmolar Na+ = 393.12
balance on Cl-
total mmolar Cl- = 457.8
total mmolar Mg++ = 44.688
total mmolar K+ = 8.568
total mmolar Ca++ = 8.568
total mmolar HCO3- = 1.9992
total mmolar SO4-- = 23.688
total umolar Fe++ = 1.97
Eh = -.359
total umolar HS- = 567.899

suppress S2O3—
extrapolate
tables
printout species = long minerals = long basis = short reactions = short
plot = character

**Depth: 4.42 m**
data = "C:\Program Files\Gwb\Gtdata\unfinished thermo_dat_modified5.dat" verify
temperature = 23.5
decouple HS-
swap e- for O2(aq)
1 kg free H2O
pH = 7.01
total mmolar Na+ = 393.12
balance on Cl-
total mmolar Cl- = 457.8
total mmolar Mg++ = 44.688
total mmolar K+ = 8.568
total mmolar Ca++ = 8.568
total mmolar HCO3- = 1.9992
total mmolar SO4-- = 23.688
total umolar Fe++ = 1.64
Eh = -.359
total umolar HS- = 506.5333

```
suppress  S2O3--
extrapolate
tables
printout  species = long  minerals = long  basis = short  reactions = short
plot = character
```

## Appendix 2: GWB REACT Inputs Files for the 9-22-05 Sampling Period with the Sampler

**Depth: 3.31 m**

data = "C:\Program Files\Gwb\Gtdata\unfinished thermo_dat_modified5.dat" verify
temperature = 23.56
decouple HS-
swap e- for O2(aq)
1 kg free H2O
Eh = -.22125
pH = 7.225
total mmolar Na+ = 379.281
balance on Cl-
total mmolar Cl- = 441.6836
total mmolar Mg++ = 43.115
total mmolar K+ = 8.266
total mmolar Ca++ = 8.266
total mmolar HCO3- = 1.929
total mmolar SO4-- = 22.854
total umolar Fe++ = 16.502

suppress S2O3--
extrapolate
tables
printout species = long minerals = long basis = short reactions = short
plot = character

**Depth: 3.42 m**

data = "C:\Program Files\Gwb\Gtdata\unfinished thermo_dat_modified5.dat" verify
temperature = 23.61
decouple HS-
swap e- for O2(aq)
1 kg free H2O
Eh = -.084
pH = 7.257
total mmolar Na+ = 378.629
balance on Cl-
total mmolar Cl- = 440.925
total mmolar Mg++ = 43.041
total mmolar K+ = 8.252
total mmolar Ca++ = 8.252
total mmolar HCO3- = 1.926
total mmolar SO4-- = 22.815

total umolar Fe++ = 23.937
total umolar HS- = 83.346

suppress S2O3--
extrapolate
tables
printout species = long minerals = long basis = short reactions = short
plot = character

**Depth: 3.5**
data = "C:\Program Files\Gwb\Gtdata\unfinished thermo_dat_modified5.dat" verify
temperature = 23.25
decouple HS-
swap e- for O2(aq)
1 kg free H2O
Eh = -.2856
pH = 7.018
total mmolar Na+ = 381.42
balance on Cl-
total mmolar Cl- = 444.175
total mmolar Mg++ = 43.358
total mmolar K+ = 8.313
total mmolar Ca++ = 8.313
total mmolar HCO3- = 1.939
total mmolar SO4-- = 22.983
total umolar Fe++ = 26.914
total umolar HS- = 1985.371

suppress S2O3--
extrapolate
tables
printout species = long minerals = long basis = short reactions = short
plot = character

## Appendix 3: GWB REACT Input Files for the 9-22-05 Sampling Period without the Sampler

**Depth: 3.26 m**

data = "C:\Program Files\Gwb\Gtdata\unfinished thermo_dat_modified5.dat" verify
temperature = 23.84
decouple HS-
swap e- for O2(aq)
1 kg free H2O
Eh = .119
pH = 7.29
total mmolar Na+ = 373.1966
balance on Cl-
total mmolar Cl- = 434.5986
total mmolar Mg++ = 42.4232
total mmolar K+ = 8.133771
total mmolar Ca++ = 8.133771
total mmolar HCO3- = 1.89788
total mmolar SO4-- = 22.48749
total umolar Fe++ = 18.095

suppress S2O3--
extrapolate
tables
printout species = long minerals = long basis = short reactions = short
plot = character

**Depth: 3.41 m**

data = "C:\Program Files\Gwb\Gtdata\unfinished thermo_dat_modified5.dat" verify
temperature = 23.57
decouple HS-
swap e- for O2(aq)
1 kg free H2O
Eh = .064
pH = 7.26
total mmolar Na+ = 377.47543
balance on Cl-
total mmolar Cl- = 440.76581
total mmolar Mg++ = 42.9096
total mmolar K+ = 8.227
total mmolar Ca++ = 8.227
total mmolar HCO3- = 1.919
total mmolar SO4-- = 22.745

total umolar Fe++ = 28.642

suppress S2O3--
extrapolate
tables
printout species = long minerals = long basis = short reactions = short
plot = character

**Depth: 3.50 m**
data = "C:\Program Files\Gwb\Gtdata\unfinished thermo_dat_modified5.dat" verify
temperature = 23.49
decouple HS-
swap e- for O2(aq)
1 kg free H2O
Eh = .03
pH = 7.27
total mmolar Na+ = 378.144
balance on Cl-
total mmolar Cl- = 440.36
total mmolar Mg++ = 42.9856
total mmolar K+ = 8.242
total mmolar Ca++ = 8.242
total mmolar HCO3- = 1.923
total mmolar SO4-- = 22.7856
total umolar Fe++ = 32.272

suppress S2O3--
extrapolate
tables
printout species = long minerals = long basis = short reactions = short
plot = character

**Depth: 3.58 m**
data = "C:\Program Files\Gwb\Gtdata\unfinished thermo_dat_modified5.dat" verify
temperature = 23.37
decouple HS-
swap e- for O2(aq)
1 kg free H2O
Eh = 0
pH = 7.3
total mmolar Na+ = 379.08
balance on Cl-

total mmolar Cl- = 441.45
total mmolar Mg++ = 43.092
total mmolar K+ = 8.262
total mmolar Ca++ = 8.262
total mmolar HCO3- = 1.928
total mmolar SO4-- = 22.842
total umolar Fe++ = 30.049
total umolar HS- = 456.681

suppress S2O3--
extrapolate
tables
printout species = long minerals = long basis = short reactions = short
plot = character

**Depth: 3.65 m**
data = "C:\Program Files\Gwb\Gtdata\unfinished thermo_dat_modified5.dat" verify
temperature = 23.15
decouple HS-
swap e- for O2(aq)
1 kg free H2O
Eh = -.147
pH = 7.27
total mmolar Na+ = 380.684
balance on Cl-
total mmolar Cl- = 443.319
total mmolar Mg++ = 43.2744
total mmolar K+ = 8.2969
total mmolar Ca++ = 8.2969
total mmolar HCO3- = 1.935
total mmolar SO4-- = 22.939
total umolar Fe++ = 13.556
total umolar HS- = 112.01

suppress S2O3--
extrapolate
tables
printout species = long minerals = long basis = short reactions = short
plot = character

## Appendix 4: GWB ACT2 Input Files for the 8-11-2004 Sampling Period

**Depth: 3.05 m**

data = "C:\Program Files\Gwb\Gtdata\unfinished thermo_dat_modified5.dat" verify
temperature = 23.5 C
decouple HS-
swap e- for O2(aq)
diagram Fe++ on Eh vs pH
log activity main = -6.309
log activity Na+ = -.586
log activity Cl- = -.548
log activity Mg++ = -1.968
log activity SO4-- = -2.604
log activity K+ = -2.275
log activity Ca++ = -2.889
log activity HCO3- = -3.022
x-axis from 0 to 14 increment 1
y-axis from -.75 to 1.25 increment .25
suppress Hematite Goethite Troilite Pyrite
extrapolate
mosaic_labels

**Depth: 3.2 m**

data = "C:\Program Files\Gwb\Gtdata\unfinished thermo_dat_modified5.dat" verify
temperature = 23.5 C
decouple HS-
swap e- for O2(aq)
diagram Fe++ on Eh vs pH
log activity main = -7.719
log activity Na+ = -.583
log activity Cl- = -.5454
log activity Mg++ = -1.965
log activity SO4-- = -2.603
log activity K+ = -2.272
log activity Ca++ = -2.888
log activity HCO3- = -3.021
log activity HS- = -3.989
x-axis from 0 to 14 increment 1
y-axis from -.75 to 1.25 increment .25
suppress Hematite Goethite Troilite Pyrite
extrapolate
mosaic_labels

**Depth: 3.35 m**

data = "C:\Program Files\Gwb\Gtdata\unfinished thermo_dat_modified5.dat" verify
temperature = 23.5 C
decouple HS-
swap e- for O2(aq)
diagram Fe++ on Eh vs pH
log activity main = -8.086
log activity Na+ = -.583
log activity Cl- = -.546
log activity Mg++ = -1.965
log activity SO4-- = -2.603
log activity K+ = -2.272
log activity Ca++ = -2.888
log activity HCO3- = -3.021
log activity HS- = -3.626
x-axis from 0 to 14 increment 1
y-axis from -.75 to 1.25 increment .25
suppress Hematite Goethite Troilite Pyrite
extrapolate
mosaic_labels

**Depth: 3.5 m**
data = "C:\Program Files\Gwb\Gtdata\unfinished thermo_dat_modified5.dat" verify
temperature = 23.5 C
decouple HS-
swap e- for O2(aq)
diagram Fe++ on Eh vs pH
log activity main = -8.257
log activity Na+ = -.583
log activity Cl- = -.544
log activity Mg++ = -1.964
log activity SO4-- = -2.604
log activity K+ = -2.272
log activity Ca++ = -2.887
log activity HCO3- = -11.69
log activity HS- = -3.531
x-axis from 0 to 14 increment 1
y-axis from -.75 to 1.25 increment .25
suppress Hematite Goethite Troilite Pyrite
extrapolate
mosaic_labels

**Depth: 3.81 m**
data = "C:\Program Files\Gwb\Gtdata\unfinished thermo_dat_modified5.dat" verify
temperature = 23.5 C

decouple HS-
swap e- for O2(aq)
diagram Fe++ on Eh vs pH
log activity main = -8.174
log activity Na+ = -.583
log activity Cl- = -.544
log activity Mg++ = -1.964
log activity SO4-- = -2.604
log activity K+ = -2.272
log activity Ca++ = -2.887
log activity HCO3- = -16.16
log activity HS- = -3.667
x-axis from 0 to 14 increment 1
y-axis from -.75 to 1.25 increment .25
suppress Hematite Goethite Troilite Pyrite
extrapolate
mosaic_labels

**Depth: 4.11 m**
data = "C:\Program Files\Gwb\Gtdata\unfinished thermo_dat_modified5.dat" verify
temperature = 23.5 C
decouple HS-
swap e- for O2(aq)
diagram Fe++ on Eh vs pH
log activity main = -8.152
log activity Na+ = -.583
log activity Cl- = -.544
log activity Mg++ = -1.964
log activity SO4-- = -2.604
log activity K+ = -2.272
log activity Ca++ = -2.887
log activity HCO3- = -16.82
log activity HS- = -3.692
x-axis from 0 to 14 increment 1
y-axis from -.75 to 1.25 increment .25
suppress Hematite Goethite Troilite Pyrite
extrapolate
mosaic_labels

**Depth 4.42 m**
data = "C:\Program Files\Gwb\Gtdata\unfinished thermo_dat_modified5.dat" verify
temperature = 23.5 C
decouple HS-
swap e- for O2(aq)

diagram Fe++ on Eh vs pH
log activity main = -8.194
log activity Na+ = -.583
log activity Cl- = -.544
log activity Mg++ = -1.964
log activity SO4-- = -2.604
log activity K+ = -2.272
log activity Ca++ = -2.887
log activity HCO3- = -16.37
log activity HS- = -3.719
x-axis from 0 to 14 increment 1
y-axis from -.75 to 1.25 increment .25
suppress Hematite Goethite Troilite Pyrite
extrapolate
mosaic_labels

## Appendix 5: GWB ACT2 Input Files for the 9-22-2005 Sampling Period with the Sampler

**Depth: 3.31 m**

data = "C:\Program Files\Gwb\Gtdata\unfinished thermo_dat_modified5.dat" verify
temperature = 23.6 C
decouple HS-
swap e- for O2(aq)
diagram Fe++ on Eh vs pH
log activity main = -5.505
log activity Na+ = -.5973
log activity Cl- = -.559
log activity Mg++ = -1.976
log activity SO4-- = -2.61
log activity K+ = -2.286
log activity Ca++ = -2.895
log activity HCO3- = -3.045
x-axis from 0 to 14 increment 1
y-axis from -.75 to 1.25 increment .25
suppress Hematite Goethite Troilite Pyrite
extrapolate
mosaic_labels

**Depth: 3.42 m**

data = "C:\Program Files\Gwb\Gtdata\unfinished thermo_dat_modified5.dat" verify
temperature = 23.6 C
decouple HS-
swap e- for O2(aq)
diagram Fe++ on Eh vs pH
log activity main = -6.839
log activity Na+ = -.598
log activity Cl- = -.5597
log activity Mg++ = -1.977
log activity SO4-- = -2.61
log activity K+ = -2.287
log activity Ca++ = -2.896
log activity HCO3- = -3.044
log activity HS- = -4.491
x-axis from 0 to 14 increment 1
y-axis from -.75 to 1.25 increment .25
suppress Hematite Goethite Troilite Pyrite
extrapolate
mosaic_labels

**Depth: 3.50 m**

data = "C:\Program Files\Gwb\Gtdata\unfinished thermo_dat_modified5.dat" verify
temperature = 23.3 C
decouple HS-
swap e- for O2(aq)
diagram Fe++ on Eh vs pH
log activity main = -7.779
log activity Na+ = -.5947
log activity Cl- = -.5562
log activity Mg++ = -1.973
log activity SO4-- = -2.609
log activity K+ = -2.284
log activity Ca++ = -2.894
log activity HCO3- = -6.383
log activity HS- = -3.13
x-axis from 0 to 14 increment 1
y-axis from -.75 to 1.25 increment .25
suppress Hematite Goethite Troilite Pyrite
extrapolate
mosaic_labels

## Appendix 6: GWB ACT2 Input Files for the 9-22-2005 Sampling Period without the Sampler

**Depth: 3.26 m**

data = "C:\Program Files\Gwb\Gtdata\unfinished thermo_dat_modified5.dat" verify
temperature = 23.8 C
decouple HS-
swap e- for O2(aq)
diagram Fe++ on Eh vs pH
log activity main = -5.469
log activity Na+ = -.6039
log activity Cl- = -.5652
log activity Mg++ = -1.981
log activity SO4-- = -2.613
log activity K+ = -2.293
log activity Ca++ = -2.898
log activity HCO3- = -3.046
x-axis from 0 to 14 increment 1
y-axis from -.75 to 1.25 increment .25
suppress Hematite Goethite Troilite Pyrite
extrapolate
mosaic_labels

**Depth: 3.41 m**

data = "C:\Program Files\Gwb\Gtdata\unfinished thermo_dat_modified5.dat" verify
temperature = 23.6 C
decouple HS-
swap e- for O2(aq)
diagram Fe++ on Eh vs pH
log activity main = -5.265
log activity Na+ = -.5996
log activity Cl- = -.5611
log activity Mg++ = -1.978
log activity SO4-- = -2.611
log activity K+ = -2.288
log activity Ca++ = -2.896
log activity HCO3- = -3.045
x-axis from 0 to 14 increment 1
y-axis from -.75 to 1.25 increment .25
suppress Hematite Goethite Troilite Pyrite
extrapolate
mosaic_labels

**Depth: 3.50 m**

data = "C:\Program Files\Gwb\Gtdata\unfinished thermo_dat_modified5.dat" verify
temperature = 23.5 C
decouple HS-
swap e- for O2(aq)
diagram Fe++ on Eh vs pH
log activity main = -5.213
log activity Na+ = -.5986
log activity Cl- = -5601
log activity Mg++ = -1.977
log activity SO4-- = -2.61
log activity K+ = -2.287
log activity Ca++ = -2.896
log activity HCO3- = -3.044
x-axis from 0 to 14 increment 1
y-axis from -.75 to 1.25 increment .25
suppress Hematite Goethite Troilite Pyrite
extrapolate
mosaic_labels

**Depth: 3.58 m**
data = "C:\Program Files\Gwb\Gtdata\unfinished thermo_dat_modified5.dat" verify
temperature = 23.4 C
decouple HS-
swap e- for O2(aq)
diagram Fe++ on Eh vs pH
log activity main = -7.262
log activity Na+ = -.5976
log activity Cl- = -.5595
log activity Mg++ = -1.976
log activity SO4-- = -2.61
log activity K+ = -2.287
log activity Ca++ = -2.896
log activity HCO3- = -3.042
log activity HS- = -3.685
x-axis from 0 to 14 increment 1
y-axis from -.75 to 1.25 increment .25
suppress Hematite Goethite Troilite Pyrite
extrapolate
mosaic_labels

**Depth: 3.64 m**
data = "C:\Program Files\Gwb\Gtdata\unfinished thermo_dat_modified5.dat" verify
temperature = 23.1 C
decouple HS-

swap e- for O2(aq)
diagram Fe++ on Eh vs pH
log activity main = -7.083
log activity Na+ = -.5958
log activity Cl- = -.5577
log activity Mg++ = -1.975
log activity SO4-- = -2.609
log activity K+ = -2.285
log activity Ca++ = -2.895
log activity HCO3- = -3.042
log activity HS- = -4.317
x-axis from 0 to 14 increment 1
y-axis from -.75 to 1.25 increment .25
suppress Hematite Goethite Troilite Pyrite
extrapolate
mosaic_labels